UNIVERSIDADE FEDERAL DE MINAS GERAIS
Instituto de Geociências
Programa de Pós-Graduação em Geologia

Tobias Maia Rabelo Fonte Boa

Thermochronology and landscape evolution of the Serra do Caparaó region, an onshore segment of the Brazilian South Atlantic continental margin

N° 58

Belo Horizonte
27/04/2022

Tobias Maia Rabelo Fonte Boa

Thermochronology and landscape evolution of the Serra do Caparaó region, an onshore segment of the Brazilian South Atlantic continental margin

Versão final

Tese apresentada ao Programa de Pós-Graduação em Geologia da Universidade Federal de Minas Gerais como requisito parcial para obtenção do título de doutor em Geologia.

Orientador: Prof. Dr. Tiago Amâncio Novo
Coorientadores: Profa. Dra. Aline Tavares Melo e Dr. Daniel Peifer

Belo Horizonte
2022

F682t
2022

Fonte-Boa, Tobias Maia Rabelo.

Thermochronology and landscape evolution of the Serra do Caparaó region, an onshore segment of the Brazilian South Atlantic continental margin [manuscrito] / Tobias Maia Rabelo Fonte Boa. – 2022.

117 f., enc. il. (principalmente color.)

Orientador: Tiago Amâncio Novo.

Coorientadores: Aline Tavares Melo e Daniel Peifer.

Tese (doutorado) – Universidade Federal de Minas Gerais, Instituto de Geociências, 2022.

Área de concentração: Geologia Regional.

Bibliografia: f. 88-105.

Inclui apêndice e anexos.

1. Tempo geológico – Teses. 2. Paisagens – Teses. Geomorfologia – Caparaó, Serra do (MG) – Teses. I. Novo, Tiago Amâncio. II. Melo, Aline Tavares. III. Peifer, Daniel. IV. Universidade Federal de Minas Gerais. Instituto de Geociências. V. Título.

CDU: 550.93(81)

Ficha catalográfica elaborada por Elisabete Quatrini Vieira – CRB6 2210
Biblioteca “Vitória Pedersoli”, Instituto de Geociências da UFMG

UNIVERSIDADE FEDERAL DE MINAS GERAIS

PROGRAMA DE PÓS-GRADUAÇÃO EM GEOLOGIA DO IGC-UFMG

FOLHA DE APROVAÇÃO

Thermochronology and landscape evolution of the Serra do Caparaó region, an onshore segment of the Brazilian South Atlantic continental margin

TOBIAS MAIA RABELO FONTE BOA

Tese submetida à Banca Examinadora designada pelo Colegiado, como requisito para obtenção do grau de Doutor em GEOLOGIA, área de concentração GEOLOGIA REGIONAL, pelo Programa de Pós-graduação em Geologia do Instituto de Geociências da Universidade Federal de Minas Gerais.

Aprovada em 27 de abril de 2022, pela banca constituída pelos membros:

Prof. Tiago Amâncio Novo - Orientador
UFMG

Prof. Antonio Carlos Pedrosa Soares
UFMG

Prof. Pedro Augusto da Silva Rosa
UFMG

Profa. Andrea Ritter Jelinek
UFRGS

Prof. Fábio Soares de Oliveira
UFOP

Belo Horizonte, 27 de abril de 2022.

Acknowledgements

Firstly, I want to thank my mentors, professors Dr. Tiago Amâncio Novo, Dr. Aline Tavares Melo, and Dr. Daniel Peifer, for their support, valuable discussion, motivating enthusiasm, and encouraging me during these almost five years of research. This doctoral's project was only possible due to the support of the Geology Pos-graduation Program of Intitute of Geosciences, PROAP (Programa de Apoio à Pós-Graduação), PRPg (Pró-reitoria de Pós-Graduação), and the Manuel da Costa Research Center (CPMTC) at the Institute of Geosciences (IGC) of the Universidade Federal de Minas Gerais (UFMG). I also thank FAPEMIG and CAPES (Coordenação de Aperfeiçoamento de Pessoal de Nível Superior – Brasil) finance code 001 for the PhD scholarship funding. Furthermore, I am very grateful to the Glasgow Low-Temperature Thermochronology (GLOW) laboratory of the University of Glasgow for providing the AFT analysis. Special thanks go to professors Dr. Cristina Persano and Dr. Mark Wildman for their technical support, patience, and assistance during and after my abroad experience at the University of Glasgow. A special mention must be made to Ana Fonseca, Fernando Crincolli, Carla Sofia Marques, Márcio Vinícius Dantas, Alex Freitas, Anderson Magalhães Victória, Maria José Oliveira, Mariana Bandeira, and many other colleagues who have worked and spent time together in the 'salinha da pós' providing countless scientific discussions and friendships over the past few years. Finally, I want to thank my family and friends for their love, comprehension, and emotional support.

"The result, therefore, of this physical inquiry, is that we find no vestige of a beginning, no prospect of an end." (James Hutton)

Resumo

A origem e evolução de margens passivas elevadas tem intrigado a comunidade geocientífica uma vez que se encaixam melhor no contexto de riftes juvenis do que de riftes maduros. Um exemplo clássico é a margem continental brasileira que evoluiu de um rifte continental cretácico, há cerca de 130 Ma, e atualmente apresenta elevações que atingem mais de 2000 m acima do nível do mar. Por apresentar a morfologia considerada típica de margens passivas elevadas, o sistema de escarpas da Serra do Mar e Serra da Mantiqueira tem sido o principal foco da maioria dos estudos. No entanto a margem passiva elevada brasileira se estende por mais de 3000 km em um cinturão montanhoso que mostra padrões morfológicos bastante variados. Além do mais essa diversidade morfológica contradiz alguns estudos que frequentemente generalizam a margem brasileira como uma estrutura continua e homogenia ao invés de uma paisagem mais complexa e diversa. Com o intuito de explorar a diversidade morfotectonica da margem continental brasileira, este trabalho busca investigar as variações espaciais e temporais do padrão de denudação obtidas através de dados de termocronologia de baixa temperatura. O estudo se concentrou na Margem Continental do Sudeste do Brasil (CMSEB) que inclui a região onshore às bacias de Santos, Campo e Espírito Santo, com foco especial na região da Serra do Caparaó, um trecho montanhoso adjacente à Serra do Mar que é relativamente menos estudado e que não mostra a clássica morfologia escarpada. De forma geral a análise termocronológica da CMSEB mostra um perfil assimétrico de denudação no qual as idades de traço de fissão em apatita (AFT) tendem a aumentar com a elevação e em direção ao interior continental. O divisor de drenagem continental delimita uma região costeira intensamente dissecada (i.e., onde as idades ATF são geralmente mais jovens ou possuem valores similares à idade do rifte) de um interior continental relativamente menos dissecado (i.e., onde as idades AFT são mais antigas que o evento de quebra continental). Este perfil assimétrico é associado à denudação diferencial generalizada da região costeira em respostas a diversos processos associados com a ruptura da litosfera continental. Além disso, diferentemente de outras margens passivas, a costa brasileira mostra idades AFT substancialmente mais jovens que o evento rifte o que indica que esse setor da margem passiva Sul Atlântica experimentou uma quantidade de denudação superior ao previsto nos modelos genéricos. Modelos térmicos frequetemente mostram um pulso de resfriamento desassociado ao evento de rifteamento sugerindo que, além da denudação prolongada relacionada ao processo de rifteamento, a exumação da margem foi influenciada por algum fator transiente. A relação entre a trama estrutural e o contraste nos dados termocronológicos, que foi pela primeira vez caracterizada em detalhe na região onshore da Bacia do espírito Santo, indica que a exumação pós-rifte da CMSEB foi controlada pela reativação de estruturas litosféricas herdadas que acomodaram a deformação associada à movimentação relativa entre blocos do embasamento (i.e., soerguimento e subsidência relativos) colaborando para o complexo padrão denudacional ao longo da costa. Neste contexto, a Serra do Caparaó representa uma região interfluvial costeira desenvolvida nos primeiros estágios do rifte do Atlântico Sul que vem sofrendo modificações

(i.e., capturas fluviais) decorrentes das reativações pós-rifte. Por fim, este estudo destaca que variações nos padrões de denudação à longo prazo corroboram as diferenças morfológicas ao longo da margem sugerindo que a margem continental brasileira não é um ambiente geotectônico homogêneo e contínuo. Além disso, apesar do reconhecimento de vários processos que atuaram durante a evolução pós-rifte da margem, a herança tectônica (i.e., trama estrutural, litologia, rigidez flexural da litosfera) impactou significativamente no padrão de denudação contribuindo para a diversidade morfológica ao longo da costa Sul Atlântica brasileira.

Palavras-chave: Margem Sul Atlântica brasileira; a evolução a longo prazo de margens continentais passivas elevadas; termocronologia de traços de fissão em apatita; evolução geomórfica da Serra do Caparaó.

Abstract

The origin and evolution of elevated passive continental margins have intrigued geoscientists since their prominent topography is more reasonably explained in the context of an active rift than a mature 'passive' setting. A classic example is the Brazilian continental margin which evolved from a rift in Cretaceous, ca. 130 Ma ago, yet presents elevations that reach more than 2000 m above sea level. The Brazilian South Atlantic marginal upwarp extends for more than 3000 km and shows substantial morphological variation. Nevertheless, geoscientists have been mainly focused on studying the escarpment-form segments (e.g., the Serra do Mar in southeast Brazil) and frequently assuming the Brazilian elevated continental margin as a well-defined and continuous marginal upwarp instead of a diversified and more complex landscape. Attempting to understand the landscape variation along the Brazilian South Atlantic passive margin, this work uses the low-temperature thermochronology to explore how time-space denudation patterns differ along the southeast Brazilian coast with a particular focus on the Serra do Caparaó segment; a relatively less-studied area found adjacent to the Serra do Mar and where the typical escarpment form is absent. Overall, the thermochronology analysis shows an asymmetric denudation profile in which AFT ages tend to increase with elevation and toward the continental interior. The continental drainage divide delimits a dissected coastal region (i.e., where AFT ages are generally younger or similar to the rifting event) from a less denudated continental interior area (i.e., where AFT ages are older than continental breakup). This asymmetric denudation profile is associated with the generalized differential exhumation of the coastal region due to the continued erosion and unloading isostatic rebound triggered by the continental breakup processes, which are expected in generic passive continental margins evolution models. However, the Brazilian continental margin shows AFT ages substantially younger than rifting event, suggesting that the margin has experienced increased post-rift exhumation. Thermal models frequently show a pulse of cooling occurring long after rifting event, indicating that an additional transient factor than continued rifting-related denudation may have influenced the exhumation of the margin. The post-rift exhumation seemed to have been controlled by the reactivation of lithospheric inherited structures that triggered the relative uplift/subsidence between basement blocks resulting in contrasting denudation patterns along the coastal region, including the onshore segment related to the Espirito Santo basin (i.e., the Serra do Capraó region). In this situation, the Serra do Capraó is currently a high-elevation coastal interfluve segment that includes relicts of ancient long-lived syn-rift coastal catchment areas (i.e., syn-fit less-denudated coastal interfluve region) that has been changed and reestablished during the post-rift reactivation. Finally, this study highlights that the thermochronology pattern corroborates the morphological differences along the margin, supporting that the Brazilian continental margin is not a single and continuous tectonic setting. Furthermore, besides the variety of proposed mechanisms operating over the post-rifting evolution of the margin, tectonic inheritance (i.e., structural framework, lithology,

the effective flexural strength of the lithosphere) has strongly impacted the denudation pattern contributing to the geomorphic diversification along the Brazilian South Atlantic coast.

Keywords: Brazilian South Atlantic continental margin; long-term landscape evolution of elevated passive continental margins; apatite fission track thermochronology; Serra do Caparaó geomorphic evolution.

List of Figures

List of Tables

Contents

1 Introduction

1.1 Rifted continental margins: a general overview

The study object of this thesis is the Serra do Caparaó, a sector of the western South Atlantic rifted continental margin in southeast Brazil (Fig. 1). To create an appropriate framework for the ensuing discussion is essential to have in mind the concepts and definitions of rifted continental margins.

Rifted continental margin (RCM)(i.e., passive continental margin, Atlantic-type continental margin, trailing-edge margin, divergent margin) comprise a distinct geological environment resulting from the divergent movement between plate boundaries. They evolved from continental breakup and subsequent seafloor spreading and thus represent the transition of new oceanic basins with the fragment of the broken continents within the same plate. In this situation, because rifted continental margins configure ancient active environments (i.e., rift system) preserved in the plate interior, they are referred to as 'passive' compared to other continental margins located at plate boundaries called active continental margins.

During the Cenozoic, RCMs had been the most common tectonic feature on Earth's surface (Fig. 1), computing more than 100,000 km in length (Bradley, 2008). Most of them were sculpted by the fragmentation of the Pangea supercontinent during the Mesozoic, when Africa, South America, Australia, Antarctica, India, North America, and Eurasia almost simultaneously spread apart (Bradley, 2008; Moulin et al., 2010; Brune, 2016). Although mature RCMs are commonly thought of as tectonically stable environments (McKenzie, 1978), studies focusing on geomorphology, tectonics, and neotectonics (e.g. Bezerra and Vita-Finzi, 2000; Paton, 2012; Salomon et al., 2015; Péron-Pinvidic and Manatschal, 2009; Peron-Pinvidic et al., 2013; Huismans and Beaumont, 2011) show a consensual post-rift (i.e., occurred long after rifting process) tectonic activity which incites the rethinking the terminology and the processes that have been used to describe the evolution of RCMs.

Guided by the expressive hydrocarbon deposits, the first studies on RCM were developed offshore, while the onshore region was relatively neglected (Gallagher and Brown, 1997). Furthermore, due to erosion of the rift flanks, the tectono-sedimentary record of the continental counterpart is often missed imposing an extra challenge to geoscientists to depict the onshore evolution of RCM and illustrating the importance of the advent of additional methods, such as low-temperature thermochronology (LTT), that enable unravelling the exhumation history of RCM.

LTT is a branch of isotopic geology used to examine the thermal evolution of rocks and minerals present within the upper crust ($\sim$1-5 km of depth). Among other applications, it gives

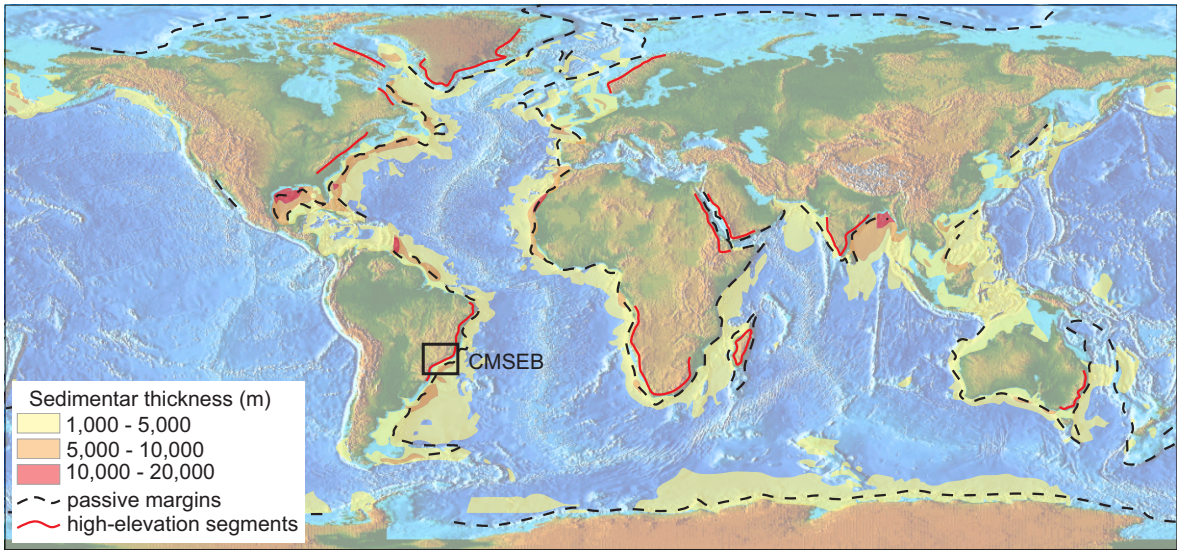

Figure 1 – Topography of the Earth showing the global distribution of passive margins (dashed black line), high-elevation segments (red line), and total sediment thickness. Based on Divins (2003), Frisch et al. (2011), Bally et al. (2012), and Japsen et al. (2012).

powerful information about the denudation history of an area, being an alternative approach for studying exhumed terrains such as onshore regions of continental margins (Gallagher and Brown, 1999; Green et al., 2013; Wildman et al., 2016; Gallagher and Brown, 1997). Furthermore, LTT has been used to model the thermal evolution of sedimentary basins. Among other subjects (e.g. infer the burial rates and subsidence), LTT is mainly used to investigate the maturation of organic material into petroleum (Schneider and Issler, 2019; Gleadow et al., 1983) characterizing the LTT as an essential and multiple-task tool to study RCMs.

Many RCMs are characterized by a high-elevation topography which is often featured by a prominent escarpment that separates an interior low-relief elevated plateau from a low-lying coastal plain (i.e., elevated passive continental margin, rifted margins upwards Green et al., 2018; Gilchrist and Summerfield, 1990). Because such salient topography is most expected in active rifts (i.e. young continental margins) rather than mature passive margins, the origin and longevity of this prominent feature are still being ardently debated (Ollier, 1982; van der Beek et al., 1995; Braun, 2018; Japsen et al., 2019; Braun, 2019; Braun and van der Beek, 2004; Gilchrist and Summerfield, 1990; Persano et al., 2002).

Some authors agree that the high-elevation topography at RCM is a long-lasting feature resulting from the continuous erosion and isostatic adjustments of an ancient topographic feature that pre-dates or was generated during the rifting process(e.g. Lister et al., 1991; Redfield et al., 2005; Persano et al., 2006; Ziegler and Cloetingh, 2004; Braun and Beaumont, 1989). On the other hand, other authors believe that the topography at RCMs are much younger due to multiple events of uplift and subsidence that occurred during the post-rift evolution of the margin (e.g. Japsen and Chalmers, 2000; Japsen et al., 2006, 2012; Green et al., 2013). This multistage evolution somehow corroborates with the play of post-rift uplift and tectonic reactivation observed by

some studies that have questioned the long-term stability of RCMs (e.g. Cogné et al., 2011, 2012; Wildman et al., 2016; Calegari et al., 2021; Bezerra and Vita-Finzi, 2000; Paton, 2012; Salomon et al., 2015; Péron-Pinvidic and Manatschal, 2009; Peron-Pinvidic et al., 2013; Huismans and Beaumont, 2011).

Overall, the RCM uplift has been attributed to several thermo-mechanical processes related or not to the extension, thinning, and rupture of the lithosphere, such as domal or dynamic uplift (Ruetenik et al., 2016), depth-dependent extension (Royden and Keen, 1980), secondary convection (Armitage et al., 2013), and magmatic underplating (McKenzie, 1984). Uplift has also been expected according to the type of deformation mechanism operating during the continental rifting (i.e. pure and simple shear; Summerfield, 1991; Lister et al., 1991; Kusznir and Ziegler, 1992), the style of rifting (i.e. active and passive rifting; McKenzie, 1978; Wernicke, 1985), and depending on the presence and volume of magma (i.e. magma-rich or volcanic, and magma-poor or non-volcanic margins; Wernicke, 1985). However, such geodynamic elements are merely key parts of end-members scenarios that operate at different temporal-spatial scales. In fact, models for RCM often show aspects in between these end-members where elements operate simultaneously. In this situation, a consensus has been reached that the evolution of RCM is extremely complex and, consequently, explain the uplift of RCM is not an easy task (see Peron-Pinvidic et al., 2019; Wildman, 2015, for a review and historical perspective).

In the Mid ‘90s, with the improvement of computational approaches, several studies using numerical models that integrate analytic information (e.g. LTT, cosmogenic) and physical processes models, at both mantle and crustal levels, were performed to improve and test the current theories about the evolution of RCMs (e.g. Kooi and Beaumont, 1994; Gilchrist et al., 1994; Gallagher et al., 1994; Tucker and Slingerland, 1994). Although the complexity of steps regarding the thermo-mechanical uplift processes, these studies have shown the importance of the prior topography and tectonic inheritance in the evolution of the RCMs. Factors such as the position and presence of a preexisting drainage divide (van der Beek et al., 2002), bedrock density and resistance to erosion (Braun et al., 2014), structural framework (Gunnell and Harbor, 2010), and flexural strength of the lithosphere (Braun, 2018) are fundamental aspects that influence the geomorphological evolution and diversification of the RCMs.

1.2 Study area

The study area comprises the continental margin of southeast Brazil (CMSEB), a segment of the Brazilian South Atlantic continental margin that runs from Curitiba to Vitória cities and includes more than 1,000 km of the Brazilian coastline (Fig. 2). The CMSEB correspond to the segment related to Santos, Campos and Espírito Santo offshore basins (França et al., 2007; Moreira et al., 2007; Winter et al., 2007) which formed following the fragmentation of West Gondwana in Early Cretaceous (ca. 138 Ma; Pérez-Díaz and Eagles, 2014).

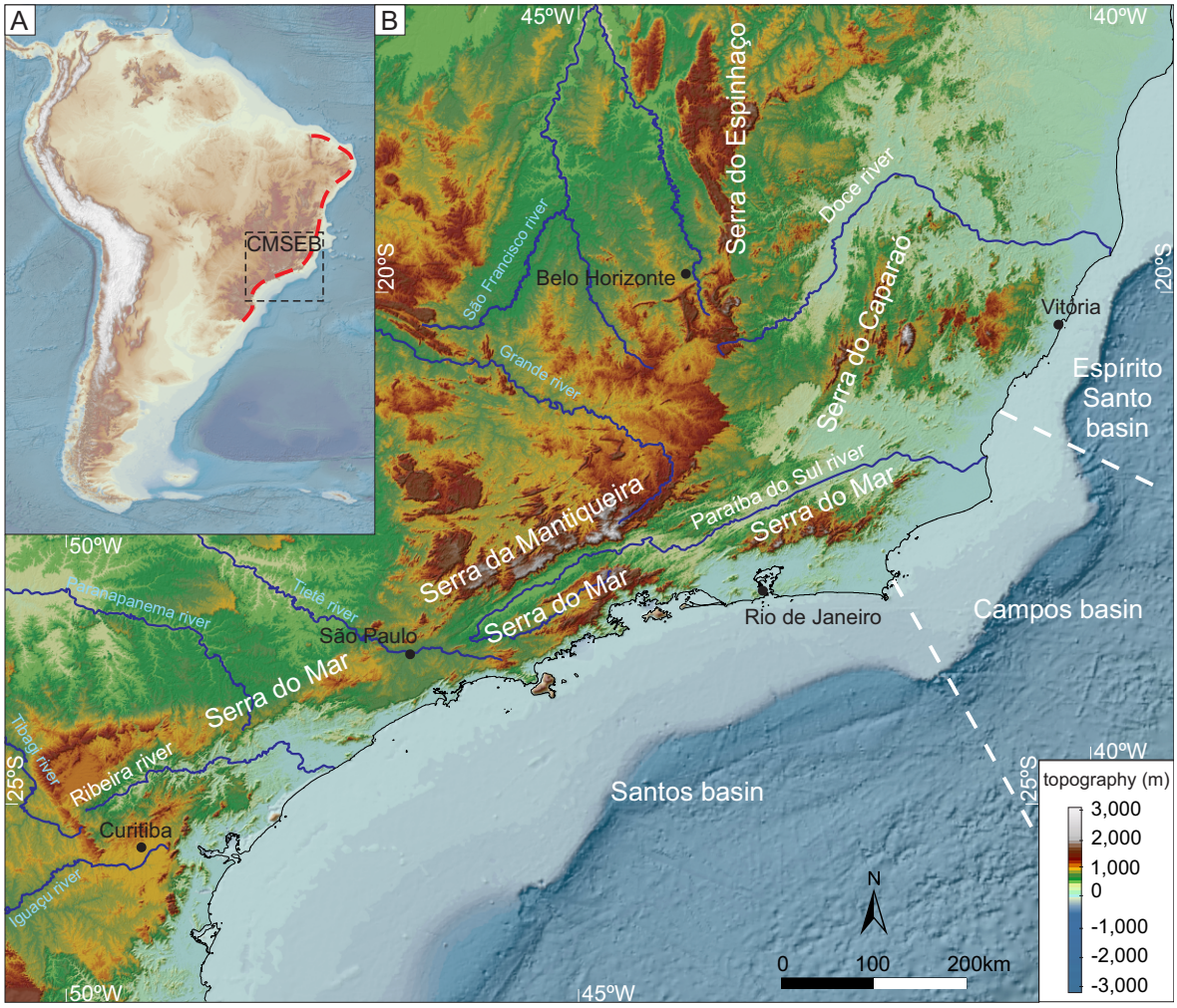

Figure 2 – A)Location of the study area in a South American context (red dashed line indicate the segment commonly referred to as the Brazilian elevated passive continental margin); B)Digital elevation model of the continental margin of SE Brazil (CMSEB) showing the spatial distribution of the Serra do Mar, Serra da Mantiqueira, Serra do Espinhaço, and Serra do Caparaó, as well as the main rivers systems. The onshore digital elevation model is derived from COP30 DEM. South America and offshore topography was obtained from topex global 1-minute grids (https://topex.ucsd.edu/cgi-bin/get_data.cgi).

The CMSEB is a segment of the high-elevation topographic belt (i.e. Brazilian elevated passive continental margin) that extends for more than 3000 km parallel to the Brazilian coast (Fig. 2A). The CMSEB southern extension is represented by the Serra da Mantiqueira and Serra do Mar, a series of prominent escarpments that occur adjacent to Santos and Campos offshore basins (Moreira et al., 2007; Winter et al., 2007), and includes the Cenozoic Rift System of Southeastern Brasil (Almeida, 1976; Melo et al., 1985; Riccomini, 1989; Zalán and Oliveira, 2005). The CMSEB northern extension occur adjacent to Espírito Santo offshore basin (França et al., 2007) and is represented by the Serra do Caparaó that runs relatively close to the coastline, and the Serra do Espinhaço that is found more than 400 km inland (Fig. 3). In contrast to the southern extension, the escarpment form is absent in the CMSEB northern extension.

The basement of CMSEB comprises part of the Mantiqueira province that includes the Araçuaí and Ribeira belts. Inland, the Mantiqueira province is bordered by São Francisco craton, Basília belt (i.e. Tocantins province), and Paraná basin (Almeida et al., 1981). Except for the Paraná basin, all these sectors are tectonic compartments related to the West Gondwana assembly. São Francisco craton comprises a collection of Archean and Paleoproterozoic terrains that constituted the paleocontinent São Francisco-Congo assembled to other terrains during Pan-African/Brasiliano orogenic cycle to form West Gondwana in the Neoproterozoic-Paleozoic boundary (Pedrosa-Soares et al., 2001; Cordani et al., 2003; Pedrosa-Soares et al., 2008; Alkmim et al., 2006; Heilbron et al., 2010). Brasilia, Araçuaí, and Ribeira belts comprise the orogenic settings developed during this amalgamation event. Paraná basin, as well as Bauru and Sanfranciscana basins (Batezelli and Ladeira, 2016) form a series of Phanerozoic intracontinental depocenters systems developed during the interval between the fragmentation of the West Gondwana and the establishment of the South Atlantic platform, which are also associated with retroarc-foreland system in response to Andean orogenic events (Menegazzo et al., 2016). In addition to the Cenozoic Rift System of Southeastern Brasil developed in the region of the Serra do Mar and Serra da Mantiqueira, along the Brazilian coast occur Paleogene-Neogene continental-to-shallow-water marine sequences related to the uppermost proximal portions of the onshore sedimentary basins (Barreiras Formation; Dias et al., 2021).

1.3 Problem rationale

The Brazilian South Atlantic coast has long been considered a classic example of a passive continental margin (e.g. Asmus and Porto, 1972; Asmus and Ponte, 1973; Figueiredo and Gabaglia, 1986). Yet, the origin and longevity of its high-elevation topography remain open to discussion. This mature rift setting evolved from the development of a divergent plate boundary that led to the fragmentation of Gondwana in the Early Cretaceous. However, after a long period of continental drifting and seafloor spreading (ca. 140 Ma), this ancient active plate boundary presents elevations that reach more than 2000 m above sea level.

Studies performed in the region of Serra do Mar have shown that the segment related to Santos and Campos basins has been quite ‘active’ since after the opening of the South Atlantic ocean. The onshore geological record suggests the development of a continental rift system during the Cenozoic in response to the reactivation of Precambrian basement inherited structures (Almeida, 1976; Melo et al., 1985; Riccomini, 1989; Zalán and Oliveira, 2005). This event was accomplished by alkaline magmatism (e.g. Thompson et al., 1998) and development of a series of small continental sedimentary basins (Fig. 3) along the main structural trend (e.g. Negrão et al., 2020). The LTT information corroborates with this scenario and indicates significant pulse of denudation during the Late Cretaceous, and the Early Cenozoic (e.g. Gallagher et al., 1994; Cogné et al., 2012; Hiruma et al., 2010).

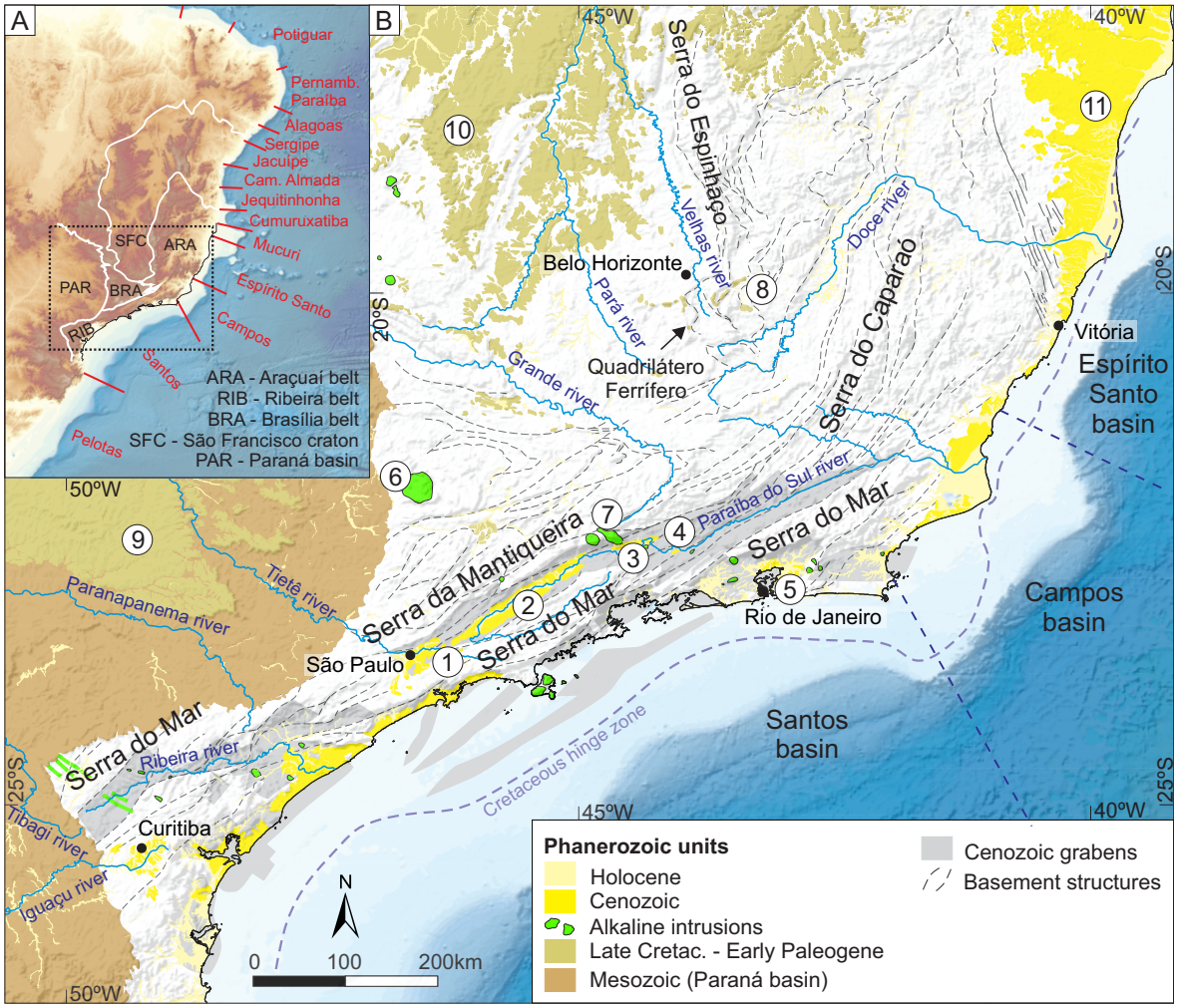

Figure 3 – Phanerozoic units of CMSEB. A) Localization map showing the Brazilian offshore basins and the tectonic provinces compartmentalization. B) Simplified geologic map showing the main Phanerozoic units, including the Cenozoic rift system of SE Brazil according to Zalán and Oliveira (2005), the main bodies of the Serra do Mar igneous province after Thompson et al. (1998), the basins of the Continental Rift of Southeastern Brazil after Riccomini et al. (2004). (1) São Paulo basin; (2) Taubaté basin; (3) Resende basin; (4) Volta Redonda basin; (5) Guanabara graben; (6) Poços de Caldas massif; (7) Passa Quatro and Itatiaia massifs; (8) Fonseca and Gandarela basisn; (9) Bauru basin; (10) Sanfranciscana basin; (11) Barreiras Formation.

Besides the consensus that the landscape of the Serra do Mar reflects post-breakup reactivation of preexisting structures, the mechanisms responsible for this reactivation remains controversial. Some studies attributed it to the gravitational collapse of a wide-elevated plateau in response to the drifting of the South American Plate over a Trindade thermal anomaly (e.g. Zalán and Oliveira, 2005). On the other hand, the reactivation of the CMSEB has been associated with tectonic activity due to intraplate-wide compressive stress transmitted from the Andean orogeny and the Atlantic spreading axis (e.g. Riccomini et al., 2004). Furthermore, the existence of the Trindade hot-spot, or even a mantle plume, is sustained by the several alkaline intrusions along the southern segment of CMSEB (the Serra do Mar igneous province; Thompson et al., 1998).

However, the accommodation of rifting-related stresses in the lithosphere due to the delamination of the subcontinental lithospheric mantle has been proposed as an alternative mechanism for this magmatic activity (Ernesto et al., 2002).

Contrasting with the Serra do Mar region, the Serra do Caparaó region is relatively less studied, and most of what is known came from few LTT (Carmo, 2005; Jelinek et al., 2014; Amaral-Santos et al., 2019; van Ranst et al., 2020)(Fig. 3). Similar to other segments of the Brazilian South Atlantic margin (e.g., northeastern Brazil; Nóbrega et al., 2005), these LTT data indicate a spatially contrasting denudation history in response to post-rift reactivation (van Ranst et al., 2020). Nevertheless, although this scenario corroborates other local non-thermochronology studies that emphasize the influence of normal faulting during the post-rift evolution of the study area (e.g., Mello, 1997; Mello et al., 1999; Noce et al., 2003; Romano and Castañeda, 2006), the region lacks LTT data with a proper spatial resolution to constrain the link between the structural framework and the long-term denudation pattern. Moreover, in contrast to the region of Serra do Mar that shows several geological evidences that help reconstruct the Cenozoic geological history (e.g., sedimentary successions and igneous intrusions), the lack of such stratigrafic clues in the region of Serra do Caparaó imposes an extra challenge to depict the evolution of this specific segment of the South Atlantic margin. Thus, the importance of having a robust LTT data.

This work seeks to fill this information gap. By presenting a detailed revision of the extensive LTT data available for the CMSEB, and by including new high-resolution data for the region of Serra do Caparaó, this study will contribute to the understanding of the long-term landscape evolution of the CMSEB, as well as, will provide a broader perspective on the long-standing debate about the evolution of 'passive' continental margins. Specifically, this work aims to address the following main hypotheses:

(i) Even thought being characterized as a elevated rifted continental margin, the Brazilian South Atlantic coast show geomorphic variations that reflect particular geological histories evidenced by the thermochronology data;

(ii) Despite the complexities regarding the mechanisms and driving forces operating over the tectonic evolution of the continental margin of southeast Brazil, tectonic inheritance has an essential role in its geomorphic diversification and geological evolution;

(iii) The reactivation of preexisting tectonic structures controlled the syn- and post-rift evolution of the onshore region related to Espírito Santo basin (i.e., Serra do Caparaó region).

1.4 Thesis outline

This study presents a detailed revision of the apatite fission track data available for the continental margin of southeast Brazil, as well as, new apatite fission track data for the region

of Serra do Caparaó (i.e. the Serra da Boa Vista area). In addition to being used to infer the magnitude and rate of denudation experienced by the margin, these data is used to highlight differences in the long-term landscape evolution through the margin.

Chapter (2) is a brief explanation about the the fission track analysis, historical aspects, relevant concepts, applications, and methodological procedures.

Chapter (3) is a review article discussing the available apatite fission track data and the landscape diversity along the continental margin of southeast Brazil entitled 'The southeast Brazilian rifted continental margin is not a single, continuous upwarp: variations in morphology and denudation pattern along the continental drainage divide' and under revision on *Earth-Science Reviews journal*.

Chapter (4) presents a set of new apatite fission track samples collected in the region of Serra da Boa Vista in the region of Serra do Caparaó and discusses the influence of reactivation of bedrock inherited structures in the long-term landscape evolution of the onshore region related to Espírito Santo basin.

Chapter (5) presents the general discussion and conclusions of this work.

Appendices (A) - Supplementary material

Annexes (A) - Additional scientific production. This section present a compendium of parallel scientific publications, as first author or collaborator, performed during the doctorate period.

2 Fission track analysis

2.1 Introduction

Thermochronology is a branch of isotope geology that embraces several methods, including fission track analysis. For over 60 years, it has been applied in geologic and planetary science with a particular interest in the earth-surface processes and the interactions between tectonics, erosion, and climate. There are many differences between geo- and thermochronology, but this distinction is often fuzzy. The main difference of thermo- over geochronology is, for example, the capability to solve both temporal and thermal aspects of geologic processes, rather than determine a singular absolute stratigraphic or magmatic formation age (Reiners et al., 2005).

This work focuses on fission track analysis (FTA). Therefore here, I attempt to introduce the general idea of this procedure. I start with a brief historical perspective of the fission track discovery, as well as the principles behind fission track formation (2.2) and the use of FTA to dating (2.3) and to investigate the thermal history of rocks and minerals (2.4).

2.2 The fission track

Fission track (FT) is a microscopic-trail-like radiation damage (Fig. 4A) present in the structure of a solid-state material (i.e. detector) due to the nuclear fission of a heavy and unstable nuclide (Fleischer et al., 1975). The study and characterization of these features in minerals (e.g., apatite, zircon) and other materials (e.g., volcanic glasses, glass shards, and plastics) characterizes the FTA (Fleischer et al., 1965b; Gleadow et al., 1983; Gallagher et al., 1998; Donelick et al., 2005).

As with other conventional isotopic methods (e.g. U-Pb geochronology), the basis of FTA is the accumulation of FT (i.e. decay-daughter product) over geological time, which, among other applications, can be used as a dating tool (Price and Walker, 1963). FT records processes at lower temperatures than conventional geochronometers, thus, FTA is also called low-temperature thermochronology (LTT) (Fig. 4B). Furthermore, because FTA enables the access of information over a protracted temperature range rather than estimating the timing of a closure temperature, it has its advantages over conventional chronometers.

Apatite and zircon are ideal for FTA because they present adequate content of uranium (i.e. uranium impurities) that accumulate a comfortable number of tracks over geological time. Moreover, because these minerals are widely present in crustal rocks, FTA has been used to study many geological settings (e.g., sedimentary basin, orogenic and non-orogenic settings) and for different purposes (e.g., sedimentary provenance, timing tectonic events, long-term landscape

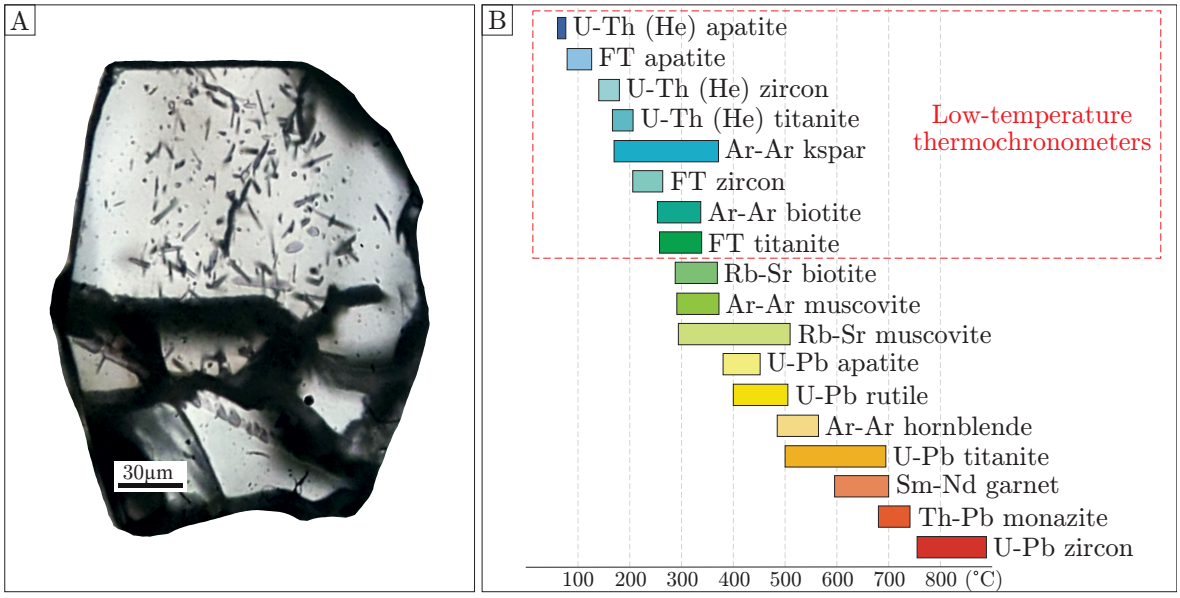

Figure 4 – A) Photomicrography of an apatite crystal showing its fission tracks. B) Temperature ranges for some thermochronometers, the red rectangle highlights the LTT.

evolution, and hydrocarbon and ore exploration; Donelick et al., 2005; Gallagher et al., 1998).

The base knowledge of FTA begins with the advent of nuclear research in the '30s. During that time, the term 'fission' was established to describe the reaction of the break-up of uranium into two lighter products (Fermi, 1934; Meitner and Frisch, 1939). The uranium fission track was firstly recognized in 1958 by Young (1958) using a fluoride crystal detector. One year later, it was confirmed by Silk and Barnes (1959) using a mica detector. Then, Price and Walker (1963) firstly suggest the use of FTA as a mineral dating method.

As with some conventional isotopic dating approaches in geosciences, the FTA is based on the chain decay of the ^{238}U, which reaches stability through two alternative paths, α-decay or spontaneous fission (Fig. 5). The former occurs with a very high probability (99.9998%) in comparison to the latter (0.0002%). Each decay path has its constant decay, mechanism, products, and applications (Table 1). For example, the ^{238}U α-decay series constitutes the primary basis for U-Pb and (U-Th)/He geochronology, while the ^{238}U spontaneous fission series is the basis for FTA.

In the α-particle decay the ^{238}U nuclei emits He-nuclei and β radiation on a complicated series of nuclear disintegration until reaches a stable ^{206}Pb nucleus (Figure 5). The α-decay causes little lattice damage (i.e. alpha recoil damage) due to the small size and low charge of the ^{4}He ion (Table 1).

In the spontaneous fission decay, the ^{238}U nuclei splits into heavy-high-energy nuclei fragments plus high-energy neutrons (Figure 5). This nuclear reaction is generally binary and asymmetric, and the fission fragments are massive and highly charged in comparison to alpha-particles (Table 1), causing much more lattice damage than alpha recoil. However, even though

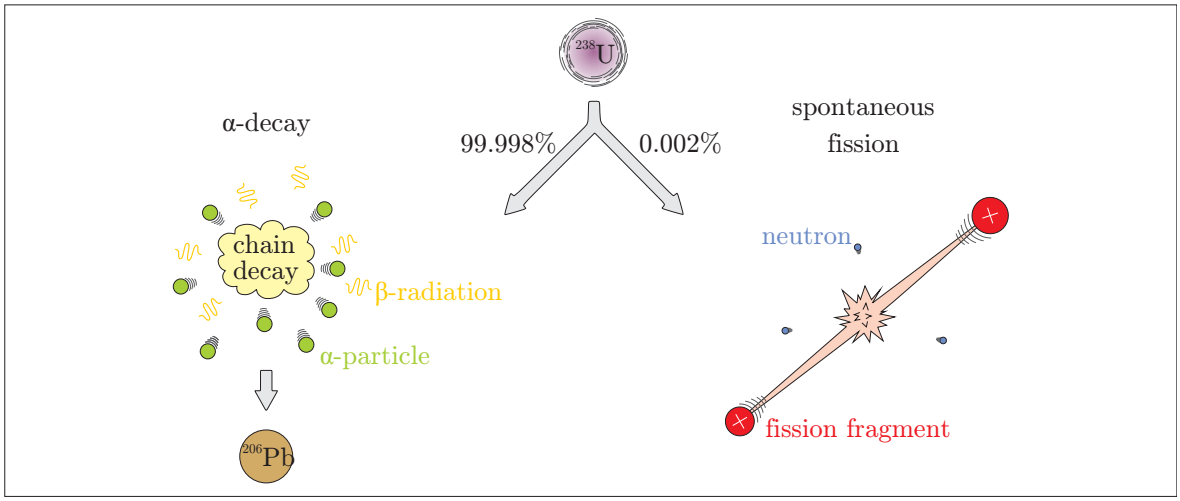

Figure 5 – ^{238}U nuclei can reach stability according to two alternative nuclear reactions, α-decay and spontaneous fission. In α-decay the ^{238}U nuclei emits He-nuclei and β radiation on a chain reaction until reaches a stable ^{206}Pb nucleus. While in the spontaneous fission decay, the ^{238}U nuclei splits into heavy-high-energy nuclei fragments and high-energy neutrons.

Table 1 – Phisical properties of the two resulting particles of ^{238}U decay: alpha-particle resulting from α-decay and fission fragments resulting from spontaneous fission.

	alpha-particle	fission fragment
Mass (amu)	4	80-155
Size (relative)	small	big
Energy (MeV)	70 $\times 10^{-3}$ to 140 $\times 10^{-3}$	160
Ionic charge	+2	+30 to +50
Occurrence (relative)	$\sim \times 10^{7}$	1

an alpha recoil event causes less damage than a fission reaction, α-particle decay is $\sim 10^7$ times more frequent, depositing more energy into lattice than fission tracks. Therefore, both the decay processes need to be considered in LTT.

The proposed mechanism by which fission fragments interact with the detector causing the disrupted zone remains controversial. In the 'ion spike' model the damage is caused by electronic repulsion (Fig. 6). According to this mechanism, the fission generates fragments that would have enough energy to leave their electron cloud behind, acting as highly charged cations inducing atomic displacements (Fleischer et al., 1975). Alternatively, in the 'thermal spike' model, the displacements would be caused by the thermal process. Furthermore, another theory predicts the recoil nuclei acting as 'wrecking balls' as the fragments travel through the enclosing material.

The stopping distance of fission fragments depends on their kinetic energy and the detector chemical composition. As the pieces interact with the detector, they lose kinetic energy

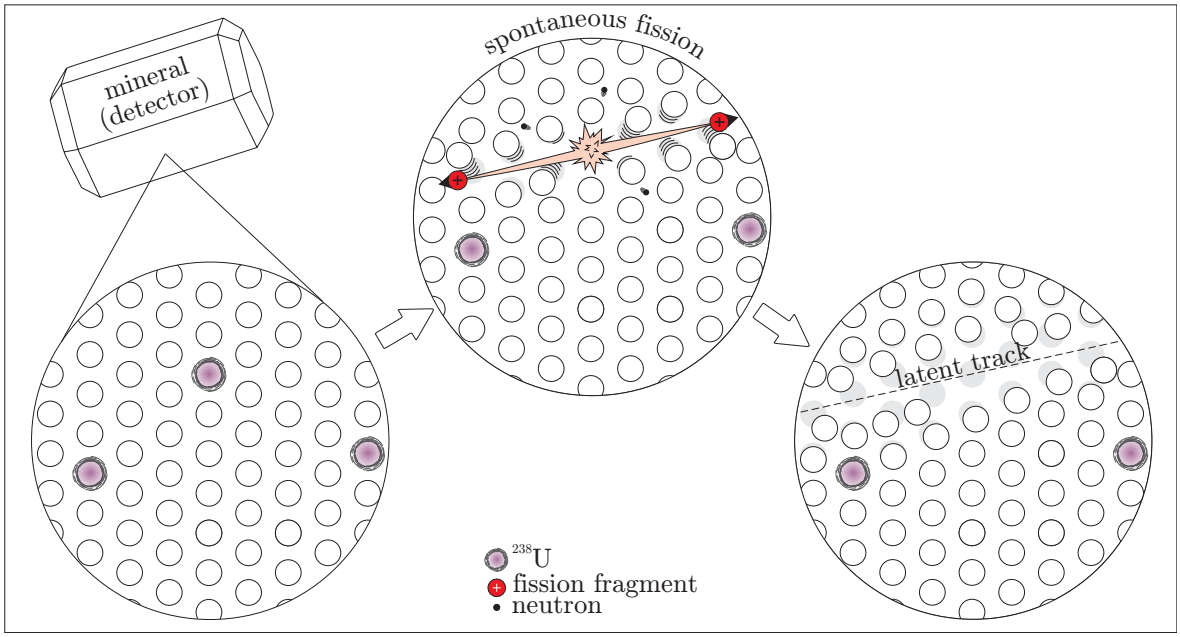

Figure 6 – The latent track formation due to the fission of an ^{238}U nucleus.

until they stop, forming one linear trail called latent track (Figure 6). In apatite, for example, this distance is 21.2 $\pm$ 0.9 μm, while in zircon it reaches 16.7 $\pm$ 0.8 μm. Generally, the latent track width is nano-metric (ηm) being too small to be observed under an optical microscope, thus for FTA, they must be revealed (i.e. enlarged) by chemical etching.

Another essential characteristic of FT is that they are temperature sensitive, which makes FTA a powerful tool to study the thermal evolution of minerals and rocks (Fleischer et al., 1975; Gleadow and Duddy, 1981; Green et al., 1986; Laslett et al., 1987). This aspect is detailed in section 2.4.

2.3 Fission track dating

2.3.1 Isotopic chronometer

In FTA we assume that each FT represents one ^{238}U spontaneous fission decay event, since:

1. Induced fission events occur just on extraordinary conditions on earth;
2. Fission track in minerals of the crust are not cosmogenic in origin, since they were buried;
3. ^{238}U is relatively the most abundant isotope (Table 2);
4. ^{238}U has small half-life of spontaneous fission relative to other isotopes such as ^{235}U and ^{232}Th which take too long to naturally produce sufficient number of tracks.(Table 2).

Table 2 – Abundance, half-lives, and decay frequency of the four major naturally nuclides exhibiting spontaneous fission (Wagner and van der Haute, 1992).

Isotope	Abundance relative to ^{238}U	Total ($t_{1/2}$) (year)	Spontaneous fission ($t_{1/2}$) (year)
^{232}Th	4[a]	1.40×10^{10}	1.0×10^{21}
^{234}U	5.44×10^{-5}	2.46×10^{5}	1.5×10^{16}
^{235}U	7.25×10^{-3}	7.04×10^{8}	1.0×10^{19}
^{238}U	1	4.47×10^{9}	8.2×10^{15}

[a] Geochemical average

Because FTs continuously accumulate over geological time, the ratio between the number of FT (i.e. decay product daughter) and the total amount of ^{235}U (i.e. radioactive parent isotope) act as a chronometer. This relationship is demonstrated by the law of radioactive decay that is based on a decay constant λ and is expressed by:

$$\frac{dN}{dt} = -\lambda N \tag{2.1}$$

where N is the number of unstable nuclide remaining after any time t.

By integrating equation (2.1) with respect to time, the number of decays D_t is given by:

$$D_t = N(e^{\lambda t} - 1) \tag{2.2}$$

Then the solution to t is:

$$t = \frac{1}{\lambda}\, ln\left(\frac{D_t}{N} + 1\right) \tag{2.3}$$

As we can see, the isotopic chronometer equation (2.3) basically depends on three parameters: the nuclide decay constant λ, the number of decays over time D_t, and the number of nuclide remaining N.

There are several studies that establish the λ for each nuclide decay series. In FT dating we use the total decay constant for ^{238}U (λ_d). However, as introduced before, ^{238}U nuclei can decay by following two alternative paths. It means that, at the same time, there are ^{238}U nuclei disintegrating to ^{206}Pb by α-decay ($\lambda_\alpha \approx 1.6\times10^{-10}\ yr^{-1}$; Steiger and Jäger, 1977) and there are ^{238}U nuclei decaying by fission ($\lambda_f \approx 8.57\times10^{-17}\ yr^{-1}$; Thiel and Herr, 1976). Thus, we have to considerate both decay constant to determine the λ_d, that is why we call it total constant decay. Fortunately, λ_α is several orders of magnitude greater than λ_f, thus only λ_α is considerate in the calculus. It has to be stressed that, although we do not consider λ_f in the calculus of λ_d, it is used to calculate the other parameters of the FT dating equation.

$$\lambda_d = \lambda_\alpha + \lambda_f \approx \lambda_\alpha = 1.6 \times 10^{-10}\ yr^{-1} \tag{2.4}$$

The heart of any isotopic approach is to determine the number of stable daughter product D_t(i.e. fission tracks) over total parent isotope, or remaining parents N after time t.

Since FT dating has consolidated as a robust way to study minerals and rocks, several procedures have been developed to determine these two parameters (e.g., the population method, the subtraction method, the external detector method, the re-etch method, and the re-polish method; Gleadow, 1981). Although each method is subject to different limitations, the most common and efficient one is the external detector method (EDM; Tagami and O'Sullivan, 2005). The great advantage of EDM is that it can deal with the problem of variation in uranium concentration (i.e. zonation) at each grain enabling to calculate single grain ages. This issue is very important in terms of the method's precision. Recently, thermochronologists are committed to establish a new procedure using laser ablation inductively coupled plasma mass spectrometry (LA-ICP-MS; Cox et al., 2000; Hasebe et al., 2004; Cogné et al., 2020) which main advantage against the other classical methods is the absence of the irradiation step that speeds up the process. This work approaches the EDM.

2.3.2 The external detector method - EDM

In the EDM the D_t is basically determined from the number of spontaneous fission tracks over an area, ρ_s, (i.e. spatial density of spontaneous fission tracks). For this, an internal section of the crystal is exposed by polishing and then etched to reveal the tracks (Figures 7A and B). In this procedure only the tracks that intersect this specific section are revealed, thus it needs a geometry factor g. The spontaneous FT are counted manually under a microscope and a square grid is commonly used to help delimit the area in which the tracks were counted (Fig. 7D).

The N is indirectly obtained from the density of induced fission tracks, ρ_i, by irradiating the sample with neutrons in a reactor. The flux of thermal neutrons inside the reactor induces synthetic fission of ^{235}U that is used to infer the ^{238}U content. It is done by attaching to the grain surface an external low-uranium detector, usually a sheet of low-uranium muscovite, used to record the ^{235}U induced fission tracks (Figure 7C). Then, similarly to the determination of ρ_s, the induced FTs are counted in the external detector using the same area used to determine the ρ_s. Furthermore, to avoid discrepancies regarding the internal variation of uranium content in the analysed crystal, the ρ_i must be counted in the same relatively-to-the-crystal position used to count ρ_s(Figure 7D). It can be done automatically, using a computer-controlled microscope stage system (Smith and Leigh-Jones, 1985) or manually by positioning the external detector on the apatite grain mounts with the same configuration when irradiated. Then, by changing the focus of the microscope, it is possible to count both spontaneous and induced tracks in the same area without moving the sample.

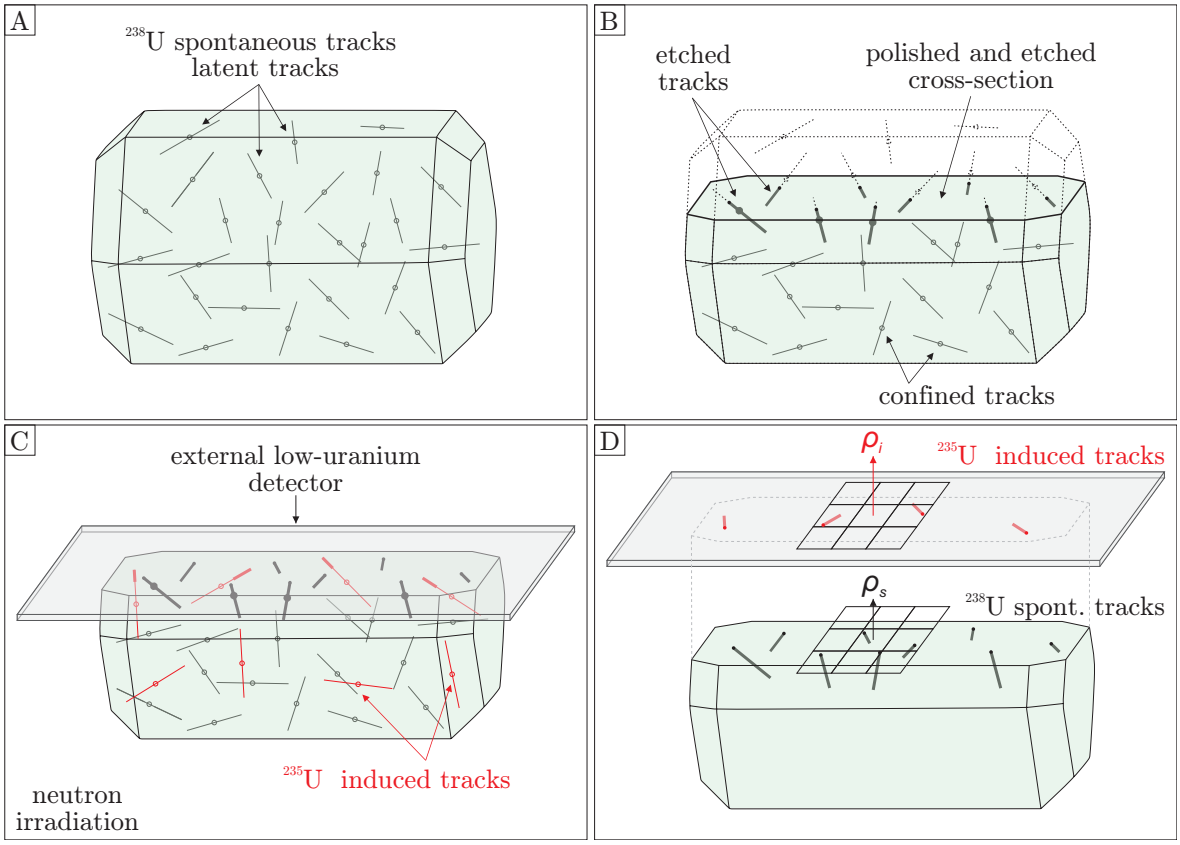

Figure 7 – Obtaining the D_t by the external detector method. A) Apatite crystal showing latent tracks due to spontaneous fission of ^{238}U. B) Revealing the fission tracks after poliching and etching procedures. C)Recording the amount of induced tracks using a external detector during neutrons irradiation in a nuclear reactor. D) Obtaining ρ_s and ρ_i using a square grid. Modified from Galbraith (2005).

The reformulation of equation (2.3) to EDM is given by:

$$t = \frac{1}{\lambda_d}\, ln\left(1 + \frac{\lambda_d}{\lambda_f}\,\frac{\rho_s}{\rho_i}\,\Phi\sigma I\right) \tag{2.5}$$

where Φ is the thermal neutron fluency in cm^{-2}, σ is the cross-section for induced fission of ^{235}U ($\sigma = 580.2\times10^{-24} cm^2$)(Hanna et al., 1969), and I is the isotopic ratio ^{235}U/^{238}U ($I = 7.25\times10^{-3}$) (Steiger and Jäger, 1977).

Since FT dating is based on relatively small number of fissioned uranium atoms in comparison to other methods based on the measurements of many ions on a mass spectrometer, FTA has very low analytical precision in contrast to other conventional geochronology methods. Besides that, the fact that some parameters of FT dating are measured manually (e.g., ρ_s, ρ_i) caused serious criticism by the geochronology community regarding the confidence of results from different workers and laboratories. Thus, after the Pisa Workshop in 1980, it was recommended a series of protocols, in agreement with IUGS Subcommission on Geochronology, to solve the calibration issue and other questions including methodological and statistical approaches. Other important discussed topics were the significance of annealing process to reveal thermal

history and the establishment of the ^{238}U spontaneous fission decay constant λ_f. After that, the thermochronological community has put great effort to define a calibration factor, ζ, yielding interlaboratory results to be compared and reproducible (Hurford and Green, 1982, 1983; Cogné et al., 2020). The reformulation of equation (2.5) to introduce the ζ-calibration factor is given by:

$$t = \frac{1}{\lambda_d} ln \left(1 + \lambda_d \zeta g \rho_d \frac{\rho_s}{\rho_i}\right) \tag{2.6}$$

where g is the geometry factor for spontaneous fission track registration (~ 0.5), ρ_d is the density of the induced fission tracks in a known uranium-bearing dosimeter. The ζ factor is determined empirically by analysing a set of samples of known ages.

As we can see, this new formulation brought several improvements to the FT dating method. Parameters such as λ_f and Φ, which are extremely difficult to be measured, imposing a big obstacle for FTA. The advent of the ζ factor came up to overcome most of those barriers.

Another improvement was the possibility of calculating the single-grain ages and their respective uncertainties. The symmetrical error σ_i for single grain FT dating using the EDM is given by:

$$\sigma_i = \left[\frac{1}{N_{s,i}} + \frac{1}{N_{i,i}} + \frac{1}{N_d} + \left(\frac{\sigma_\zeta}{\zeta}\right)^2\right]^{\frac{1}{2}} \tag{2.7}$$

where $N_{s,i}$ is the number of spontaneous tracks counted over area, $N_{i,i}$ is the number of induced tracks counted over area, N_d is the total of induced tracks to determine ρ_d (Donelick et al., 2005).

2.4 Fission track annealing and thermal sensitivity

Besides the FT density, another powerful subject in FTA is the FT length distribution. Observation in laboratory and geological environment (i.e. field) have shown that FTs shorten under specific temperature range (Fleischer et al., 1965a). For example, FTs in apatite start to decrease in size if heated above ~60 °C and completely disappear at temperatures higher than ~120 °C.

This thermal sensitivity is called annealing and, in terms of cooling, the concept is similar to the 'closure temperatures' for other isotopic methods (i.e. retention temperature of the daughter product; Dodson, 1973). However, the significance of closing temperature has to be used carefully in FTA since temperature can influence the FT density causing serious implications on FT age interpretation. Empirical procedures have shown that apatite and zircon demonstrate annealing anisotropy. Factors such as chemical composition and orientation of the FT in relation to the mineral crystallographic axis can influence how 'easy' or 'difficult' the lattice damage anneals.

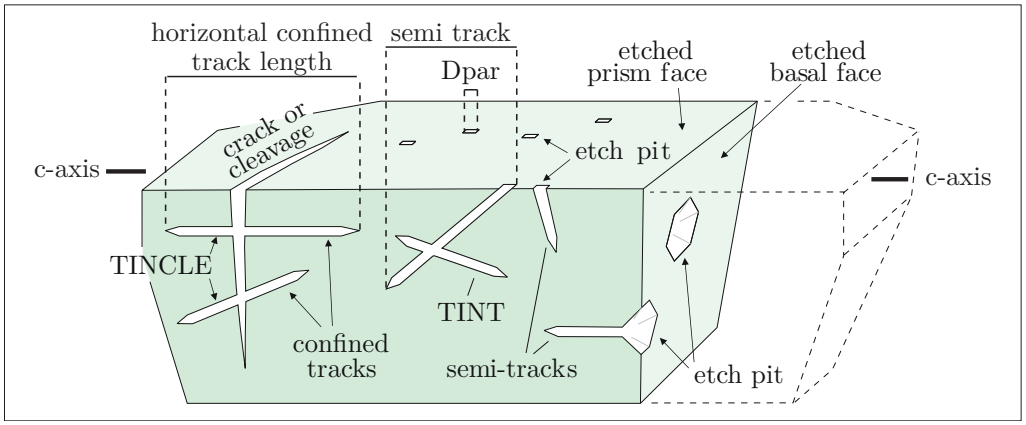

Figure 8 – Schematic diagram illustrating some elements of an apatite crystal regarding counting fission tracks under a microscope. Modified from (Hurford, 2019)

As firstly suspected by Gleadow and Duddy (1981), the content of Cl and F would substantially affect annealing properties in apatite (Green et al., 1985). F- and OH-apatites appear to be more susceptible to annealing, while Cl-apatites are more resistant (Carlson et al., 1999; Ravenhurst et al., 2003; Spiegel et al., 2007). However, rates of annealing vary widely and a useful correlation between annealing and composition remains poorly determined. Alternatively, researches have correlated the annealing kinetics to etch figure diameter parallel to the c-axis (D_{par}). Great D_{par} values correspond to resistance to annealing and vice-versa (Donelick et al., 2005).

Annealing kinetics also varies according the crystallographic orientation (Green and Durrani, 1977; Green, 1981; Laslett et al., 1984; Crowley et al., 1991; Donelick, 1991; Ravenhurst et al., 2003). In apatite, for example, tracks parallel to the crystallographic c-axis are more resistant, while tracks perpendicular to c-axis anneals easily. Thus, concerned to improve the measurement issues, some authors propose c-axis projection model that estimates the length a track would have if it was formed parallel to the c-axis (e.g., Carlson et al., 1999; Donelick et al., 1999; Barbarand et al., 2003; Ketcham, 2003; Ketcham et al., 2007; Jonckheere et al., 2019; Tamer et al., 2019; Tamer and Ketcham, 2020). However, some authors believe that c-axis correction is not effective since it would interfere with the length anisotropy erasing part of the thermal history information (e.g. Galbraith, 2002).

Horizontal confined tracks are preferred in FT length analysis because they are full length (i.e. both track ends are preserved from polishing) and they show their true 2D-projection dimension (Figure 8). Some common criteria to identify horizontal confined tracks are: tracks giving a bright reflection and track in full focus (Galbraith, 2005). In contrast to the semi-tracks (i.e. tracks that intersect the polishing surface and are used to calculate the FT density), the confined tracks are etched because they cross some feature which allows a pathway for the etchant such as a semi-track, a crack, or a cleavage plane. Tracks intersecting another track are called ‘TINTs’ (track-in-track) and tracks crossing a cleavage plane are the ‘TINCLEs’

(track-in-cleavage)(Lal et al., 1969).

2.4.1 Modeling thermal histories

Because FTs are formed continuously throughout time and the annealing process occurs gradually, the AFT age can be combined with track length distribution to investigate the thermal history of rocks and minerals (Fleischer et al., 1975; Gleadow and Duddy, 1981; Green et al., 1986; Laslett et al., 1987).

Due to the number of possible solutions to a given observed data (i.e., fission-track length distribution), solving thermal histories from FTA is better treated as an inversion problem (Gallagher, 2012). Furthermore, due to the complexity of the issue (i.e. complex misfit objective function; Sambridge and Mosegaard, 2002), it cannot be properly solved by conventional inversion procedures (e.g., partial derivatives, matrix inversion; Gallagher et al., 1991; Gallagher and Sambridge, 1994). Thus, as an alternative, stochastic sampling methods have been widely applied to infer time-temperature paths of rocks and minerals, such as, Monte Carlo (Lutz and Omar, 1991; Gallagher, 1995, 2012), genetic algorithms (Gallagher, 1995) and, random search (Willett, 1997).

2.4.2 The Bayesian transdimensional Markov Chain Monte Carlo approach

In this work, we use the Bayesian transdimensional Markov Chain Monte Carlo approach introduced by Gallagher (2012). Instead of looking for the best single solution, the Bayesian framework is concerned to find the most probable thermal history defined by a set of joint models known as posterior probability density function (i.e. posterior ‘pdf’). As a starting clue, the method requires some prior information which can include some thermal history constraints and other additional information known about the sample (e.g., AFT age, stratigraphic age, annealing model). This information will define the temperature-time model space (i.e. prior ‘pdf’) over which to search.

Basically, the procedure consists of (i) sampling the model space, (ii) solving the forward model for a given thermal history (i.e. proposed model), and (iii) calculating the misfit (i.e. likelihood function). Following the Markov chain idea, the proposed model is rejected, or not, based on an acceptance criterion. If accepted, the proposed model becomes the current model, which will be re-sampled (perturbed) in the next loop. This perturbation is ruled by the Monte Carlo approach where a random number is generated and used to change the parameters of the current model. The process is repeated many times and all the accepted models are collected to compose a posterior distribution. The final product is a joint of accepted thermal histories rather than a single model.

Among the output models, we mainly consider three representative models, the maximum likelihood model, the maximum posterior model, and the expected model. The first is the model that best fits the data, even though it is often relatively complex. The second is the model with maximum probability which tries to balance fitting the data with keeping the model relatively simple. The third is a single weighted mean model, where the weighting is provided by the posterior probability for each model. Differently from the maximum likelihood and maximum posterior models, the expected models are not directly sampled from the posterior distribution.

To produce the proposed model, a series of possible transformations on the current model has to be defined by the user (e.g. to move a point in the model space). Based on the acceptance rates of proposed model parameters (being around 20-50$\%$) and the behavior of the parameter sampling chain (being stationary) it is possible to monitor the 'well behavior' of the inversion process over the iterations. A final check is made by examining the final model predictions.

3 The southeast Brazilian rifted continental margin is not a single, continuous upwarp: variations in morphology and denudation pattern along the continental drainage divide

Tobias Maia Rabelo Fonte-Boa[a*]; Daniel Peifer[a]; Ana Carolina Fonseca[b]; Tiago Amâncio Novo[a]

[a] Geology post-graduation program, Institute of Geosciences, Federal University of Minas Gerais, 6627 Antônio Carlos Avenue, Belo Horizonte, MG 31270-901, Brazil.
*Corresponding author: tobiasfonteboa@gmail.com
[b] Department of Geology, Ghent University, Ghent, Belgium.

Abstract

Rifted continental margins (RCM) are large-scale features of Earth's surface that show substantial morphological variations. However, geoscientists have been mostly focused on studying the classical escarpment feature, while there is a lack of studies on other morphologies that characterizes this tectonic environment. The case of the Brazilian South Atlantic margin is not an exception. Most landscape evolution studies concentrate on the Serra do Mar escarpment system, while other segments with no escarpments have been partially neglected. Moreover, various authors assume the Brazilian elevated continental margin as a well-defined and continuous marginal upwarp instead of a diversified and more complex landscape. Here we debate this issue and explore how the first-order topographic forms and time-space denudation patterns differ along the Brazilian South Atlantic margin. We focus on the continental margin of southeast Brazil (CMSEB) that includes the Serra do Mar and Serra da Mantiqueira escarpment system and the adjacent northern segment known as Serra do Espinhaço and Serra do Caparaó, where the seaward-facing steep escarpment is absent. We show that, similar to other RCMs, the CMSEB presents a continental drainage divide separating two distinct regions with contrasting denudation patterns, (i) an inland continental interior, characterized by high elevation and relatively low relief with a predominance of AFT ages significantly older than South Atlantic rifting event, and (ii) a coastal region characterized by low elevations and high relief with the predominance AFT ages younger than the rifting. However, besides the differential denudation associated with the South Atlantic opening, the margin has experienced substantial post-rift exhumation attributed

to rock uplift triggered by the reactivation of inherited basement structures. The morphological differences between CMSEB's southern (Serra do Mar and Serra da Mantiqueira) and northern (Serra do Espinhaço and Serra do Caparaó) extensions reflect sectors with contrasting geomorphic evolution supporting the idea that the rifted Brazilian RCM is not a single and continuous tectonic setting. Finally, our findings indicate that tectonic inheritance strongly impacts the denudation pattern, which contributes to the geomorphic diversification along the Brazilian RCM.

Keywords: South Atlantic rifted continental margin evolution; continental drainage divide morphology; apatite fission track thermochronology; tectonic inheritance.

3.1 Introduction

The morphology of elevated rifted continental margins (RCM) is commonly defined by a steep sea-ward escarpment running parallel to the coast with more than 1 km of elevation, and separating an upland continental interior plateau with low relief from a medium to high relief coastal plain of varying width, with examples including southeastern Brazil, eastern Australia, southern Africa, and western India (Braun, 2018). Such high and steep topography is more reasonably explained in the context of active rifts than in mature 'passive' margins, and thus many authors have attempted to resolve its enigmatic persistence (e.g., Ollier, 1982; Gilchrist and Summerfield, 1990; van der Beek et al., 1995; Persano et al., 2002; Braun and van der Beek, 2004; Braun, 2018, 2019; Japsen et al., 2019). High relief in RCM has been attributed to the operation of thermo-mechanical processes in the lithosphere-asthenosphere interface capable of driving rock uplift long after the continental breakup, such as domal or dynamic uplift (e.g., Ruetenik et al., 2016), depth-dependent extension (e.g., Royden and Keen, 1980), secondary convection (e.g., Armitage et al., 2013; Sacek, 2017), lithospheric necking (e.g., Braun and Beaumont, 1989), denudational flexural-isostatic rebound (e.g., Gilchrist and Summerfield, 1990), and magmatic underplating (e.g., McKenzie, 1984). However, these factors are generally suggested as components of end-member scenarios that, nonetheless, do not fully address the intricate topographic evolution of one particular RCM or apply to all cases (Gallagher and Brown, 1997). To date, the evolution of rifted margins is generally agreed to involve a highly complex, multiphase process (Peron-Pinvidic et al., 2019).

Marginal upwarps on RCMs are significant large-scale features of Earth's surface. Their topographic configuration differs from high elevation domains flanked by wall-like escarpments (e.g., southern Africa, western India, and southeastern Australia) to low amplitude upwarps located at low elevations in settings such as eastern India, eastern Argentina, and southern Australia. However, even rifted margins characterized by the classic morphology of a sharp escarpment form, in reality, far more complex landscapes, where relief varies from one part to

another along their length of thousands of kilometers. In this situation, it is reasonable to assume that differing landscape histories likely explain substantial morphological variations along the length of a RCM, similar to consensual interpretations in vast mountain systems such as the Andes (e.g., Schildgen and Hoke, 2018). Nonetheless, the majority of empirical and numerical studies in these settings concentrated on the formation and evolution of 'Great Escarpments', and generic conceptual models of margin evolution (e.g., 'downwarp'; Ollier and Pain, 1997, 'scarp retreat'; Gilchrist et al., 1994, 'pinned divide or downwearing'; Kooi and Beaumont, 1994) were proposed to explain the long lifespan of such escarpments. In contrast, fewer studies explored links between lateral changes in relief and bedrock geology and the post-breakup evolution in RCM (e.g., Persano et al., 2006; Calegari et al., 2021; Codilean et al., 2021), even though some authors have highlighted that topography changes substantially along the extensive length of these settings (e.g., Gallagher et al., 1998; Persano et al., 2002; Bishop, 2007; Japsen et al., 2012; Braun, 2018).

In this contribution, we concentrate on investigating the landscape variability along the Brazilian elevated RCM by exploring quantitatively how first-order topographic forms and the pattern and chronology of the long-term denudation differs throughout the length of one such vast rifted setting extending for more than 3,000 km along the western South Atlantic coast. In this situation, it is symbolic that numerous studies show the Brazilian elevated-RCM as a single, well-defined and continuous continental margin upwarp (e.g., Summerfield, 1991; Matmon et al., 2002). Nevertheless, some authors emphasized significant morphological changes along the Brazilian coast (e.g., Jelinek et al., 2014; Braun, 2018; Calegari et al., 2021), although the precise ways through which topography and post-breakup denudation patterns differ spatially over the length of the Brazilian RCM remain to be evaluated. Here, we focus on the onshore segment related to Santos, Campos, and Espírito Santo offshore basins (Mohriak et al., 2008), which is referred to as the continental margin of southeast Brazil (CMSEB). We perform quantitative topographic analysis to define the marginal drainage divide and explore differences in topography between the inland and seaward-dipping sides of the divide along the Brazilian South Atlantic rifted margin. In addition, we take advantage of the large set of apatite fission track data available to explore variations in denudation patterns and the thermal evolution of the crust from the inland plateau to the continental water divide and up to the baselevel. We concentrate on differences in these inland-to-coast exhumation profiles over the margin's southern and northern extensions addressing interactions with potential controls such as the basement structural framework, lithological variability, and flexural strength of the lithosphere.

3.2 Geological setting

The study area is the continental margin of southeast Brazil (CMSEB), a continental-scale topographically pronounced terrain, roughly NE-SW trending, covering more than 1,000

km of the western South Atlantic rifted margin, between parallels 17°S and 27°S (Fig. 9). It comprises the onshore region adjacent to Santos, Campos, and Espírito Santo offshore basins that includes the Cenozoic Rift System of Southeastern Brazil (Riccomini et al., 2004; Zalán and Oliveira, 2005). The complex evolution of the CMSEB has been addressed by numerous studies using different methods, such as stratigraphic analysis (e.g., Chang et al., 1992; Mello et al., 1999; Riccomini et al., 2004; Negrão et al., 2020), structural geology (e.g., Calegari et al., 2016, 2021), geophysics (e.g., Zalán and Oliveira, 2005; Mohriak et al., 2008; Cogné et al., 2013; Stanton et al., 2021), geomorphology (e.g., Salgado et al., 2016; Souza et al., 2019; Souza et al., 2021), and thermochronology (e.g., Gallagher et al., 1994; Cogné et al., 2011, 2012; Jelinek et al., 2014). Nevertheless, our knowledge of its geological history is incomplete. In the sequence, we summarize common interpretations about the establishment and tectonic evolution of the CMSEB, emphasizing the amalgamation and subsequent fragmentation of West Gondwana.

3.2.1 West Gondwana assembly and bedrock tectonic evolution

The bedrock of CMSEB resulted from successive tectonic cycles that culminated in the amalgamation of West Gondwana during the Early Paleozoic (Fig. 10A). This orogenic event, commonly referred to as the Pan-African/Brasiliano orogenic cycle, was characterized by diachronous accretion of multiple terranes during the Neoproterozoic–Cambrian (Pedrosa-Soares et al., 2001; Cordani et al., 2003; Alkmim et al., 2006; Pedrosa-Soares et al., 2008; Heilbron et al., 2010). In general, these terranes comprise several associations of Paleoproterozoic–Archean basement blocks and Mesoproterozoic–Neoproterozoic supracrustal sequences, mostly intruded by Neoproterozoic granitic rocks (i.e., magmatic arcs). The study area includes the Southern Brasília belt, the Araçuaí-Ribeira belt system, and the southern portion of the São Francisco craton (Fig. 10B).

The São Francisco craton designates an area of the São Francisco-Congo paleocontienent that was not profoundly affected by the Pan-African/Brasiliano orogenic cycle (Heilbron et al., 2017). The CMSEB includes the sector of the São Francisco-Congo paleocontinent composed of Archean TTG-type granitoid nuclei (the Belo Horizonte and Guanhães units in Fig. 10C) encompassed by several metamorphic complexes resulting from tectonic events during the Rhyacian–Orosirian (ca. 2.1–2.0 Ga; Noce et al., 2007). Essentially, these metamorphic complexes comprise the following: a granite-greenstone belt occurring in the Quadrilátero Ferrífero region (the Mineiro belt unit), an intra-oceanic arc (the Juiz de Fora unit), and an arc-related active continental margin (the Mantiqueira unit; Ávila et al., 2010; Bruno et al., 2020; Araujo et al., 2021). In addition, several metasedimentary associations (e.g., calcissilicatic rocks, mica schists, paragneisses, quartzites, and paraconglomerates) occur along the São Francisco craton boundary related to the continental margin environment that surrounded the São Francisco paleocontinent during the Mesoproterozoic (the quartzose rocks in Fig. 10C).

The southern sector of the Brasília belt resulted from the consumption of a large oceanic

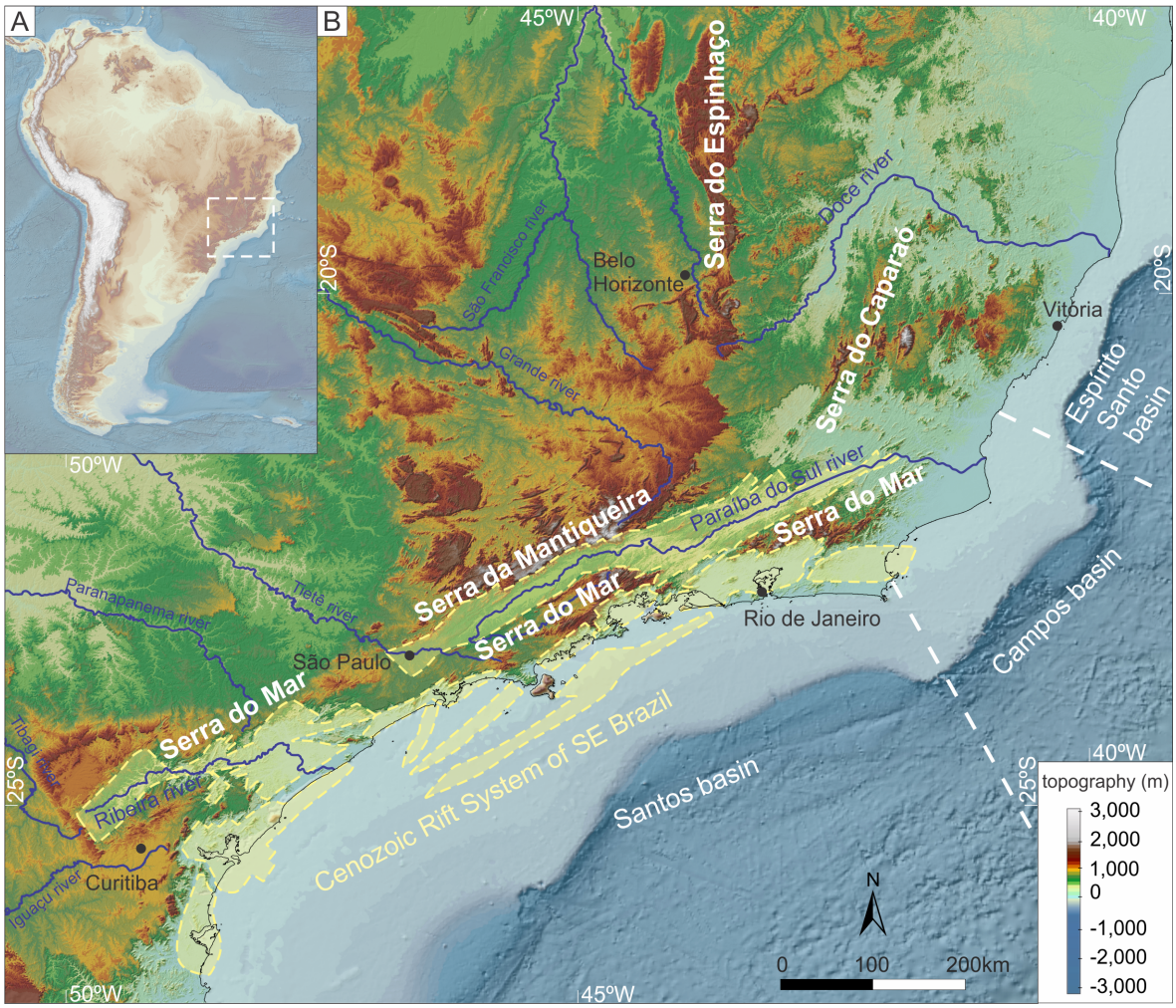

Figure 9 – **Topographic configuration of the continental margin of southeast Brazil (CMSEB)**. A) Location of the study area in the context of South America. B) Elevation map of the continental margin of SE Brazil showing the main rivers, the twin range system, and the offshore sedimentary basins. The onshore digital elevation model is derived from COP30 DEM, and the offshore digital elevation model was obtained from topex global 1-minute grids https://topex.ucsd.edu/cgi-bin/get_data.cgi. The highlighted yellowish region delimits the Cenozoic Rift System of Southeastern Brazil, according to Zalán and Oliveira (2005).

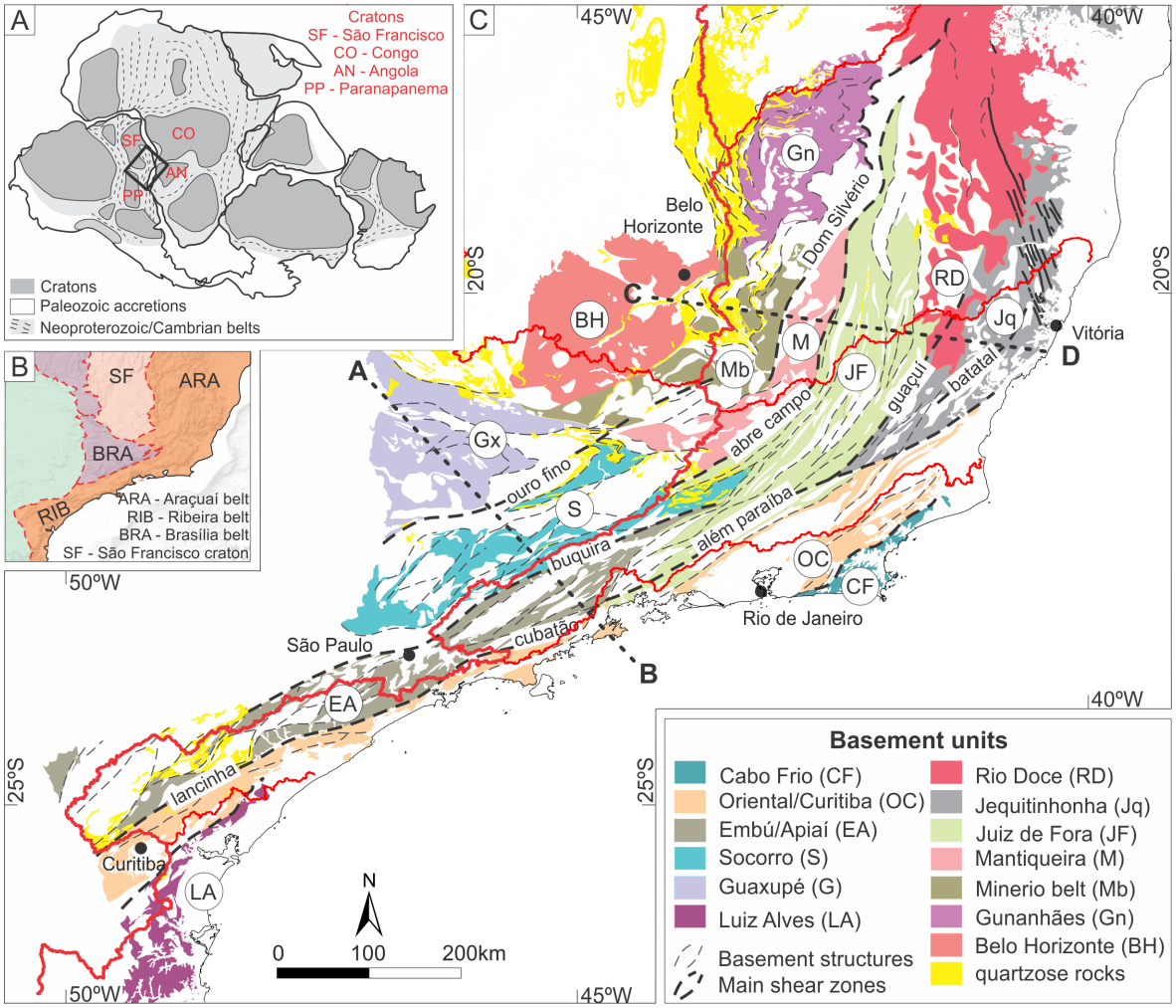

Figure 10 – **The basement bedrock geology of the CMSEB**. A) Reconstruction of Gondwana, after Schmitt et al. (2018). B) Tectonic provinces in the CMSEB setting. C) Simplified geologic map showing the main tectonic structures and basement units, based on Trouw et al. (2000); Heilbron et al. (2004, 2008). We explore fission track data along the representative transects A-B and C-D. These profiles traverse the bedrock geology and tectonic structures of the CMSEB (see Figs. 18 and 19).

slab due to the convergence of the Paranapanema paleocontinent towards the western margin of the São Francisco paleocontinent during the Neoproterozoic (Reno et al., 2009). The collision produced a stack of flat-lying nappes verging to the east (the Guaxupé unit). As a result, an interference zone (the Socorro unit), that is characterized by superposed structures with contrasting vergence, marks the transition between the southern sector of the Brasília belt and the Araçuaí-Ribeira belt system (Trouw et al., 2013).

The Araçuaí-Ribeira belt system comprises the northern extension of the Mantiqueira Province (Almeida et al., 1981). The Ribeira sector (southern Araçuaí-Ribeira belt) results from the protracted consumption of the Neoproterozoic Adamastor ocean by accretion of Archean/Paleoproterozoic terranes (the Luiz Alves unit), arc terranes (the Occidental/Curitiba and Embú/Apiaí units), and small plates (the Cabo Frio unit) across the southern and southeastern

sectors of the São Francisco paleocontinent (Heilbron et al., 2010; Caxito et al., 2021). Differently from the Ribeira sector, the Araçuaí sector comprises a confined orogen involving intense granitic production (the Rio Doce unit) and arc-related settings (the Jequitinhonha unit) (Pedrosa-Soares et al., 2011). In the Araçuaí-Ribeira belt system, the major tectonic framework consists of a series of anastomosed sub-vertical shear zones that extend over hundreds of kilometers and outline the basement units (Fig. 10C). These structures configure significant lithospheric discontinuities (e.g., the Dom Silvério shear zone as the suture zone of the Araçuaí orogen; (Alkmim et al., 2006) that are susceptible to successive reactivations (e.g., Fontainha et al., 2021). In the south, the primary orientation of the main structures is SW-NE, while in the north, the primary trend is S-N (Silva et al., 2009; Egydio-Silva et al., 2018).

During the Paleozoic, the Pan-African/Brasiliano orogenic cycle was completed, and the West Gondwana was consolidated as a supercontinent (Schmitt et al., 2018). Thus, what is currently the CMSEB region was located, at this time, in the relatively stable continental interior of this continent (Fig. 10A). Nevertheless, from the Early Ordovician to Middle Permian, the Famatian and Gondwanic orogenic cycles occurred in the southwestern margin of West Gondwana, inducing long-wavelength denudation in the continental interior and sediment accumulation in the Paraná basin (Milani and Thomaz Filho, 2000, Fig. 11)).

3.2.2 West Gondwana fragmentation and the establishment of the CMSEB

The West Gondwana breakup and the following opening of the South Atlantic Ocean took place during the Early Cretaceous (138 Ma; Pérez-Díaz and Eagles, 2014), with the ocean spread propagating from south to north. The extension and crustal thinning of the newly-formed South Atlantic continental margin coincided with the eruption of the massive and widespread continental flood basalts of the Paraná LIP (Janasi et al., 2011).

Based on the sedimentary records of the Santos, Campos, and Espírito Santo offshore basins, the first stages of the rifting process are generally interpreted as associated with strong tectonic subsidence and the development of intra-continental rifts filled with fluvial, lacustrine and alluvial fan sediments (França et al., 2007; Moreira et al., 2007; Winter et al., 2007). The inherited tectonic framework of the basement controlled rifting structures (Mohriak et al., 2008). In addition, the presence of Early Cretaceous volcanoclastic rocks, which comprise the primary basement-bedrock type of the Santos and Campos basins (Fig. 12), suggests an intense magmatic activity during the continental breakup. In turn, Aptian/Albian evaporites mark the transition from a continental to a shallow-marine environment, representing thus the end of tectonic subsidence and the predominance of thermal subsidence (Mohriak et al., 2008). In the Late Cretaceous, the increment of thermal subsidence led to a typical drift marine transgression with the deposition of deep marine siliciclastic sediments over the Aptian carbonate platforms (Fig. 12).

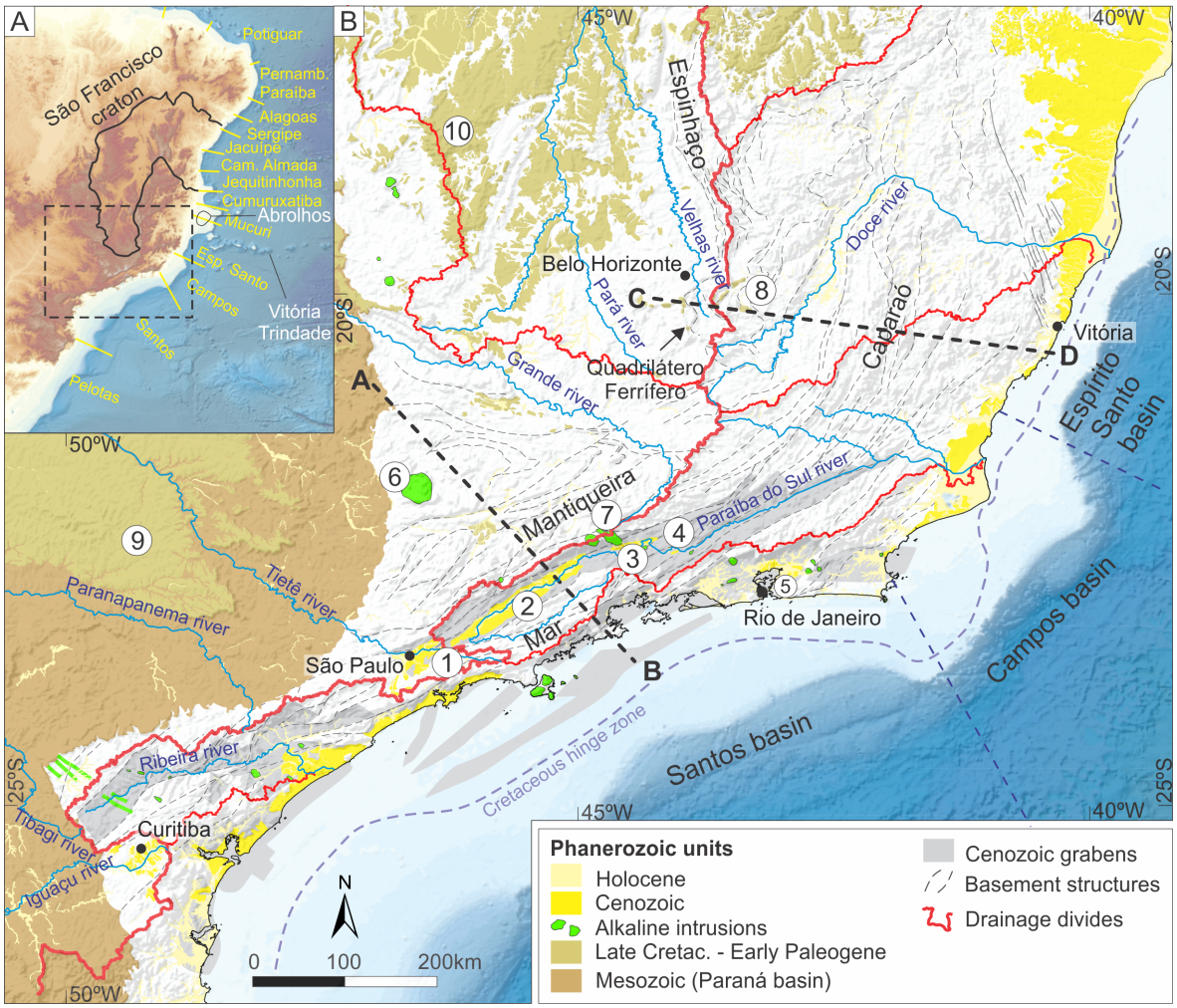

Figure 11 – **The phanerozoic units of CMSEB**. A) Geographical context of the study area emphasizes the offshore basins' limits, the São Francisco craton (SF) limit, the Abrolhos bank, and Vitória-Trindade seamounts. B) Simplified geologic map showing the main Phanerozoic units, including the Cenozoic rift system of SE Brazil according to Zalán and Oliveira (2005), the main bodies of the Serra do Mar igneous province after Thompson et al. (1998), the basins of the Continental Rift of Southeastern Brazil after Riccomini et al. (2004). (1) São Paulo basin; (2) Taubaté basin; (3) Resende basin; (4) Volta Redonda basin; (5) Guanabara graben; (6) Poços de Caldas massif; (7) Passa Quatro and Itatiaia massifs; (8) Fonseca and Gandarela basisn; (9) Bauru basin; (10) Sanfranciscana basin. Note that transects A-B and C-D traverse phanerozoic units of CMSEB (see Figs. 18 and 19).

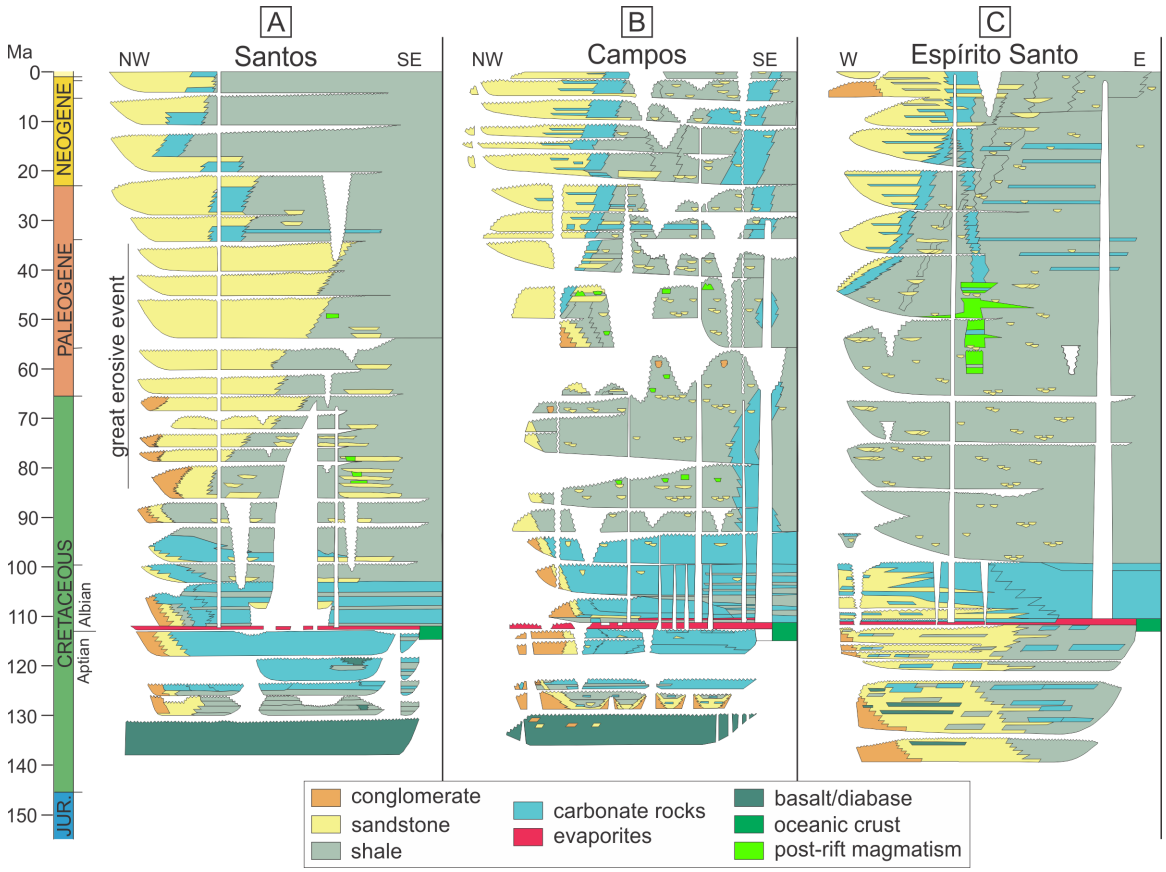

Figure 12 – **Simplified stratigraphic chart of A) Santos basin; B) Campos basin; C) Espírito Santo basin**. Modified from Moreira et al. (2007), Winter et al. (2007), and França et al. (2007).

The offshore and onshore geological records suggest that the post-rift evolution of the southeast Brazilian passive margin was unsteady in space and time, involving volcanism, variations in erosion rates, sediment influx, and topographic rejuvenation long after continental rupture (Mohriak et al., 2008). For instance, a Late Cretaceous to Paleogene magmatic pulse is recorded at the Santos basin (ca. 85.8 Ma; Moreira et al., 2007; Winter et al., 2007), and onshore at the Serra do Mar igneous province (ca. 85 to 55 Ma; Thompson et al., 1998). Simultaneously, the reactivation of basement structures in the Paleogene resulted in the development of a series of NE-SW-trending intra-continental depocenters (e.g., Resende and Volta Redonda basins; Negrão et al., 2020). The Serra do Mar and Serra da Mantiqueira uplifts are also commonly hypothesized as resulting from these reactivations (e.g., Continental Rift of Southeastern Brazil; Riccomini et al., 2004); Fig. 11B). Concomitantly, a major erosive event in the form of a massive clastic progradation is often attributed to an increment in subsidence rates recorded in the Santos basin during the Late Cretaceous and Paleogene (Fig. 12A) (Moreira et al., 2007; Mohriak et al., 2008).

Based on these tectono-magmatic constraints, the post-rift reactivation of the CMSEB has been often interpreted as associated with the drifting of the South American plate over the Trindade mantle plume (Thompson et al., 1998), resulting in regional uplift and arching of the

lithosphere with posterior extensional collapse (e.g., Zalán and Oliveira, 2005). Different views assume that Meso-Cenozoic magmatic activity was associated with the accommodation of rifting-related stresses in the lithosphere and delamination of the subcontinental lithospheric mantle (Ernesto et al., 2002). Furthermore, several authors attributed the post-rift tectonic manifestation along CMSEB to far-field compressional stresses transmitted from Andean orogenic pulses likely combined with the mid-Atlantic ridge push (e.g. Riccomini and Assumpção, 1999).

The continental interior of the South Atlantic platform also records Late Mesozoic-Cenozoic tectonic activity which is generally attributed to the intense tectonic restructuring of the South Atlantic platform after the continental breakup (Batezelli and Ladeira, 2016). In addition, the development of post-rift chrono-correlated intracontinental continental-scale depocenters is also associated with retroarc-foreland systems in response to Andean orogenic events (e.g., Bauru and Sanfransiscana basins; Batezelli and Ladeira, 2016; Menegazzo et al., 2016). In the region of Serra do Mar, the Cenozoic Rift System of Southeastern Brazil and the Cenozoic sedimentary successions undoubtedly record the post-rift tectonic activity, in contrast with the continental sector adjacent to Espírito Santo basin, where similar empirical Cenozoic constraints are scarce. The region of Quadrilátero Ferrífero shows post-rift chrono-correlated (i.e., Cenozoic) continental basins associated with brittle deformation (e.g., Fonseca and Gandarela basins, and Doce river middle valley lake system; Sant'Anna et al., 1997; Mello et al., 1999), however these occurrences are very thin and localized. Therefore, there is no consensus about the magnitude and significance of this geological record in the context of the tectonic evolution of the CMSEB. Furthermore, despite the magmatic pulse recorded offshore (Abrolhos and Vitória-Trindade seamonts, ca. 59 to 37 Ma; França et al., 2007; Stanton et al., 2021), the related-onshore region lacks evidence for the post-rift magmatic activity.

3.3 Existing apatite fission track data

Over the last three decades, more than 35 AFT thermochronology studies were conducted in the CMSEB, amounting to more than 500 individual samples (Fig. 13 and Appendix A.1.1, for a review see (Novo et al., 2021). A significant portion of these empirical studies focused on exploring the tectonic evolution of the Serra do Mar escarpment and its correlation with the post-rift history of the Brazilian South Atlantic passive continental margin (e.g., Tello Saenz et al., 2003; Hackspacher et al., 2004; Hiruma et al., 2010; Cogné et al., 2011, 2012; Gezatt et al., 2021). Other recurrent objectives in these studies include the investigation of the alkaline intrusions and their role during the post-rift tectonic evolution and establishment of the South Atlantic platform (e.g., Amaral et al., 1997; Franco et al., 2005; Soares et al., 2016), as well as the thermo-tectonic evolution of the Santos and Campos offshore sedimentary basins and their expressive hydrocarbon related-reservoirs oil maturation (e.g., Engelmann de Oliveira et al., 2016, 2018). This context explains the substantial concentration of AFT samples (more than 300

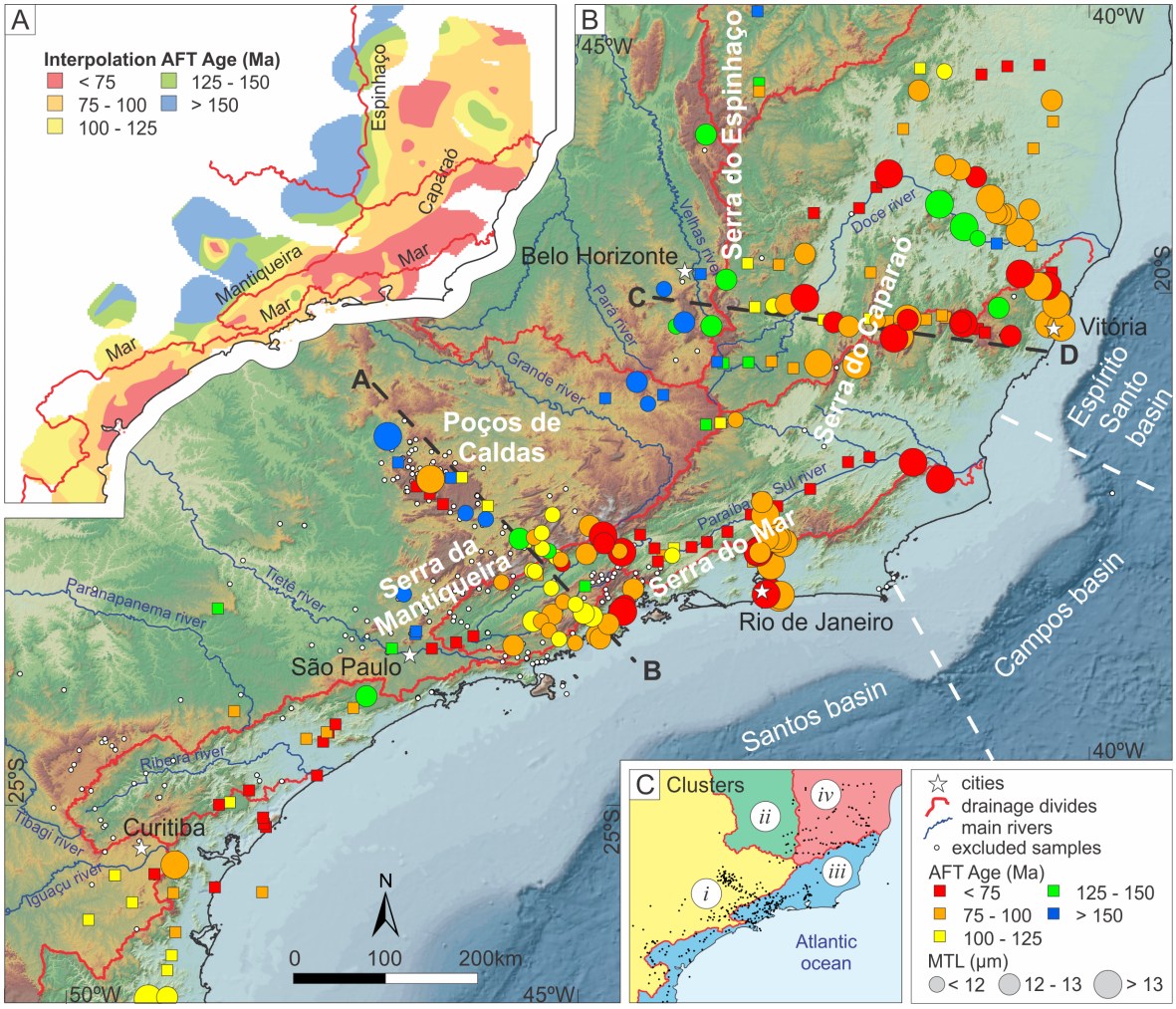

Figure 13 – **Available AFT data for the CMSEB**. A) AFT age interpolation (natural neighbor). B) AFT age distribution according to our compilation criteria (see Methods). Squares represent samples that passed in the age but not the MTL criterion, while circles represent samples that passed in both age and MTL criteria. Small white dots represent criterion-excluded samples. C) AFT samples clusters according to major drainage basins: (i) Paraná, (ii) São Francisco, (iii) Paraíba do Sul, and (iv) Doce. The abundance of fission track data along lines A-B and C-D allowed us to use them to produce two regional transects exploring along-profile variations in the long-term cooling path of the rocks (see Figs. 18 and 19).

samples) collected in the area extending from Poços de Caldas to the Serra do Mar (Fig. 13). Furthermore, the denudation history of the southernmost portion of the Serra do Mar was the target of several thermochronological studies (e.g., Gallagher et al., 1994; Karl et al., 2013; Krob et al., 2019). More recently, a few authors investigated AFT data collected in areas located more to the north of the CMSEB, including the area adjacent to the Espírito Santo basin (e.g., Jelinek et al., 2014; van Ranst et al., 2020) and inland settings within the Brazilian South Atlantic platform such as São Francisco craton and related Proterozoic mobile belts (e.g., Amaral-Santos et al., 2019; Fonseca et al., 2021).

The thermochronological data from CMSEB is generally interpreted as recording three

main cooling events, (i) Middle Paleozoic (ca. 350 Ma), (ii) Early Cretaceous, and (iii) Late Cretaceous-Early Paleogene. The Middle Paleozoic cooling event (ca. 350 Ma) is primarily recorded by samples collected inland, deep in the continental interior, and is referred to as the pre-rift phase (e.g., Jelinek et al., 2014). The authors generally associate this event with the Famatian and Gondwanic orogenic cycles affecting the southwestern margin of the Western Gondwana paleocontinent during the Ordovician to Permian (e.g., Amaral-Santos et al., 2019; Fonseca et al., 2021). These orogenic systems induced long-wavelength denudation and deposition cycles in the West Gondwana continental interior (e.g., the Paraná basin; (Milani and Thomaz Filho, 2000). The Early Cretaceous event is commonly interpreted as linked to the breakup of West Gondwana and the South Atlantic opening (138 Ma; Pérez-Díaz and Eagles, 2014). This event is mainly associated with an increment in exhumation rates due to the formation of a new erosional baselevel and the uplift and erosion of the rift-shoulders (e.g., Tello Saenz et al., 2003; Cogné et al., 2011, 2012; Jelinek et al., 2014).

The Late Cretaceous-Early Paleogene cooling event is widely attributed to the post-rift tectonic reactivation of the margin rather than the progressive and continuing exhumation of the coastal region (e.g. Cogné et al., 2012). To date, we have not fully understood the time interval, the drivers, the magnitude, and the spatial extent of this post-rift event. Nonetheless, various authors hypothesized multiple post-rift cooling pulses in different parts of the CMSEB, triggered by magmatic underplating (e.g., Hackspacher et al., 2004; Gallagher et al., 1994), mantle plume activity (e.g., Franco-Magalhaes et al., 2010, 2014), and, more commonly in the literature, intraplate-wide compressive stress transmitted from the Andean orogeny and the Atlantic spreading axis (e.g., Cogné et al., 2011, 2012; Jelinek et al., 2014; Amaral-Santos et al., 2019; van Ranst et al., 2020; Fonseca et al., 2021). Furthermore, some thermal models suggest an individual extra Neogene cooling episode interpreted as an increment in denudation rates resulting from either climate change (e.g. Jelinek et al., 2014) or a tectonic event in the Andes (e.g., Cogné et al., 2011, 2012; Engelmann de Oliveira et al., 2016). Finally, some stratigraphic and structural studies conducted in the Cenozoic continental basins (e.g., Riccomini et al., 2004; Cogné et al., 2013; Negrão et al., 2020) indicate multiple reactivation events, despite being poorly constrained by low-temperature thermochronology, highlighting the complexity of the post-rift evolution of the CMSEB.

3.4 Methods

The continental drainage divide that forms in rifted continental margins in response to the rift-related establishment of a new baselevel for continental erosion is a unique feature of their topographic configuration. This continental drainage divide, commonly extending over hundreds to thousands of kilometers parallel to the shoreline, separates seaward-dipping catchments with rivers flowing directly to the baselevel from inland catchments with rivers that flow far longer

distances, of thousands of kilometers, over the continental interior before reaching the distant baselevel. In addition, what has generally been assumed as a rift-related major escarpment on many occasions coincides spatially with the continental water divide or is located nearby in its seaward-dipping flank. Hence, there is a stark morphological contrast in rifted continental margins between the inland and seaward-dipping sides of the drainage divide. Because steep slopes amplify the efficiency of erosion, we commonly predict (and there is extensive empirical evidence of that; e.g. Wang and Willett, 2021), that the prominent escarpment, and consequently the continental water divide, retreats inland due to the significant differences in erosion between each side of the divide, with occasional river captures of inland areas. Therefore, the topographic configuration of rifted continental margins, especially the location of the main water divide and the escarpment and their interactions with potential controls such as lithological variability and flexural strength, are key elements in understanding the evolution of these settings (Braun, 2018).

To explore the post-rift evolution of the continental margin of southeastern Brazil (CMSEB), a continental-scale and geologically complex area, we combined topographic and thermochronological analysis to quantify the present-day position and geometry of the continental drainage divide as well as differences in morphology and denudation rates on either side of the divide. As the continental drainage divide in the CMSEB extends for more than one thousand kilometers, we concentrate on how topography and denudation patterns in either side of the divide vary along the entire length of the Brazilian South Atlantic continental water divide. We take advantage of the high AFT data density available for the CMSEB to explore the spatial distribution of AFT ages and mean track length data. We clustered these samples according to the four main river systems in the study area: the Paraná, the São Francisco, the Doce, and the Paraíba do Sul (Fig. 13C; note that the Doce and Paraíba do Sul AFT sample clusters also include samples collected in smaller neighboring river basins). In particular, the abundance of fission track data along lines A-B and C-D in Figs. 10, 11 and 12, allowed us to use an inverse modeling approach to produce two regional transects exploring variations in the thermal history of rocks from the inland plateau to the continental drainage divide and up to the coastal plain in the northern and southern parts of the CMSEB.

3.4.1 Topographic analysis

Following recommendations by Guth and Geoffroy (2021) and Purinton and Bookhagen (2021), we used a seamless Copernicus (COP30) digital elevation model (DEM) with a spatial resolution of 30 m to perform topographic analysis. The topographic data was downloaded from OpenTopography (`https://opentopography.org/`) and projected to South America Albers Equal Area Conic (ESRI:102033) with custom standard parallels because the study area covers three different UTM zones.

We used the COP30 DEM to extract the position and geometry of the continental drainage divide in the Brazilian South Atlantic continental margin. For achieving that, we employed the

DIVIDEobj algorithm implemented in TopoToolbox (Scherler and Schwanghart, 2020a,b) to extract all drainage divide segments in the study area in an objective and reproducible manner. Because the algorithm determines catchment boundaries from tributary junctions and drainage outlets where interfluves initiate or end (referred to as 'endpoints', Scherler and Schwanghart, 2020a,b), the resulting drainage divide segments depend on the initial extraction of the river network. In this situation, following standard pre-processing using carving routines, we extracted the hydrologically conditioned drainage network using a D8 algorithm employing a threshold upstream contributing area of 10 km^2 in TopoToolbox (Schwanghart and Scherler, 2014). We took advantage that the DIVIDEobj algorithm organizes and sort the divide segments in a tree-like network structure to define the continental drainage divide, and we computed the maximum along-divide distance from endpoints. The sorted drainage divide network by divide distance indicated the position of the continental water divide due to its higher values of divide distance compared to divide segments distributed in other areas. Thus, we used a 'selection by attributes' to extract the continental water divide. However, some interfluves other than the continental water divide also exhibited high values of divide distance, yet because such interfluves are separating coastal catchments from other coastal catchments instead of dividing inland from coastal river basins, we managed to identify the continental water divide reliably (see Fig. 14).

To explore how topography varies along the continental drainage divide and on each of its sides, we created complex swath profile objects in TopoToolbox that were defined using the sorted XY coordinates of all nodes of the drainage divide segments composing the main divide extracted using the DIVIDEobj algorithm. Each of these points (n = 365620) defined bends in swath objects, and thus we computed descriptive statistics for how the topographic metrics 'elevation' and 'local relief' varies along the continental divide considering a swath width of 30 km. Local relief is a topographic metric traditionally shown to be a reliable proxy for erosion rate (e.g., Ahnert, 1970; Montgomery and Brandon, 2002), and we used the localtopography algorithm in TopoToolbox to compute local relief as the maximum difference in elevation in a circular neighborhood with a diameter of 2 km. Given that an extreme asymmetry in relief defines an escarpment (Braun, 2018), we have chosen a reasonable window size that was adequately equipped to capture the locally (and laterally continuous) substantial difference in elevation associated with an escarpment (i.e., we have chosen a local relief window that was plausible and not too large. In addition, we also computed descriptive statistics on how local relief and elevation differ from the inland plateau to the continental drainage divide and up to the coastal plain over the entire CMSEB.

3.4.2 Fission track analysis

Apatite fission track (AFT) thermochronology is a method based on the accumulation of microscopic-trail-like radiation damage (i.e., the fission track) caused by the spontaneous fission decay of ^{238}U in apatite crystals. Apatite fission tracks are sensitive to temperature

(Fleischer et al., 1965a) and completely anneal at temperatures higher than 120°C, while the track annealing is minimal at temperatures lower than 60°C (Green et al., 1985). The temperature interval between 120 and 60°C is the boundary for fission track stability referred to as the partial annealing zone (PAZ), and within this temperature interval fission tracks shorten. Given that fission tracks are formed continuously throughout time and that the annealing process occurs gradually, one can explore the density of fission tracks (i.e., fission track age) combined with the length distribution of these fission tracks to investigate the thermal history of rocks and minerals (Gleadow and Duddy, 1981; Green et al., 1986; Laslett et al., 1987; Fleischer et al., 1975). Nonetheless, such thermal evolution recorded by fission tracks may reflect the movement of isotherms (e.g., the thermal anomaly of an igneous intrusion in the shallow crust) or the movement of rocks towards the surface due to denudation (Malusà and Fitzgerald, 2019a). Therefore, AFT is a widely used technique to evaluate the timing and rate of exhumation of continental passive margins (Wildman et al., 2019).

Constraining the timing and magnitude of rock uplift (or even surface uplift) using thermochronology data independently is challenging principally due to an absence of reasonable constraints on spatial and temporal variation of thermal reference frames (i.e., isotherms England and Molnar, 1990; Malusà and Fitzgerald, 2019a). This is a concern in this study as we estimated thermal histories from fission track data available for the CMSEB. However, the thermal state of onshore sectors of passive margins is generally considered relatively simple since these settings do not seem to be affected by rifting thermal processes (e.g., Gallagher et al., 1994). Therefore, we assumed a theoretical time-space fixed geothermal gradient, which is unrealistic and an important limitation to our study, yet the most reasonable choice. We take that into account when interpreting our results and their implications.

The large AFT dataset available for the CMSEB has been acquired following different protocols (see Appendix A.1.1). As such, we applied compilation criteria based on AFT age and the mean track length (MTL) to ensure that our analyzed AFT data are comparable and complete, excluding all samples that did not meet the standards. Regarding the AFT age, we compiled all samples analyzed employing the external detector method using the ζ calibration approach (Hurford and Green, 1983), and we excluded all samples with less than 15 apatite crystals analyzed or that have failed the chi-square homogeneity test (p(χ^2)>5%; Galbraith, 2005). For the MTL filter, we excluded samples with less than 70 track-length measurements. All samples in our compilation meet both the AFT age and MTL standards. Furthermore, we excluded all samples with missing information, such as, for example, samples where the method or p(χ^2) value has not been specified.

We employed the Bayesian transdimensional Markov Chain Monte Carlo approach introduced by Gallagher (2012) to estimate the thermal history of AFT samples collected in the study area. In this situation, we used the annealing model of Ketcham et al. (2007), which requires some kinetic parameters to produce the time-temperature models (e.g., D_{par}; Donelick

et al., 2005, crystal composition; Carlson et al., 1999). Following a similar approach reported by Wildman et al. (2015, 2017), we used a range in D_{par} values defined as 2.00 ±1.00 μm to produce thermal models when this information was not given in the literature. We performed the inversion algorithm for a minimum of 200,000 iterations after discarding an initial 50,000 iterations (Gallagher, 2012). These modeling results were monitored through the acceptance rates of proposal model parameters with parameter sampling being stationary as suggested by Gallagher (2012). Final models were represented by the predicted model and associated uncertainty measures (i.e., 95% credible intervals), thus defining the most representative model to the overall thermal history posterior collection. Each sample's prior information was set to the central age ± central age on time and 70 ±70 °C on temperature. The present-day temperature was set at 20 ±10 °C. All samples used for modeling are outcrop samples taken from the crystalline basement. Thus, except for the samples from the São Francisco craton area, we used an initial constraint of 550 ±50 Ma and 200 ±200 °C to account for the uncertainty in paleotemperatures of the sample during the last orogeny event. We exclusively employed samples with at least 20 analyzed crystals and 100 track-length measurements for our thermal modeling. Finally, samples located next to each other were modeled together.

3.5 Results

3.5.1 Macro-geomorphological characterization of the CMSEB

The continental drainage divide extends for more than 2,500 km over the CMSEB (Fig. 14). From its southern to its northern extension, the continental drainage divide (CDD) passes through several large-scale morphostructures of southeastern Brazil, including parts of the Serra do Mar, the Serra da Mantiqueira, the Quadrilátero Ferrífero, and the Serra do Espinhaço, in a laterally continuous manner. The Paraná and the São Francisco rivers compose the two major drainage systems draining the inland region from the CDD. In this situation, the Paraná River, which is, in fact, a tributary of one of the most extensive South American drainage systems, the Platine river basin, flows over nearly 4,000 km before reaching the distant baselevel, Atlantic Ocean, while the São Francisco River flows over nearly 3,000 km. In contrast, the seaward-draining area from the CDD comprises many relatively small river basins (n = 113) with a wide range of sizes, amongst which the Ribeira, Paraíba do Sul, and the Doce river basins are the largest. Furthermore, we also highlight, using white lines in Fig. 14, interfluves characterized by high values of divide distance that do not separate inland and coastal catchments. In particular, some of these interfluves are marked by high elevations, such as the Serra do Caparaó interfluve separating the Doce and Paraíba do Sul river basins (with a maximum elevation of 2,892 m), and the northeast extension of the Serra do Mar separating the Paraíba do Sul and Ribeira river basins (with a maximum elevation of 2,366 m).

Overall, the shoreline-to-the-CDD distance varies substantially along the length of the

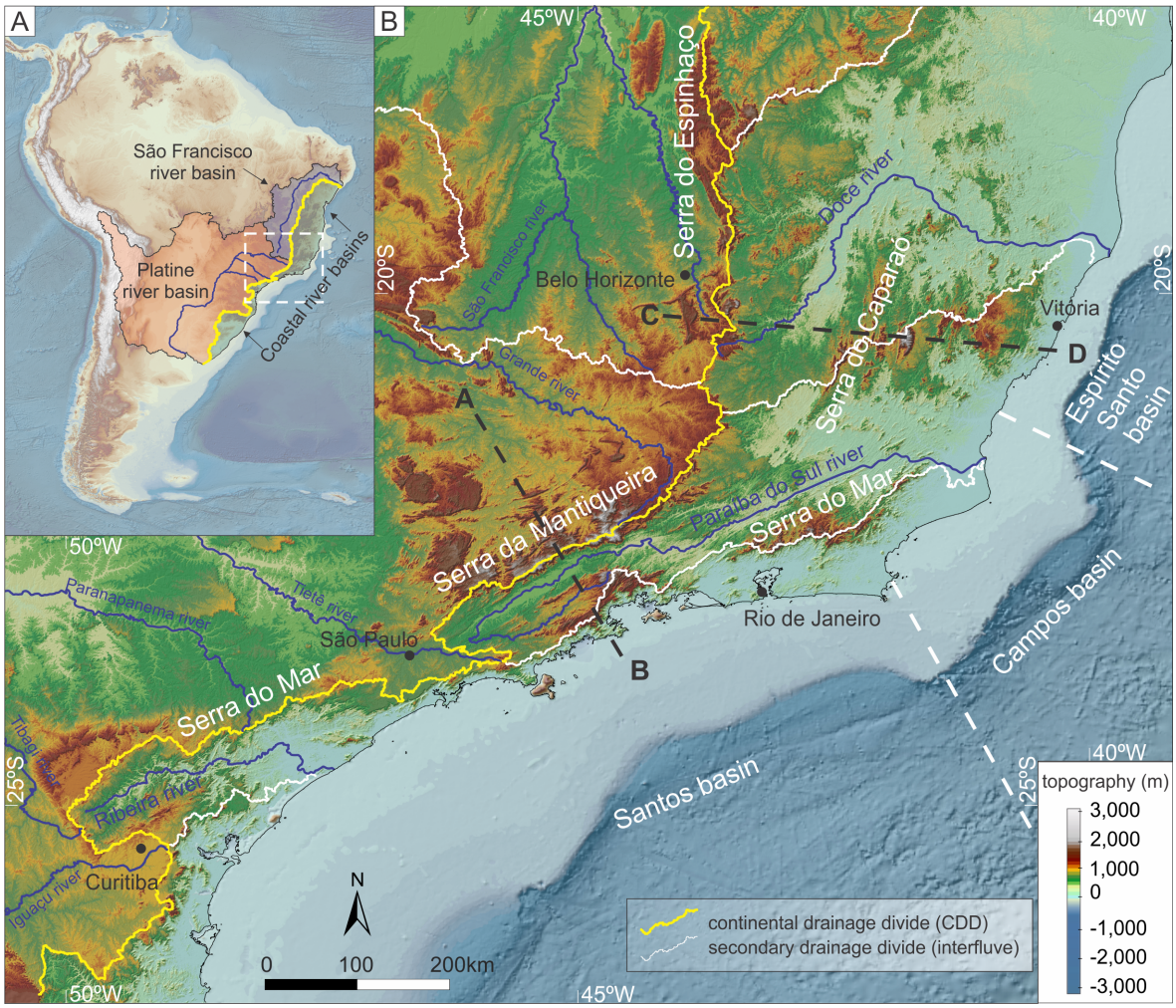

Figure 14 – **The first order drainage system of the CMSEB**. A) Location of the study area in a South American context indicating the macro-scale drainage configuration which is represented by two continental-scale interior drainage basins (Platine and São Francisco) and a group of smaller drainage basins grouped in the costal river basins. B) Topographic map of the study area showing the main rivers, range systems, main drainage divides, as well as the offshore sedimentary basins. Yellow continuous line indicates the continental drainage divide, and the white lines indicate the main interfluves, or secondary drainage divides that delimits the coastal and continental interior drainage basins. The topographic transects A-B and C-D cross cut the main macro-geomorphological elements of the CMSEB (see Figs. 18 and 19).

CDD, ranging from ca. 10 km to more than 400 km (Figs. 15 A and 15B). The southern CDD extension related to the Serra do Mar alternate segments that are positioned very close to the shoreline, such as nearby the city of São Paulo, where the CDD is ca. 10 km from the coast, with segments that are located more inland, such as in the Curitiba region, where the divide is located more than 150 km away from the baselevel. The CDD extension associated with the Serra da Mantiqueira is positioned roughly ca. 100 km inland, while in CDD's northern part, in the Serra do Espinhaço, the divide is located substantially deeper into the continental interior, in all cases more than 300 km away from the coast and, in the northernmost CMSEB, more than 400 km inland. We also find significant differences in the angular relationship between the CDD and the coastal interfluves (white lines in Fig. 14) along the margin. Specifically, the CDD and the coastal interfluves run roughly parallel in the area between the cities of Curitiba and Rio de Janeiro, whereas in areas north of the Serra da Mantiqueira, the CDD and coastal interfluves run roughly perpendicularly. We note that different parts of the same regional morphostructure in southern CMSEB, namely the Serra do Mar, constitute both CDD and coastal interfluve segments, such that the Serra do Mar coastal interfluve appears to be the continuation of the Serra do Mar CDD segment (Fig. 14).

The swath profile extending along the continental drainage divide indicates that relief varies significantly along the CDD, ranging from values lower than 200 m to higher than 2,200 m (Fig. 15B). We observe that CDD segments characterized by steep morphologies (i.e., range in elevation of more than 1 km over the swath profile) are substantially more frequent and laterally broader along the Serra do Mar and Serra da Mantiqueira CDD segments compared to the gentler morphology on either side of the Serra do Espinhaço CDD segment. Furthermore, steep escarpments along the Serra do Mar and Serra da Mantiqueira CDD segments frequently extend continuously for more than 200 km. In contrast, in the northern CMSEB along the Serra do Espinhaço CDD segment, steep escarpments are scarce and, where present, are spatially restricted to local occurrences.

We find that the areas surrounding the CDD (CD in Fig. 16) present high median values of elevation and local relief, the continental interior domain (CI in Fig. 16) show high median values of elevation and the lowest median values of local relief, and the coastal region (CR in Fig. 16) exhibits the lowest median values of elevation and the highest median values of local relief. Surprisingly, the high end of the distribution of elevation of the coastal region significantly surpasses that of the continental interior domain and is higher than what we observe for the areas surrounding the CDD (Figs. 16B and 16C). Such prominent areas of high elevation positioned seaward from the CDD comprise segments of the coastal interfluves separating the most extensive coastal river basins from each other (Figs. 14 and 15). The highest peaks in the CMSEB are part of such coastal interfluves, and, for example, the highest elevation occurs at the Serra do Caparaó (2,892 m; see swath profile C-D in Figs. 15A and B1 in appendix A.1.2), whereas maximum elevations along the CDD or in inland areas from the CDD rarely overcome 2,000 m.

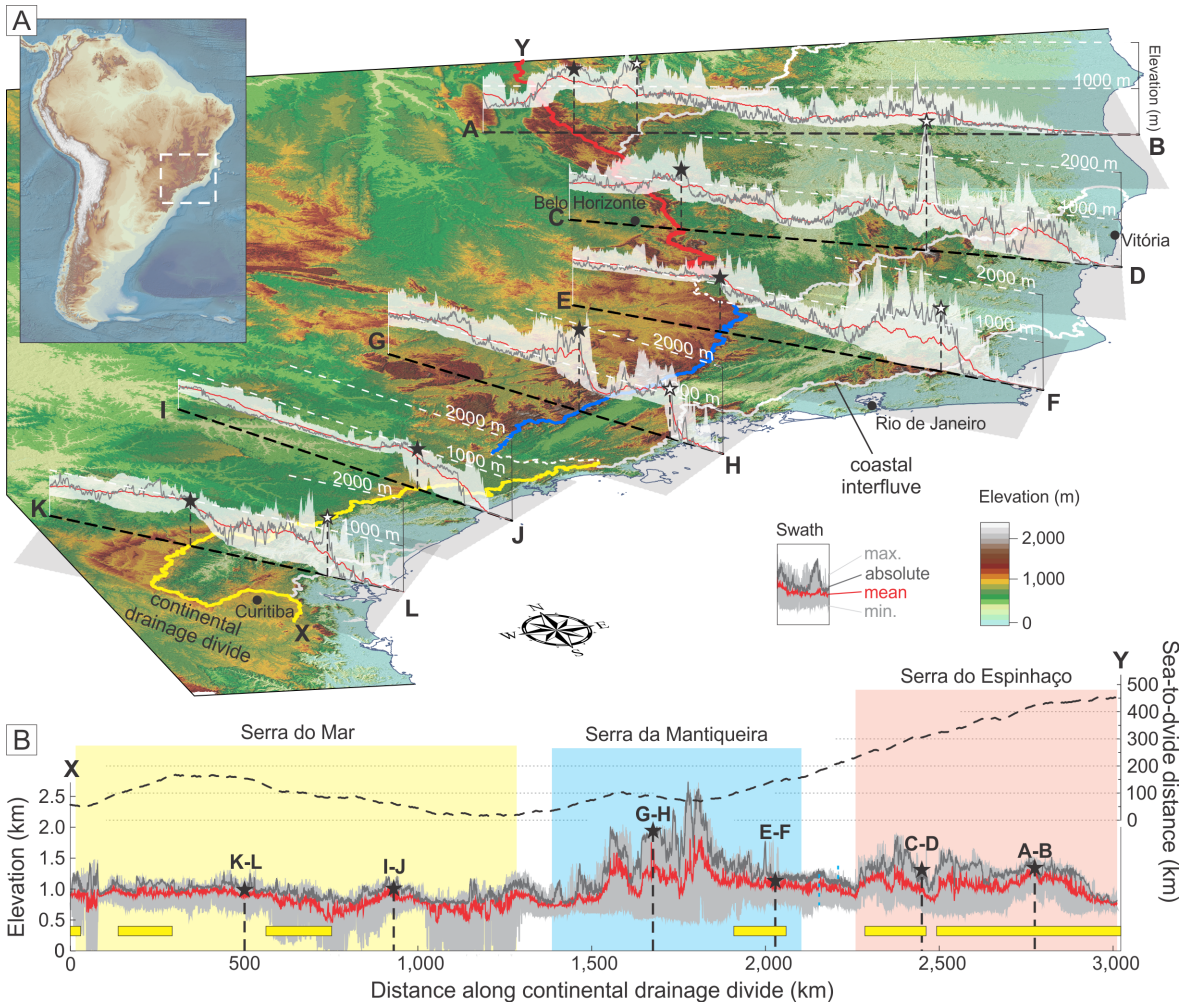

Figure 15 – **The geomorphic characterization of the CMSEB**. A) Series of swath profiles showing the lateral variations in the macro-geomorpholy along the CMSEB; B) Swath profile along continental divide (X-Y) including a plot showing the variation of the distance between the continental divide and the shoreline (black dashed line). The yellow rectangles indicate the segments of the continental divide with predominance of quartzose rocks. The black stars mark the intersection between the series of perpendicular-to-the-coast swaths and the continental divide, and the white stars spot the intersection between the swaths and the coastal interfluves. For more details see Fig. B1 in appendix A.1.2.

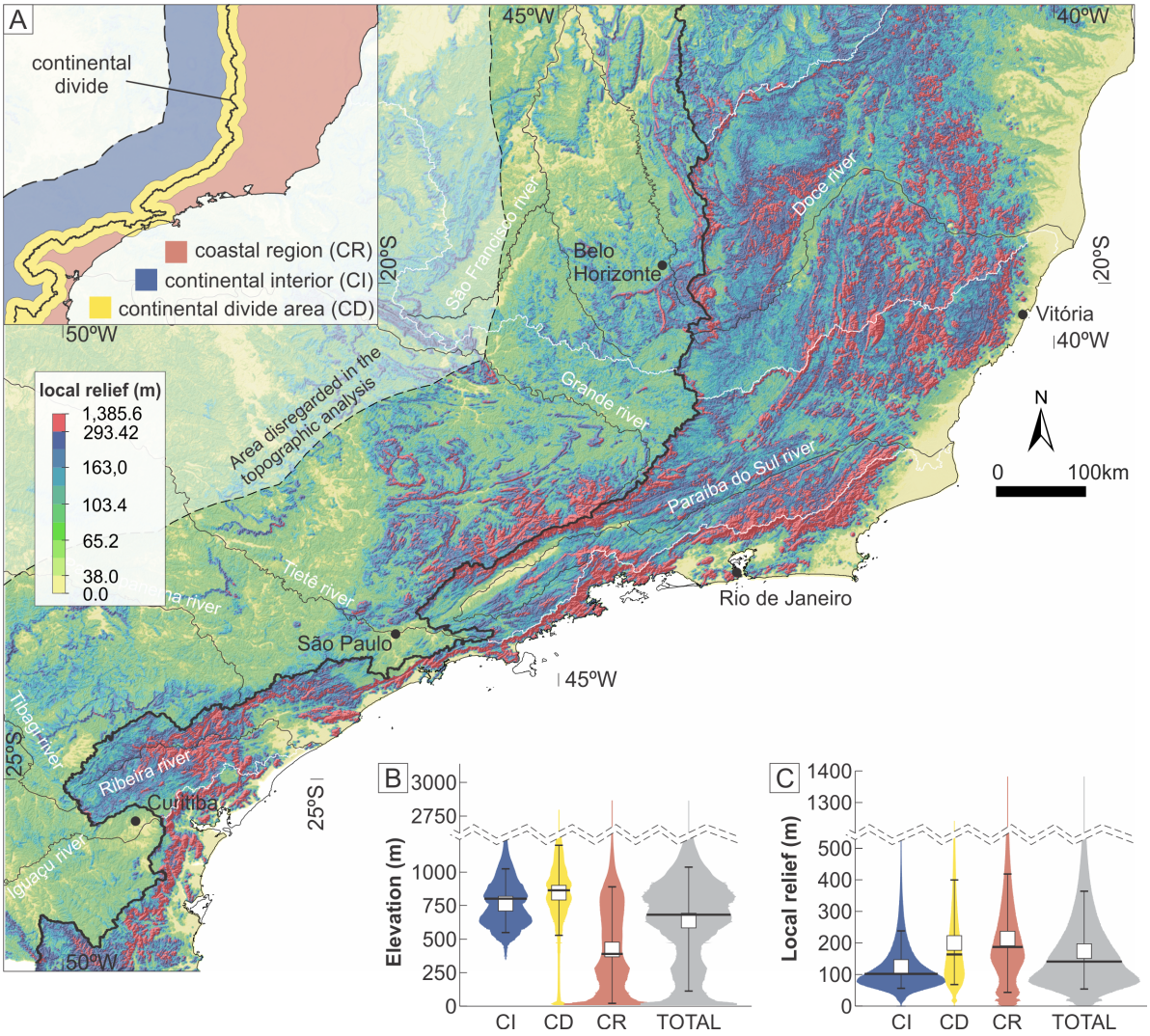

Figure 16 – **Map of topographic local relief of the CMSEB considering a 2 km circular window**. A) Sectors used in the topographic analysis: (i) continental interior, (ii) continental divide area which includes 30 km Swath along the CDD, and (iii) coastal region. B) Violin plots showing the distribution of elevation for each sector; C) Violin plot showing the distribution of local relief for each sector. Whiskers show the interval between the 10th and 90th percentiles of the data, white squares represent mean values, and thick black lines exhibit median values. The shades of red in the map of local relief represent the superior 10th percentiles of the data indicating the steepest areas.

For instance, the highest inland peak is at Serra do Caraça in the Quadrilátero Ferrífero region (2,072 m), which is located ca. 400 km away from the distant base level. The swath profile E-F (Fig. 15A) shows another example of high elevations occurring in a coastal interfluve, with values often reaching more than 2,000 m, while maximum elevations at the CDD in this profile do not reach more than 1,800 m.

3.5.2 The spatial distribution of AFT data

We find that pre-rift AFT ages (i.e. ages that are older than 138 Ma; Pérez-Díaz and Eagles, 2014) mostly occur in the continental interior of the CMSEB, while post-rift AFT ages tend to predominate in the coastal region (Fig. 17 A). For example, the São Francisco river basin sector includes AFT ages ranging from 129.0 ±8.0 to 289.0 ±13.0 Ma, with the predominance of pre-rift ages. The Paraná river basin sector presents AFT ages ranging from 51.0 ±5.0 to 337.0 ±27.0 Ma, showing a relatively broader and mixed-age spectrum with an expressive contribution of post-rift ages in addition to the pre-rift ones. In contrast, the Doce river basin sector shows AFT ages ranging from 39.0 ±4.0 to 187.0 ±18.0 Ma distributed in a narrow age spectrum with the predominance of post-rift ages. Similarly, the Paraíba do Sul river basin sector includes AFT ages ranging from 21.0 ±1.8 to 150.0 ±12.0 Ma displaying a narrow age spectrum with the predominance of post-rift AFT ages.

The relationships between AFT age and elevation above sea level suggest that AFT age tends to increase with elevation for samples younger than rifting (i.e., with ages younger than 138 Ma; Pérez-Díaz and Eagles, 2014), whereas samples older than rifting tend to remain in a wide but steady elevation range of ca. 700 and 1,300 m irrespective of sample age (Figs. 17B and 17C). However, despite this general tendency, the Paraná and Paraíba do Sul river basin sectors include a set of syn- to post-rift samples positioned in elevations higher than 1,300 m, which are unusually young for their high elevations (Group 1 in Fig. 17B). Furthermore, some samples that present syn-rift AFT age from the Doce river basin sector are positioned at elevations lower than 250 m (Group 2 in Fig. 17C), which is substantially lower than other samples with syn-rift AFT age observed in the surrounding areas of the CDD characterized by high elevations. In addition, although agreeing with the general distribution of AFT age and elevation aforementioned, the samples that were excluded from our compilation criteria (see Methods) suggest a group of samples with pre-rift AFT ages located in areas with high elevation. We observe that these high-elevation relatively-old AFT samples are positioned at the coastal interfluves (Serra do Mar; Group 3 in Fig. 17B, and Serra do Caparaó; Group 4 in Fig. 17C).

The relationships between AFT age and distance from the CDD indicate that AFT ages increase towards the continental interior in both southern (Paraná and Paranaíba do Sul river basin sectors; Fig. 17D) and northern (São Francisco and Doce river basin sectors; Fig. 17E) parts of the CMSEB. However, in the Paraná and Paranaíba do Sul river basin sectors, the CDD coincides spatially with samples with post-rift ages (Fig. 17D), while in the São Francisco and Doce river basin sectors, the CDD coincides spatially with samples of syn-rift ages (Fig. 17E). We also observe that the set of samples with syn- to pre-rift ages from the Paraná river basin sector, located more than 100 km inland from the divide in the Poços de Caldas region (Group 5 in Fig. 17D), suggests an age-distance trend that is different from the trend indicated by the bulk of the AFT data.

The outlier groups we identify in age-elevation plots (Figs. 17B and 17C) also stand

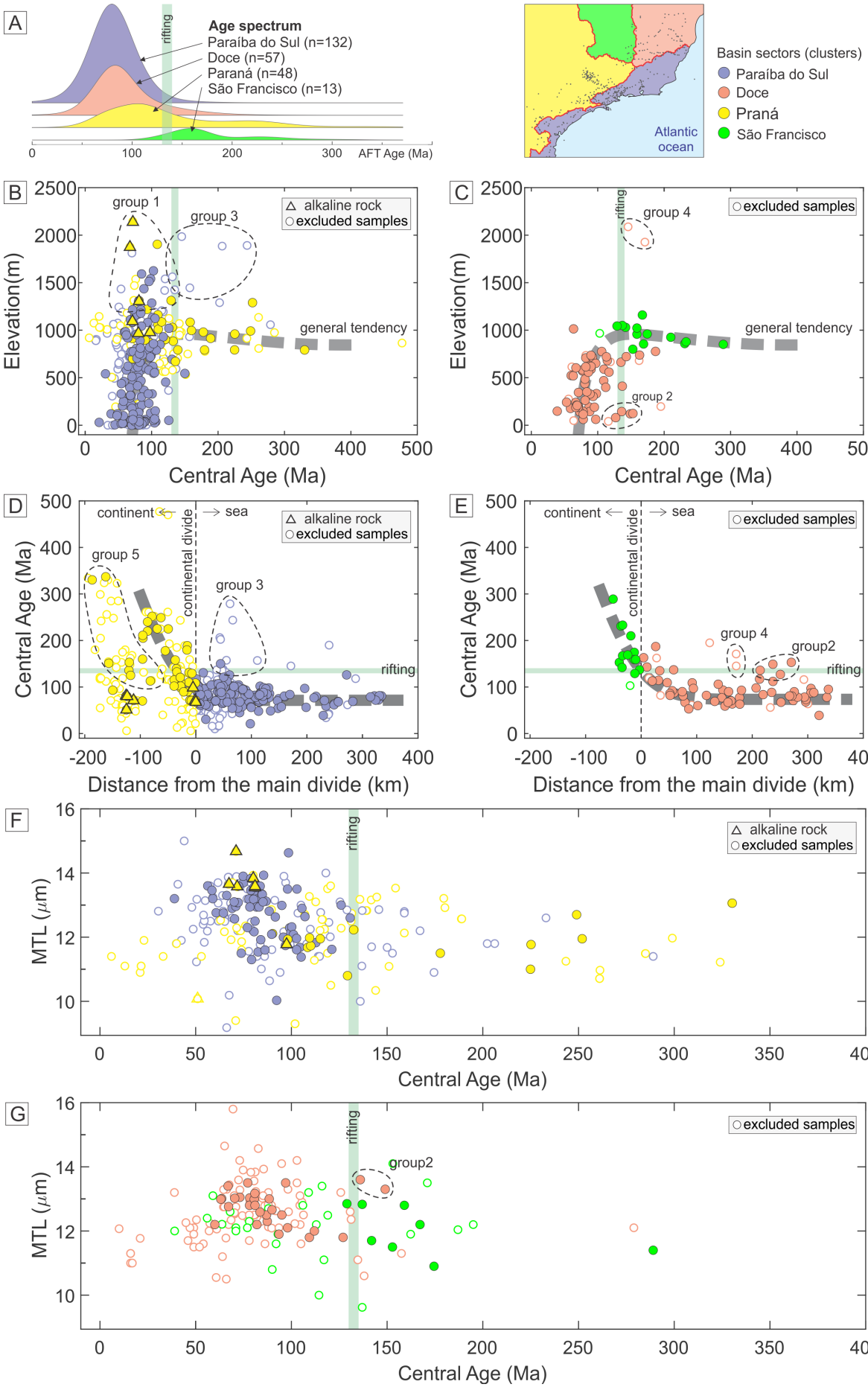
A
rifting
Age spectrum
Paraíba do Sul (n=132)
Doce (n=57)
Paraná (n=48)
São Francisco (n=13)
0
100
200
300
AFT Age (Ma)
Atlantic ocean
Basin sectors (clusters)
Paraíba do Sul
Doce
Praná
São Francisco
B
group 1
group 3
alkaline rock
excluded samples
general tendency
Elevation(m)
Central Age (Ma)
C
rifting
group 4
excluded samples
general tendency
group 2
Elevation(m)
Central Age (Ma)
D
continent
sea
continental divide
alkaline rock
excluded samples
group 5
group 3
rifting
Central Age (Ma)
Distance from the main divide (km)
E
continent
sea
continental divide
excluded samples
group 4
group2
rifting
Central Age (Ma)
Distance from the main divide (km)
F
rifting
alkaline rock
excluded samples
MTL (μm)
Central Age (Ma)
G
rifting
group2
excluded samples
MTL (μm)
Central Age (Ma)

Figure 17 – **Analysis of AFT age and mean track length (MTL) of the data available for the CMSEB**. A) AFT age spectrum for the four clusters of the CMSEB defined from the major drainage basins: Paraíba do Sul, Paraná, São Francisco, and Doce; B) Plot of AFT age against elevation for the southern segment of CMSEB (Paraná and Paraíba do Sul river basin sectors); C) Plot of AFT age against elevation highlighting for the northern segment of CMSEB (São Francisco and Doce river basin sectors); Plot of AFT age against distance from divide plot for the southern segment of CMSEB (Paraná and Paraíba do Sul river basin sectors); D) Plot of AFT age against distance from divide plot for the northern segment of CMSEB (São Francisco and Doce river basin sectors); F) Plot of AFT age against MTL (i.e., boomerang plot) for the southern segment of CMSEB (Paraná and Paraíba do Sul river basin sectors); G) Plot of AFT age against MTL (i.e., boomerang plot) for the northern segment of CMSEB (São Francisco and Doce river basin sectors).

apart from general age-distance tendencies (Figs. 17D and 17E). For example, the set of samples with syn-rift ages from the Doce river basin sector positioned at low elevations is also located relatively abnormally close to the sea, between 200 and 300 km seaward from the CDD (Group 2 in Figs. 17C and 17E). Additionally, the samples from the Serra do Caparaó interfluve segment also configure a set of syn- to pre-rift samples that are located more than 150 km away from the CDD in the seaward direction (Group 4 in Figs. 17C and 17E), which is at odds with the syn- to pre-rift samples we observe at or nearby to the CDD. Likewise, the Serra do Mar samples show predominantly syn- to pre-rift ages (Group 3 in Figs. 17B and 17D), are positioned at high elevations at a coastal interfluve, and are distributed between the CDD and the shoreline.

We find that MTL values range from ca. 10 to 15 μm (Figs. 17F and 17G). The relationships between AFT age and MTL (i.e., boomerang plots) indicate that samples with ages between 50 to 100 Ma tend to show MTL values ranging between 12 to 14 μm (which is high to moderate), whereas samples within the time interval of 100 Ma and rifting tend to show MTL values lower than 13 μm (low to moderate). In this situation, the Doce river basin sector shows a set of syn-rift samples with relatively high MTL values (Group 2 in Fig. 17G), including samples from the outlier Group 2 in Figs. 17C and 17E. Finally, samples collected deep in the continental interior show moderate to low MTL values (lower than 13 μm).

3.5.3 The southern AFT transect

The southern regional AFT transect extending from the Poços de Caldas highlands to the Atlantic coast shows a complex along-profile distribution of AFT ages and MTL data (Figs. 18 and B2 in appendix A.1.2). At the Poços de Caldas plateau, deep in the continental interior, AFT samples with Paleozoic-Mesozoic ages and high to moderate MTL values predominate if we keep apart samples related to the intrusive alkaline bodies (Fig. 18B). AFT ages tend to decrease towards the coast, reaching Mid to Late Cretaceous (i.e., syn- to post-rift) ages in the Serra da Mantiqueira region. In contrast, from this point and in the direction to the coast, there is

an overall tendency of progressively younger AFT ages, with samples reaching Paleocene ages nearby the coastline. However, such overall tendency is broken in the transition between Paraíba do Sul river depression and the Serra do Mar uplift (positioned at a coastal interfluve), where we observe samples with pre- to syn-rift AFT ages that are substantially older than suggested by the tendency of younger ages in the direction of the coast. Our results indicate that MTL values decrease from high to moderate values (13-14 μm) in the continental interior to ca. 11 μm at the Serra da Mantiqueira, and, from this point in the direction of the coast, MTL values tend to increase up to ca. 13 μm in proximity to the coast. Nonetheless, in the transition between Paraíba do Sul river depression and the Serra do Mar uplift, this tendency in the distribution of MTL data is broken, as we find moderate to small MTL values that are indicative of a relatively long permanence in the partial annealing zone since the syn-rift stage. In contrast, the higher MTL values we observe in samples at the coast may indicate accelerated post-rift cooling. In particular, the along-profile break in the general tendency in the distribution of AFT ages and MTL data we observe suggest a spatial-and-temporal complex denudation history.

The thermal histories we infer from AFT samples from the basement of Poços de Caldas plateau suggest a protracted cooling history (from $\approx$120^{o}C) since the Paleozoic without any evidence of syn- or post-rift cooling events (squares in Figs. 18C and 18D). Following along the transect, the thermal models of the two samples located seaward of the Ouro Fino shear zone register an apparent syn-rift reheating followed by a monotonic thermal evolution (plus symbol in Figs. 18C and 18D). Thermal models for samples from the Serra da Mantiqueira (concentric circles in Figs. 18C and 18D) indicate an accelerated cooling related to syn-rift event followed by a period of relative thermal stability and, subsequently, by a second cooling pulse during the post-rift phase. Further along the transect, thermal modeling of a sample from the Paraíba do Sul river depression suggests a post-rift accelerated cooling phase. Finally, thermal modeling of a sample from the Serra do Mar uplift (squares in Figs. 18C and 18D) registers a discrete syn-rift accelerated cooling phase followed by a final cooling event during the Miocene. Therefore, these thermal models suggest that denudation along the southern AFT transect of the CMSEB was variable in time and space, in agreement with the along-profile variations in AFT ages and MTL data.

3.5.4 The northern AFT transect

The northern regional AFT transect extending from Quadrilátero Ferrífero highland to the Atlantic shoreline shows an overall progressive along-profile decrease in AFT ages from the deep continental interior toward the coast, in a less complex thermochronological pattern than the identified along the southern transect (Figs. 19 and B3 in Appendix A.1.2). At the Quadrilátero Ferrífero highland, nearly 400 km away from the ocean, AFT samples with Paleozoic ages and with low to moderate MTL values predominate, suggesting a protracted cooling evolution since pre-rift times (Figs. 19B and 19C). AFT ages tend to decrease rapidly along the transect in

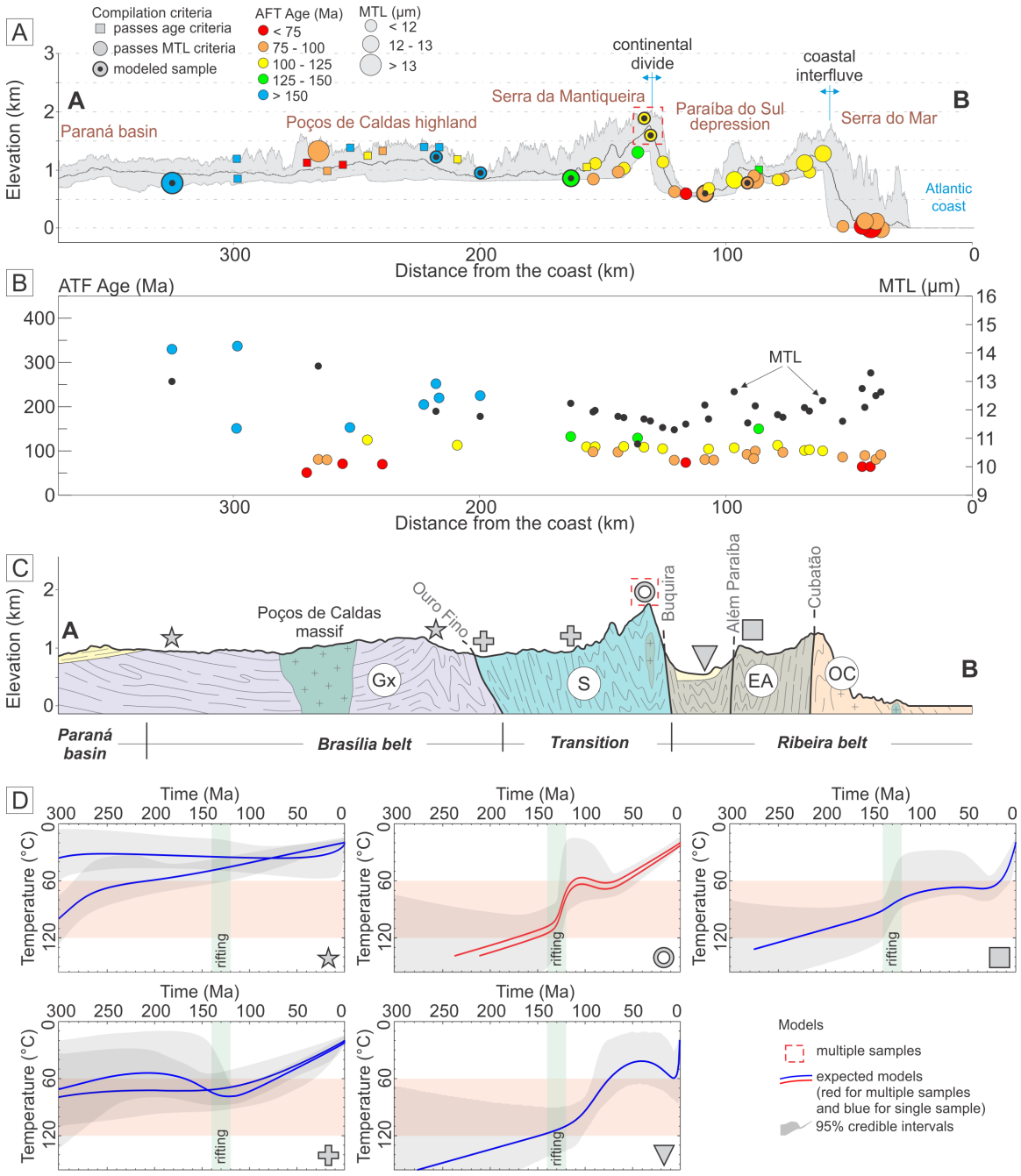

Figure 18 – **The southern CMSEB transect**. A) Swath profile including the AFT data accounting for samples within 50 km on either side of the section trace; B) AFT ages and MTL distribution along the transect; C) Simplified geological characteristics and basement units, (Gx) Guaxupé, (S) Socorro, (EA) Embú/Apiaí, (OC) Oriental/Curitiba; D) Thermal models with their along-profile positions indicated by symbols in panels C and D, and also signalized in panel A. The blue line shows the expected model for a single sample, whereas red lines represent samples that were modeled together. Gray shadows indicate 95% credible intervals for the model. Here we choose to include only the samples we consider representative in terms of geographical position and model result. For more details about the samples, see Fig. B2 (Appendix A.1.2).

the direction of the ocean, reaching Mid to Late Cretaceous ages in the Doce river depression. From this point in the transect and moving toward the coast, AFT ages remain relatively steady, yielding ca. Late Cretaceous to Paleocene ages, except for one Early Cretaceous AFT age in the transition between the Serra do Caparaó uplift and the coastline (ca. 60 km in the profile in Fig. 19A). The progressive diminishing in AFT ages is accompanied by increments in MTL values, which suggests that the region between the Doce river depression and the coastline was considerably exhumed during the post-rift evolution of the margin. We emphasize, nonetheless, that we find AFT samples with post-rift ages inland, distant from the shoreline, which contrasts with our results along the southern transect.

The thermal histories we infer from AFT samples inland from the Dom Silvério shear zone (stars, upward triangles, and plus symbols in Figs. 19C and 19D) indicate a protracted thermal history since Paleozoic with some indications of syn-rift cooling. We emphasize that although Amaral-Santos et al. (2019) do not report syn-rift denudation in the Quadrilátero Ferrífero area, our modeling outcome provide compelling evidence for an accelerated cooling event during or just before rifting (samples G1 and Cb1; see Fig. B3 in appendix A.1.2 for details about the localization of the samples and individual models). Differently, the AFT data we find along the transect from the Dom Silvério shear zone in the direction of the coast unambiguously show an expressive post-rift accelerated cooling (concentric circles and downward triangles in Figs. 19C and 19D). In this situation, the distribution of AFT ages, MTL data, and thermal models along the northern CMSEB regional transect demonstrate that denudation rates have varied in time and space in the northern portion of the CMSEB and such variations in denudation rates were markedly different along the northern transect.

3.6 Discussion

3.6.1 The post-rift exhumation of the CMSEB

The establishment of a new baselevel for continental erosion when rifting leads to the rupture of a continent is a fundamental element in the topographic evolution of a rifted continental margin (RCM) (Braun and van der Beek, 2004). In this situation, baselevel lowering along the rift axis causes reorganization of the preexisting drainage pattern and the establishment of a continental drainage divide (CDD) (Gilchrist et al., 1994). In addition, the formation of the new baselevel necessarily creates relief, given that the preexisting topography was previously elevated above sea level. In turn, this newly-created relief amplifies the efficiency of erosion processes in the resulting river network and adjacent hillslopes, particularly in rift flanks where relief is highest. As the new drainage system evolves, erosion is focused on rivers and hillslopes on the seaward-facing side of the CDD, and thus this high relief zone progressively retreats toward the inland plateau, enlarging seaward-dipping river basins and augmenting the width of the coastal plain (Wang and Willett, 2021). Therefore, in an RCM setting, we commonly expect a stark

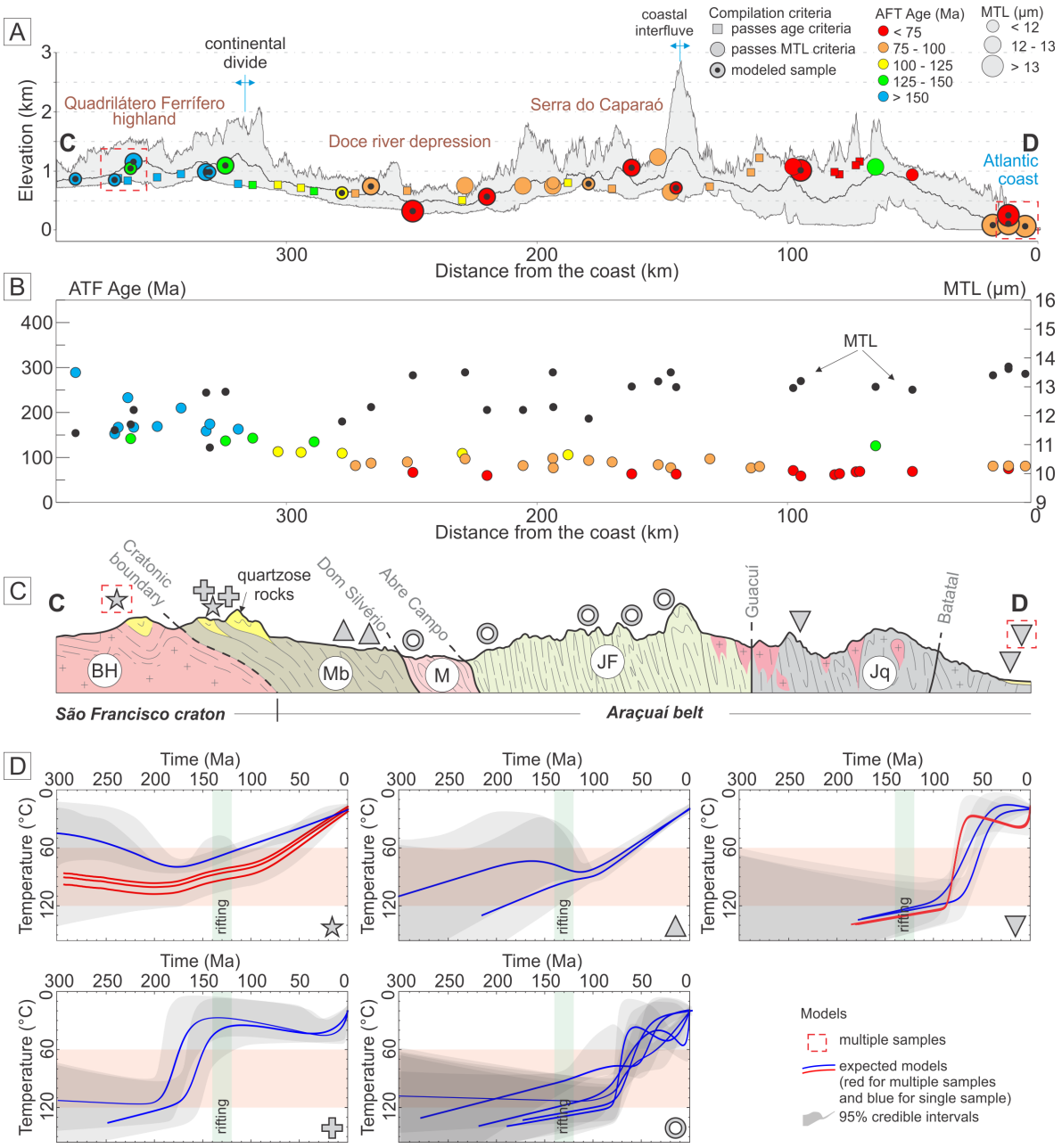

Figure 19 – **The northern CMSEB transect**. A) Swath profile including the AFT data accounting for samples within 50 km on either side of the section trace; B) AFT ages and MTL distribution along the transect; C) Simplified geological characteristics and basement units, (BH) Belo Horizonte, (Mb) Mineiro belt, (M) Mantiqueira, (JF) Juiz de Fora, (RD) Rio Doce, (PS) Paraíba do Sul, and main shear zones; D) Thermal models with their along-profile positions indicated by symbols in panels C and D, and also signalized in panel A. The blue line shows the expected model for a single sample, whereas red lines represent samples that were modeled together. Gray shadows indicate 95% credible intervals for the model. Here we choose to include only the samples we consider representative in terms of geographical position and model result. For more details about the samples, see Fig. B3 (Appendix A.1.2).

geomorphic contrast between a less dissected, elevated continental interior and a highly dissected seaward-facing region, with the CDD as an important morphological boundary (Gilchrist and Summerfield, 1990).

Our results indicate a similar scenario since the Brazilian southeast CDD marks the transition between two distinct settings, (i) an inland, continental interior sector characterized by high elevation and medium to low relief with a predominance of pre-rift AFT ages (i.e., younger than 138 Ma; Pérez-Díaz and Eagles, 2014), and (ii) a coastal region characterized by low elevations and high relief with the predominance of AFT ages younger than the rifting event. This asymmetrical continental interior-coastal denudation profile is similar to common observations in other RCMs (e.g., Gallagher and Brown, 1997; Gallagher et al., 1998). However, we highlight that variability in morphology and denudation styles between the inland and coastal domains we focus cannot fully explain the denudational pattern of the CMSEB. For instance, we show AFT samples essentially younger than the rifting event in the CMSEB, which suggests that the margin experienced substantial post-rift denudation estimated as of more than 3 km (e.g., Gallagher et al., 1994; Cogné et al., 2011; Jelinek et al., 2014; van Ranst et al., 2020). Such expressive post-rift denudation has been commonly interpreted as the result of episode (or episodes) of post-rift rock uplift affecting, at least, parts of the CMSEB (e.g., Hiruma et al., 2010; Cogné et al., 2011, 2012; Franco-Magalhaes et al., 2014; Engelmann de Oliveira et al., 2016; Souza et al., 2021), which is consistent with our findings.

Rock uplift is a plausible explanation for the unusually high elevations associated with AFT samples with syn- to post-rift ages collected at the Serra da Mantiqueira (Group 1 in Fig. 17). AFT samples with such relatively young ages are more commonly identified in lower elevations at the coastal region, yet the Serra da Mantiqueira represents a CDD segment reaching more than 2,500 m of elevation. We emphasize that these samples from the Serra da Mantiqueira, although including some samples from Late Cretaceous intrusive alkaline rocks (Figs. 17B, 17D, and 17F), originate from the crystalline basement, which is consensually considered free from the thermal effects of post-rift magmatism (Gallagher et al., 1994; Cogné et al., 2011, 2012). Other compelling evidence of post-rift uplift includes AFT samples with syn- to pre-rift ages at high elevations collected from the Serra do Mar (Group 3 in Fig. 17) and the Serra do Caparaó (Group 4 in Fig. 17). The age-elevation relationship for these samples is strikingly dissimilar from the general tendency of our AFT dataset (Fig. 17). In addition, these samples were collected in coastal interfluve areas reaching maximum elevations considerably higher than the maximum elevations we find at the CDD or the continental interior areas (Fig. 15), which can be reasonably explained as the result of post-rift uplift given that, otherwise, maximum elevation in coastal areas would be consistently lower than elevations at the CDD.

In turn, the set of AFT samples with AFT pre-rift ages which are at low elevations (less than 300 m above sea level), and near the coastline (Group 2 in Fig. 17), is at odds with general expectations of old AFT ages normally associated with high elevations. This suggests

that some coastal region areas have experienced local post-rift subsidence, given they appear to have been prevented of post-rift exhumation. These samples are principally from the low elevation valley of the Doce River, and their associated high MTL values indicate relatively fast syn-rift cooling followed by thermal stability at low temperatures (Jelinek et al., 2014). In this situation, preserving AFT samples with syn-rift ages in low elevations at the bottom of the Doce river valley, characterized by substantial upstream contributing area (drainage area) and high discharge, is not reasonable without evoking local subsidence (van Ranst et al., 2020). Therefore, our empirical data suggest post-rift uplift and subsidence over different parts of the CSMEB, which is reflected in the complex spatial denudation pattern indicated by the AFT data and thermal models along the Brazilian continental margin. Following previous studies, our results are consistent with the hypothesis of differential vertical motion between basement blocks (e.g., Hiruma et al., 2010; Cogné et al., 2011; van Ranst et al., 2020).

3.6.2 Timing and driving forces of post-rift rock uplift

Various thermochronological studies addressing the long-term evolution of the Brazilian South Atlantic coast identified enhanced post-rift denudation, prompting a search for explanations that, in most cases, favored post-rift rock uplift (e.g., Hiruma et al., 2010; Cogné et al., 2011, 2012; Franco-Magalhaes et al., 2014; Engelmann de Oliveira et al., 2016; Souza et al., 2021). In this situation, the thermochronological data, in agreement with the onshore and offshore geological record (Moreira et al., 2007), suggest an exhumation event dissociated (and substantially later) from the rifting process that is particularly detectable from boomerang plots (Fig. 17) and thermal models (concentric circles and downward triangles in Figs. 18D and 19D). However, such empirical data indicate that the post-rift topographic evolution of the CMSEB involves successive and spatial-heterogeneous uplift events rather than a well-defined, single, and general post-rift episode affecting the Brazilian margin as a whole.

The post-rift uplift and erosion affecting the Brazilian South Atlantic coast have been attributed to various driving forces. A recurrent explanation is, for example, the flexural-isostatic response of the lithosphere due to the mass flux in RCMs, where the continuing continental denudational unloading drives onshore uplift and the sediment loading cause offshore subsidence, triggering a protracted self-sustained process that is widely considered a first-order mechanism operating over their long-term evolution (Gilchrist and Summerfield, 1990; Summerfield, 1991; Gilchrist et al., 1994; Bishop, 2007; Jelinek et al., 2014; van Ranst et al., 2020). Other factors proposed as a mechanism of post-rift rock uplift in the CSEMB include the influence of secondary convection cells in the mantle (e.g., Sacek, 2017), magmatic underplating (e.g., Gallagher et al., 1994; Hackspacher et al., 2004), and mantle plume activity (e.g., Franco-Magalhaes et al., 2010), 2014), which is expected to promote a long-wavelength upwarp of the margin. In particular, intraplate-wide compressive stresses transmitted from the Andean orogeny and the Atlantic spreading axis are commonly interpreted as an essential tectonic component inducing post-rift

uplift in the CMSEB (e.g., Cogné et al., 2011, 2012; Jelinek et al., 2014; Amaral-Santos et al., 2019; van Ranst et al., 2020; Fonseca et al., 2021).

Nevertheless, these mechanisms of uplift can operate over different time-space wavelengths, which may overlap, leading to a scenario of a very complex arrangement of processes operating in the evolution of each specific sector of the CMSEB. For example, the alkaline intrusions, which are essential pieces of evidence indicative of the influence of the mantle thermal-mechanical process driving permanent post-rift uplift of the Brazilian margin, are concentrated in the southern part of the CMSEB (e.g. the Serra do Mar igneous province, ca. 85 to 55 Ma; Thompson et al., 1998, and the northern offshore region, the Abrolhos and Vitória-Trindade seamounts, ca. 59 to 37 Ma; França et al., 2007; Stantonet al., 2021). In contrast, alkaline intrusions are scarce in parts of the CMSEB, such as the onshore northern areas associated with the Serra do Caparaó and Serra do Espinhaço. Furthermore, as the continental denudation unloading has been a continuing process and the CMSEB bedrock includes several different age-composition tectonic basement blocks (Fig. 10), the flexural-isostatic compensation is an example of a permanent and spatially variable uplift mechanism occurring in the study area. In addition, the compressive forces transmitted from Andeans orogenic events in association with the push of the Mid-Atlantic spread axis are another transient input of exhumation likely operating in the post-rift evolution of the CMSEB. Finally, climate variations between drier and wetter conditions are also common elements of the Cenozoic climatic history of Brazil (e.g., Zachos et al., 2001; Behling, 2002; Stríkis et al., 2018) and are likely another process involved in the post-rift topographic evolution of CMSEB.

3.6.3 The two sectors of the CMSEB

The topographic and thermochronological data show that the southern (the Serra do Mar and Serra da Mantiqueira) and northern (the Serra do Espinhaço and Serra do Caparaó) extensions of the CMSEB compose two distinct onshore segments of the Brazilian South Atlantic passive margin. In particular, these different parts of the CMSEB are marked by stark dissimilarities in morphology. The CDD is located near the shoreline in CMSEB's southern extension, while it is positioned very deep in the continental interior at its northern extension (Fig. 15), and steep escarpment areas are more frequent and broader in southern CMSEB.

Importantly, the thermochronological data suggest that these geomorphic differences reflect different geologic and thermal histories. In CMSEB's northern extension, particularly in the Serra do Espinhaço region, the CDD separate inland areas characterized by pre-rift AFT ages and a seaward-draining domain characterized by syn- to post-rift AFT ages. In contrast, we document syn- to post-rift AFT ages positioned inland from the CDD at CMSEB's southern extension, which are significantly younger than expected and indicate that the exhumation of the coastal region associated with the opening of the Atlantic Ocean likely reached inland areas from the Serra da Mantiqueira in southern CMSEB (Fig. 13). These results suggest the presence of a

syn-rift-related continental drainage divide positioned inland from its present-day position (more than ≈100 km), implying the 'seaward-advance' of the CDD at CMSEB's southern extension instead of the otherwise expected inland retreat of the CDD (e.g., Ollier and Pain, 1997). In this situation, the region inland from Serra da Mantiqueira (referred to as the Poços de Caldas plateau) likely represents an ancient syn-rift coastal area that was uplifted at post-rift times. Localized tectonic uplift is a plausible explanation for the hypothesis of a 'seaward-advance' of the CDD at CMSEB's southern extension, and this scenario explains the set of AFT samples with unusual post-rift ages positioned at high elevations (Group 1 in Fig. 17) we document, as well as it is consistent with common interpretations that the uplift of the Serra da Mantiqueira occurred in response to the development of the Continental Rift of Southeastern Brazil long after the rifting event (Riccomini et al., 2004).

3.6.4 Tectonic inheritance and the CMSEB diversification

Spatial and temporal contrasts in denudation patterns and topographic forms over the CMSEB are primarily related to the bedrock compartmentalization and the structural framework of the basement. For example, the position of the CDD in CMSEB's northern extension coincides with the São Francisco craton boundary (Fig. 10C). This spatial correspondence suggests that the expressive contrast in flexural strength between the craton and the ancient orogen influence the width of the coastal region as well as it contributes to the long-term stability of the northern segment of the CDD (i.e., the Serra do Espinhaço, which last experienced major tectonic activity in the Neoproterozoic–Cambrian (Pedrosa-Soares et al., 2001; Alkmim et al., 2006; Pedrosa-Soares et al., 2008). In this case, the relatively weak lithosphere of the Araçuaí belt configures a terrain more susceptible to uplift and exhumation than the rigid lithosphere of the São Francisco craton (Fonseca et al., 2021). Likewise, the position of the southern portion of Brasília belt in-between two cratonic masses (i.e., São Francisco craton and Paranapanema block) (Fig. 11A) may also contribute to the long-term preservation of the Poços de Caldas plateau (i.e., the inland part of CMSEB's southern segment) from intense syn- and post-rift exhumation (Fonseca et al., 2021). The flexural strength of the lithosphere has been demonstrated as a significant control of denudation in continental margins (e.g., Braun, 2018) and in internal portions of the South Atlantic platform since Paleozoic times (e.g., Fonseca et al., 2021).

The structural framework also plays a role on the contrasts in denudation and topographic forms we report between the southern and northern parts of the CMSEB. The main ductile shear zones separate areas with contrasting denudation patterns throughout the margin, with the Ouro Fino shear zone delimiting the spatial influence of the syn-rift cooling (Fig. 18D), while the Buquira, Além Paraíba, and Cubatão shear zones control the post-rift denudation along the present-day coastal region (Figs. 18D and 19D). In addition, these ancient shear zones also influence the occurrence of the lengthy escarpment-like CDD segments in CMSEB's southern extension along the Serra do Mar and Serra da Mantiqueira (Figs. 10C and 15B). Such influence

of the shear zones in the morphology of the surface and denudation patterns likely corroborate various studies suggesting that the post-rift exhumation history of the CMSEB is associated with the reactivation of these preexisting structures (e.g., Gallagher et al., 1994; Tello Saenz et al., 2003; Ribeiro et al., 2005b,a; Hiruma et al., 2010; Cogné et al., 2011; Karl et al., 2013; Engelmann de Oliveira et al., 2016, 2018; Krob et al., 2019; van Ranst et al., 2020; Gezatt et al., 2021).

Differently from other RCMs whose continental drainage divide is positioned less than 200 km from the coast (cf., Braun, 2018), the CDD in northern CMSEB is located more than 300 km inland from ocean. The 'craton-orogen' discrepancy in flexural strength and its resultant role in the enhanced isostatic rebound of the Araçuaí belt lithosphere has undoubtedly factored in setting up the configuration of the larger width of the coastal region in CMSEB's northern sector (Figs. 10C and 15). Our thermochronological data indicate such enhanced isostatic rebound of the Araçuaí belt lithosphere through the documentation of widespread post-rift exhumation in the northern extent CMSEB, which presumably contributes to the prominent topography of the northern coastal interfluves (e.g., Serra do Caparaó). However, other processes and interactions such as the syn-rift reactivation of major lithospheric discontinuities like the Dom Silvério shear zone (Fig. 10C), which is interpreted as the orogenic suture of the Araçuaí orogen (Alkmim et al., 2006), must have contributed to the unusually wider coastal region in the northern sector. The east African rift system is a modern example of a rift setting with ∼300 km of widespread extension controlled by preexisting tectonic structures (Boone et al., 2019) which illustrates how the reactivation of preexisting major weakness zones induces the propagation of the denudation in regions not necessarily restricted to the main rift axis. Furthermore, it is plausible that the differential tectonic fabric of the Ribeira belt (southern CMSEB) compared to the Araçuaí setting (northern CMSEB), in which preexisting structural discontinuities are more pervasive and restricted to areas near the shoreline in the former, has also contributed for the contrasting coastal width between southern and northern CMSEB extents.

We also propose that the exposure of resistant rocks to weathering and erosion plays a significant role in the long-term stability of the position of pronounced topography of the northern CDD. Studies using cosmogenic isotopes (e.g., Barreto et al., 2013; Peifer et al., 2021) indicate extremely low denudation rates (of <5 m/Myr) in areas underlain by quartzose rocks that, due to their high resistance, sustain the high elevations and steep slopes of the Serra do Espinhaço and Quadrilátero Ferrífero highlands, such as Espinhaço supergroup (Chemale Jr et al., 2012) and Minas supergroup (Alkmim and Marshak, 1998). Hence, the combined effect of exposure of rocks with low erodibility underlying nearby areas of the northern CDD and the stark contrast in flexural strength between craton-orogen strengthen the topographic stability of the Serra do Espinhaço and Quadrilátero Ferrífero areas. Consequently, the presence of an ancient, preexisting inland drainage divide that was probably in place in this region (i.e., craton boundary) by the end of the Pan-African/Brasiliano orogenic cycle (Peifer Bezerra, 2018) can further support the

explanation of why the northern CMSEB coastal zone is so wide as well as the absence of a 'Great Escarpment' in this northern segment (Gilchrist et al., 1994; Brown et al., 2002; Braun, 2018). According to the pinned divide model proposed by van der Beek et al. (2002) for the southeast African margin, the presence of an inland elevated plateau as a preexisting drainage divide may influence the stability of the newborn marginal divide/escarpment, resulting in widespread rapid erosion of the area located seaward from this preexisting inland divide rather than the formation of a marginal scarp that progressively retreats toward the continental interior. Finally, given that there is a positive relationship between the density of the material being eroded and the isostatic response (Braun et al., 2014), it is reasonable to expect that lithological contrasts, implying variations in surface rock density, further contribute to the complex geomorphic and denudation patterns in CMSEB. For instance, we observe the correspondence between the coverage of the Juiz de Fora basement unit, which includes lithology denser than the surrounding units, and the prominent topography of the Serra do Caparaó (Figs. 10 and 19).

3.7 Conclusion

We perform quantitative topographic analysis and use apatite fission track available data to demonstrate how the first order topography and the denudation pattern varies along a segment of the Brazilian South Atlantic coast, more specifically throughout the well-known escarpment system of the Serra do Mar and Serra da Mantiqueira, and the adjacent northeastern segment that includes the Serra do Espinhaço and the Serra do Caparaó. We show that, similar to other mature rifted settings, the continental margin of southeast Brazil is characterized by the typical asymmetric denudation profile, and the continental drainage divide mostly delimits a less dissected continental interior from a denudated coastal region. Furthermore, we demonstrate that besides the differential denudation in response to developing a new base level (i.e. South Atlantic opening), the margin has experienced substantial post-rift exhumation with the contribution of local and relative rock uplift due to the reactivation of ancient basement structures. We highlight that the geomorphic differences along the margin reflect particular geological histories allowing, therefore, the recognition of two different sectors. The southern sector is characterized by a continental water divide that advanced seaward due to the influence of faulting (i.e., localized uplift) that occurred long after the rifting event and contributed to the maintenance of steep escarpment features along the Serra do Mar and the Serra da Mantiqueira. The northern sector is characterized by a relatively wider coastal region controlled by the reactivation of further-inland structures and a long-lived continental water divide anchored deep in the continental interior. Our results suggests that, besides the complex mechanisms involved in the post-rift evolution, which may contributed to the segmentation of the margin, the tectonic inheritance (i.e, structural framework, lithology, effective flexural strength of the lithosphere) performed a fundamental role in setting up geomorphic diversification along the Brazilian South Atlantic rifted margin.

3.8 Acknowledgements

This work was supported by the Coordenação de Aperfeiçoamento de Pessoal de Nível Superior – Brasil (Capes, the research fund of the Brazilian Ministry of Education) – Finance code 001. The first author thank Fundação de Amparo Pesquisa do Estado de Minas Gerais (FAPEMIG) for the Ph.D. scholarship funding. The second author had support from CAPES under a CAPES-PrInt Postdoctoral fellowship (nº 88887.508590/2020-00). We also thank Cristina Persano and Mark Wildman for the constructive discussion and the advice on thermal modeling. Finally, we thank Andrea Ritter Jelinek, Matheus H. Kuchenbecker do Amaral, and the reviewers for their constructive suggestions that helped to improve the final version of the manuscript.

4 The apatite fission track thermochronology data of the Serra da Boa Vista region

4.1 Geological setting

The study area includes the continental region associated with the Espírito Santo offshore basin; a segment of the South Atlantic rifted continental margin in Brazil. This geotectonic setting is commonly referred to as a passive margin established after the Gondwana breakup during the Mesozoic. However, onshore and offshore geological records suggest that it has been quite active since then. This post-rift activity has been partially associated with the reactivation of inherited lithospheric structures developed over a protracted and complex geological history marked by successive tectonic cycles. The link between the contrasting denudation patterns and basement network is relatively well characterized in other segments of the Brazilian coast (e.g., Serra do Mar region adjacent to Santos and Campos basins; Cogné et al., 2012, onshore area adjacent to Potiguar basin in northeast Brazil; Nóbrega et al., 2005). Nevertheless, the influence of fault reactivation is poorly constrained in the continental region related to Espírito Santo offshore basin. In sequence, we characterize the bedrock composition and structural framework of the study area, and then we summarize a general state of the art about the tectonic evolution of the southeast Brazilian segment of the South Atlantic rifted continental margin.

4.1.1 Bedrock composition and structural framework

In the study area, the main structural framework developed as a consequence of the Pan-African/Brasiliano orogenic cycle that is characterized by the accretion of multiple terranes (i.e., Paleoproterozoic–Archean landmasses, Mesoproterozoic–Neoproterozoic supracrustal sequences, and Neoproterozoic magmatic arcs; see the units in Fig. 20A) during the Neoproterozoic-Cambrian to form the West Gondwana supercontinent (Pedrosa-Soares et al., 2001; Cordani et al., 2003; Alkmim et al., 2006; Pedrosa-Soares et al., 2008; Heilbron et al., 2010). The study area is included in the Araçuaí-Ribeira belt, a segment of this orogenic system developed due to the interaction of São Francisco and Congo landmasses that lead to the amalgamation of Paleoproterozic units (rocks of the Juiz de Fora and Mantiqueira domains) and Neoproterozoic sequences (Raposos, Nova Venécia, Dom Silvério, and Rio Doce groups) and granitic intrusions (Rio Doce and Rio Negro metagranites). Juiz de Fora and Mantiqueira domains comprise two Paleoproterozoic crustal segments, an intra-oceanic arc and an arc-related active continental margin respectively, involved in a Rhyacian-Orosirian orogenic cycle responsible to build the São

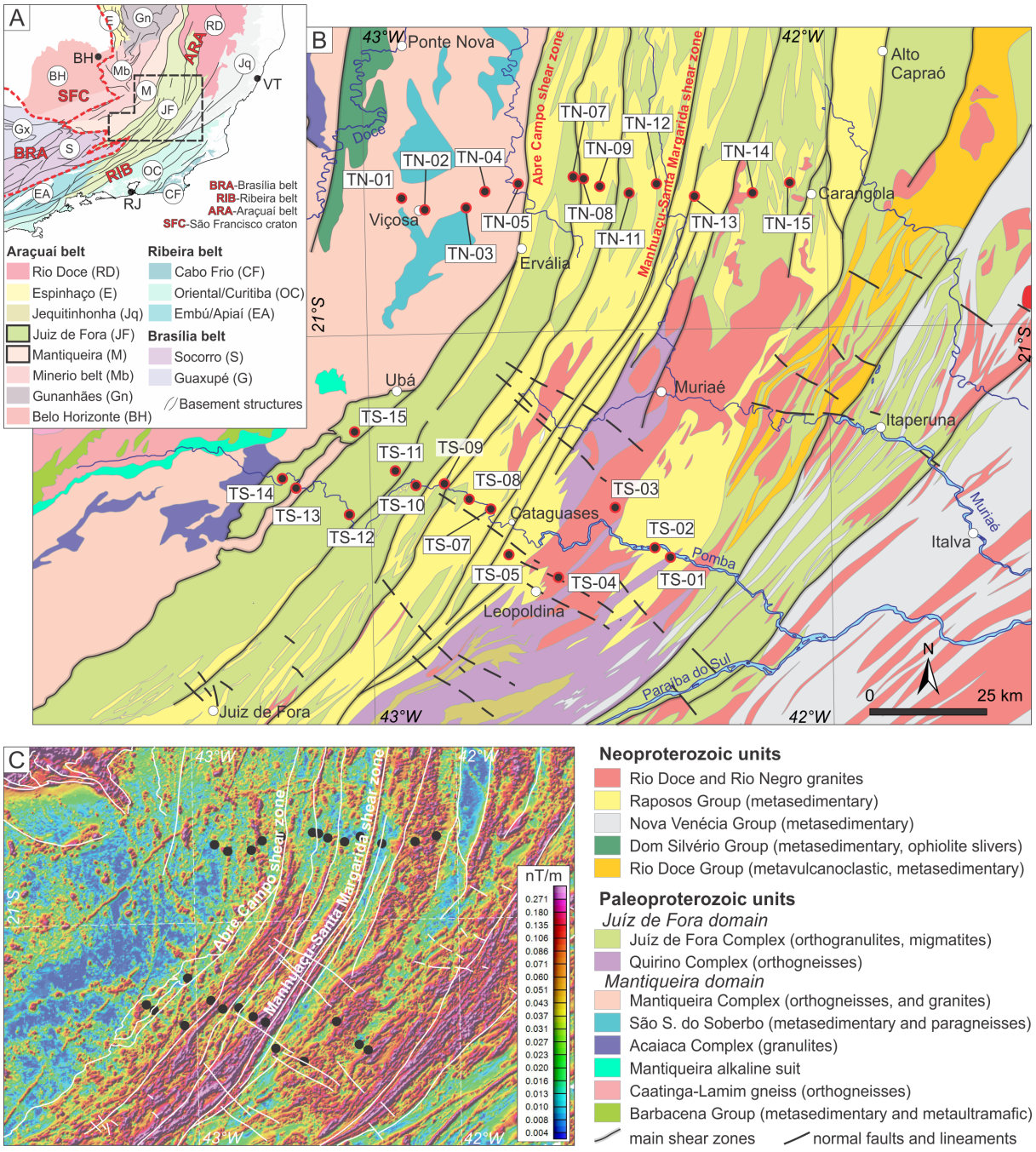

Figure 20 – **Local Geology**. A)Simplified geological map of southeast Brazil highlighting the main tectonic structures and basement units; B)Detailed geological map of the Serra da Boa Vista region; C)Map of the total gradient of the anomalous magnetic field and in white the tectonic structures presented in B.

Francisco-Congo paleocontinent. The Neoproterozoic sequences and granitic intrusions comprise the rocks related to taphrogenic, accretion, and collision event(s) of the Pan-African/Brasiliano orogenic cycle. In the study area, these units are exposed in the form of high-grade metamorphic rocks structured according to SW-NE to SSW-NNE anastomosed sub-vertical shear zones that extend over hundreds of kilometers (Fig. 20). In the center of the study area, the Abre Campo and Manhuaçu-Santa Margarida shear zone systems is an important series of SW-NE dextral strike-slip ductile shear zones associated with WNW-striking brittle fault zones and jointing resulted from poly-phase transcurrent deformation that affected the Paleoproterozoic and Neoproterozoic units during the Pan-African/Brasiliano orogenic cycle (Silva et al., 2009; Egydio-Silva et al., 2018). These lengthy structures comprise main lithospheric discontinuities and present a distinct pattern on magnetometric maps (Fig. 20B).

4.1.2 Samples and sampling strategy

In order to investigate and better constrain the influence of the structural frame work in the exhumation pattern along the Brazilian South Atlantic continental margin (Fig. 21A), we collected samples for apatite fission track analysis concentrated in two profiles across the basement main structural trend. A total of 27 samples were acquired with spacing of approximately 5 km. The northern profile comprises 13 samples collected across the Serra da Boa Vista, a SW-NE range that runs parallel to the Proterozoic shear zones (Egydio-Silva et al., 2018). This morphostructure is part of the Serra do Caparaó, a high-elevation segment of the Brazilian continental rifted margin costal interfluve (Fonte-Boa et al., 2022, Chapter 3). The southern profile comprises 14 samples collected along the Pomba river valley that cross-cut the south extension of the Serra da Boa Vista (Fig. 21B).

The apatite crystals were separated using a standard procedure of crushing, magnetic and heavy liquid mineral separation procedures (cf. Donelick et al., 2005). The grains were mounted in epoxy resin and polished until flat and then etched for 20 seconds in 5M nitric acid (HNO_3) at controlled temperature range between 18 and 23 °C. After thermal neutron irradiation the external detectors were removed and etched in 48% HF acid for c. 25 – 28 minutes at room temperature (18-23 °C).

4.2 Results

We present 27 new apatite fission track data distributed in two transects (Tabs. 3, 4, and 5; Figs. 20 and 23; and Appendix A.2.1). Eight samples failed in the chi-square (χ^2) age homogeneity test and the majority of the analyzed samples, except for samples TS-07, TS-08, and TS-15 which also failed in the χ^2 test, show moderate to low single-grain fission track age dispersion (i.e., $\leq$20%). The D_{par} values range from 1.54 to 1.86 μm and are inferior to values for Durango apatite (2.05 $\pm$0.16 μm; Sobel and Seward, 2010). Compared to other studies that show

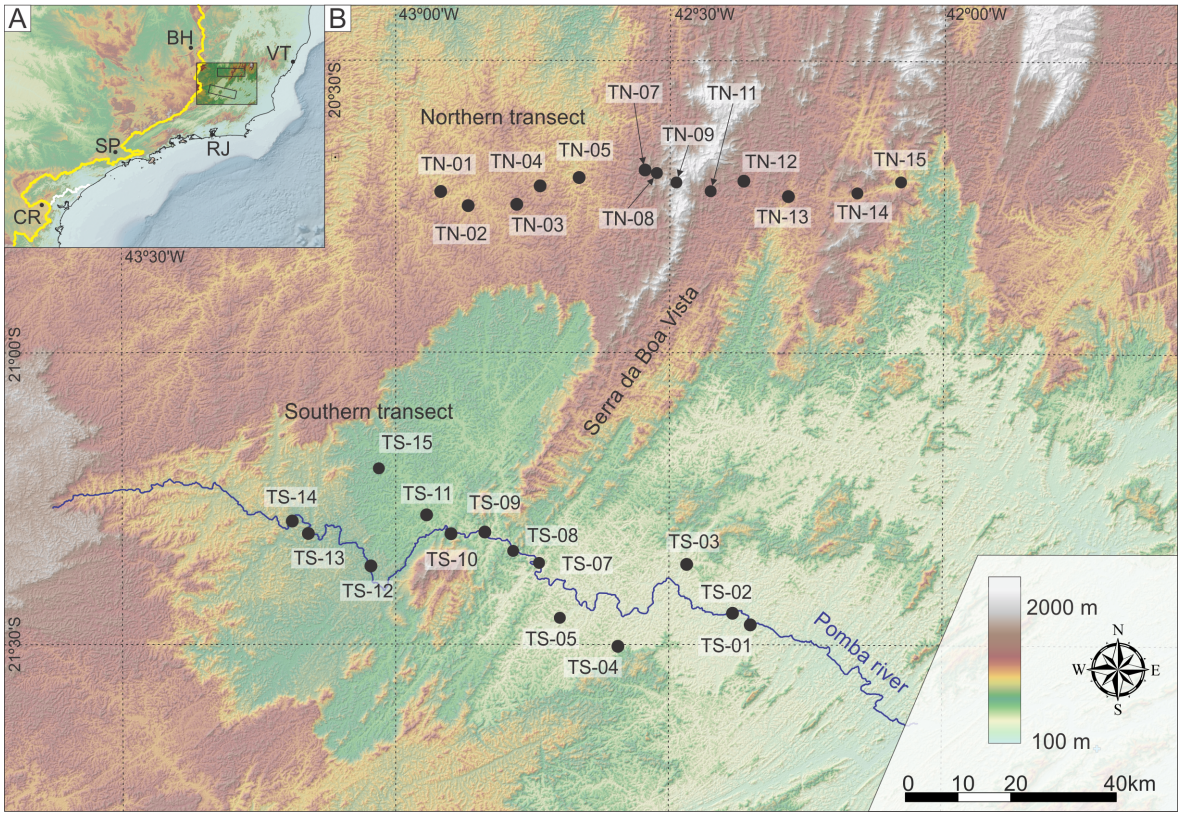

Figure 21 – **Sample locations**. A)Location of the study area in the context of the Brazilian southeast continental margin, showing the position of the continental drainage divide and the main cities: CR- Curitiba, SP- São Paulo, RJ- Rio de Janeiro, VT- Vitória, and BH- Belo Horizonte; B)The position of the northern and southern transects along the Serra da Boa Vista in the Serra do Caparaó region.

a wider D_{par} variation (e.g. Wildman et al., 2016, , which D_{par} values range from 1.45 to 3.42 μm), this narrow range suggests that the apatite crystals have similar composition. In addition, despite the samples being collected from different rock types, there is no correlation between AFT data and lithology (Fig. 22A). The c-axis uncorrected MTLs range from 11.15 $\pm$0.29 to 13.10 $\pm$0.20 μm, while the c-axis corrected MTL values are significantly higher, ranging from 13.30 $\pm$0.17 to 14.36 $\pm$0.18 μm (Fig. 22C).

Overall, the AFT ages tend to increase with the elevation (Fig. 22A) and toward the continental drainage divide (Fig. 22B). The southern transect includes samples collected between 108 and 445 m above sea level and AFT central ages ranging from 65.3 $\pm$7.9 to 167.5 $\pm$21.4 Ma resulting in a relatively slight positive age-elevation correlation with a high degree of dispersion (Figs. 22A and 23B). On the other hand, the northern transect comprises samples collected from 560 to 1360 m with AFT central ages ranging from 79.7 $\pm$9.2 to 134.6 $\pm$16.0 Ma resulting in a strikingly positive age-elevation correlation with a low degree of dispersion (Figs. 22A and 23C). Despite the overall age-elevation tendency disparity between the northern and southern transects, the spatial distribution of the samples show that the oldest AFT ages are associated to the SW-NE topographic range, referred to as Serra da Boa Vista, found in the center of the study

Table 3 – Samples location coordinates, elevation above sea level, distance from the coast and the continental drainage divide, and ithology.

Sample	Longitude (°) WGS84	Latitude (°) WGS84	Elevation (m)	Coast[a] (km)	Divide[b] (km)	Lithology
TN-01	-42.92	-20.72	652	225	69	Orthogneiss
TN-02	-42.87	-20.75	692	220	75	Orthogneiss
TN-03	-42.78	-20.75	712	211	83	Orthogneiss
TN-04	-42.74	-20.72	701	207	85	Charnockite
TN-05	-42.67	-20.70	608	199	91	Orthogneiss
TN-07	-42.55	-20.69	875	187	102	Paragneiss
TN-08	-42.52	-20.69	988	185	104	Paragneiss
TN-09	-42.49	-20.71	1360	181	108	Paragneiss
TN-11	-42.43	-20.72	846	174	115	Orthogneiss
TN-12	-42.37	-20.71	792	168	120	Orthogneiss
TN-13	-42.28	-20.73	692	160	129	Granite/Charnockite
TN-14	-42.16	-20.73	698	147	142	Orthogneiss
TN-15	-42.08	-20.71	560	139	149	Paragneiss
TS-01	-42.35	-21.47	157	134	128	Orthogneiss
TS-02	-42.38	-21.45	108	137	124	Paragneiss
TS-03	-42.47	-21.36	230	147	115	Granite/Charnockite
TS-04	-42.59	-21.50	204	159	103	Granite/Charnockite
TS-05	-42.70	-21.45	188	170	92	Gneiss
TS-07	-42.74	-21.36	280	175	87	Charnockite
TS-08	-42.79	-21.34	226	180	82	Paragneiss
TS-09	-42.84	-21.31	231	186	76	Orthogneiss
TS-10	-42.90	-21.31	247	192	70	Orthogneiss
TS-11	-42.94	-21.28	302	198	65	Orthogneiss
TS-12	-43.05	-21.37	404	207	55	Orthogneiss
TS-13	-43.16	-21.31	435	219	43	Orthogneiss
TS-14	-43.19	-21.29	445	223	40	Orthogneiss
TS-15	-43.03	-21.20	407	208	58	Orthogneiss

[a] Distance from the coastline.
[b] Distance from the continental drainage divide.

Table 4 – Results of Apatite Fission Track Analysis, Apatite Fission Track Ages.

Sample	ρ_s[c] (10^6cm^{-2})	ρ_i[c] (10^6cm^{-2})	ρ_d[c] (10^6cm^{-2})	χ^{2}[d]	D_{par}[e] (μm)	Central AFT Age (Ma)	$\pm1\sigma$	Dispersion[f] (%)
TN-01	5.0	15.9	16.9	0.96	1.65	79.7	9.2	0
TN-02	3.4	8.4	14.9	0.64	1.65	89.1	10.9	0
TN-03	6.7	13.2	16.8	0.51	1.79	126.4	14.4	3
TN-04	9.4	18.1	13.7	0.31	1.70	105.4	11.8	5
TN-05	7.5	16.9	12.2	0.55	1.63	80.0	9.0	1
TN-07	13.8	23.7	12.9	0.05	1.65	110.4	12.6	12
TN-08	16.5	26.6	13.0	0.01	1.79	119.0	13.8	15
TN-09	8.0	11.7	13.3	0.05	1.71	134.6	16.0	14
TN-11	17.5	32.2	13.9	0.11	1.59	111.2	12.6	8
TN-12	11.3	21.4	13.0	0.10	1.79	102.1	11.3	9
TN-13	13.3	37.7	18.2	0.05	1.66	94.2	10.6	11
TN-14	12.7	35.0	16.5	0.24	1.73	88.2	10.3	6
TN-15	6.4	12.9	11.9	0.62	1.60	87.6	11.8	0
TS-01	3.3	12.1	16.9	0.09	1.61	65.3	7.9	15
TS-02	6.9	24.1	18.0	0.66	1.56	76.5	8.4	0
TS-03	6.3	12.7	12.4	0.06	1.78	91.1	10.5	14
TS-04	7.4	21.9	17.4	0.20	1.72	87.7	9.7	6
TS-05	17.8	43.0	11.9	0.02	1.70	73.0	8.0	10
TS-07	3.2	7.9	13.4	0.01	1.54	86.1	11.5	23
TS-08	3.8	7.3	14.4	0.00	1.58	109.9	14.1	24
TS-09	2.9	4.6	17.9	0.23	1.86	167.5	21.4	18
TS-10	2.3	4.8	18.8	0.91	1.81	134.2	17.5	0
TS-11	3.4	5.6	13.8	0.40	1.75	122.6	7.5	0
TS-12	2.1	6.1	17.6	0.80	1.65	89.6	10.4	0
TS-13	9.0	23.3	15.3	0.46	1.60	87.4	4.8	7
TS-14	5.9	11.7	17.6	0.10	1.73	134.6	17.1	18
TS-15	5.8	11.6	11.9	0.01	1.64	88.8	11.9	24

[c] Track density of induced (i), spontaneous (s), dosimeter tracks (d).

[d] Etch pit diameters used as a proxy for the influence of chemical composition on track annealing.

[e] p value of the chi-square age homogeneity test (Galbraith, 2005). Gray for failed samples.

[f] Standard deviation of the true single-grain ages as a percentage of their central age (Galbraith, 2005). Gray for high single-grain dispersion.

Table 5 – Results of Apatite Fission Track Analysis, Mean Track Lengths.

		Measured			**c Axis Correction**			
Sample	#Xtls[f]	MTL (μm)	$\pm1\sigma$	SD[g]	MTL (μm)	$\pm1\sigma$	SD[g]	L[h]
TN-01	25	11.15	0.29	1.68	13.30	0.17	0.97	34
TN-02	22	12.71	0.21	1.60	14.15	0.14	1.05	56
TN-03	20	12.99	0.26	1.87	14.31	0.19	1.35	52
TN-04	25	12.74	0.18	1.73	14.23	0.11	1.11	94
TN-05	20	12.51	0.18	1.62	14.01	0.12	1.10	79
TN-07	20	11.77	0.16	1.73	13.57	0.10	1.10	114
TN-08	22	12.19	0.20	2.01	13.78	0.13	1.31	105
TN-09	19	12.27	0.24	1.78	13.77	0.18	1.30	54
TN-11	18	11.69	0.28	1.99	13.52	0.18	1.29	50
TN-12	24	12.20	0.13	1.44	13.72	0.09	1.05	125
TN-13	25	12.26	0.14	1.75	13.80	0.10	1.19	150
TN-14	16	12.54	0.16	1.66	14.04	0.11	1.11	102
TN-15	16	12.67	0.25	1.53	14.12	0.17	1.06	37
TS-01	22	11.85	0.14	1.42	13.55	0.09	0.93	101
TS-02	23	11.85	0.29	1.83	13.69	0.18	1.12	39
TS-03	25	12.04	0.17	1.71	13.72	0.11	1.12	102
TS-04	25	12.86	0.13	1.47	14.19	0.09	1.03	125
TS-05	20	12.02	0.15	1.75	13.68	0.10	1.11	129
TS-07	19	12.98	0.25	1.14	14.36	0.18	0.81	20
TS-08	20	11.98	0.35	1.99	13.60	0.25	1.46	33
TS-09	23	12.31	0.34	1.54	13.83	0.20	0.92	20
TS-10	21	12.49	0.28	1.72	14.07	0.19	1.13	37
TS-11	22	12.95	0.17	1.42	14.30	0.12	1.02	67
TS-12	20	12.22	0.45	2.14	13.93	0.28	1.33	23
TS-13	21	12.08	0.17	1.73	13.65	0.12	1.21	100
TS-14	25	11.55	0.26	1.79	13.40	0.17	1.18	48
TS-15	20	13.10	0.20	1.55	14.34	0.14	1.11	60

[f] Number of analyzed crystals.
[g] The standard deviation of measured horizontal confined track lengths.
[h] Number of measured horizontal confined track.

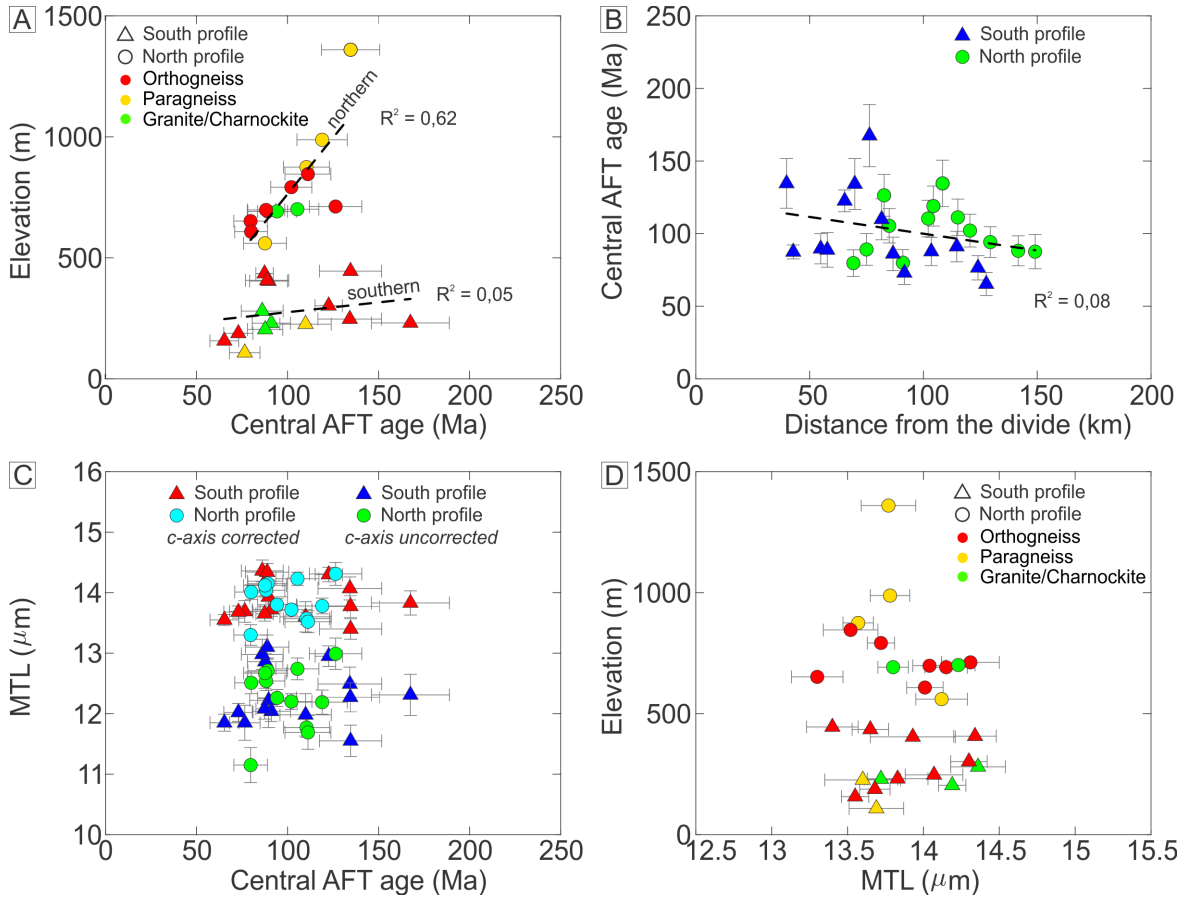

Figure 22 – **Local Plots**. A)Plot of AFT age against elevation; B)Plot of AFT age against distance from the divide; C) Plot of AFT age against MTL; D) Plot of MTL against elevation.

area (Figs. 23A, 23B, and 23C). Note that the oldest samples from southern transect are found at relatively low elevation when compared to the oldest samples of the northern transect. This relationship indicates that the distribution of AFT ages are associated to the morpho-structure (i.e., high-elevation and high relief belt land form) rather than to the values of altitude. In contrast to the interesting correlation between the AFT ages and morphology, the MTL data does not present any clear correlation with the AFT ages (Fig. 22C), nor with the elevation (Figs. 22D, and the relief (Figs. 23B and 23C).

4.3 Discussion

4.3.1 The local denudation pattern

Our new thermochronology data show that the AFT ages vary considerably along the study area. This variation is observed in the W-E direction (i.e., along each transect) and in the S-N direction (i.e., from one transect to the other). Although not directly linked to elevation, the AFT ages tend to increase toward the transect center in both transects. We interpreted this distinct thermochronology pattern as the result of spatially differential cooling in response to

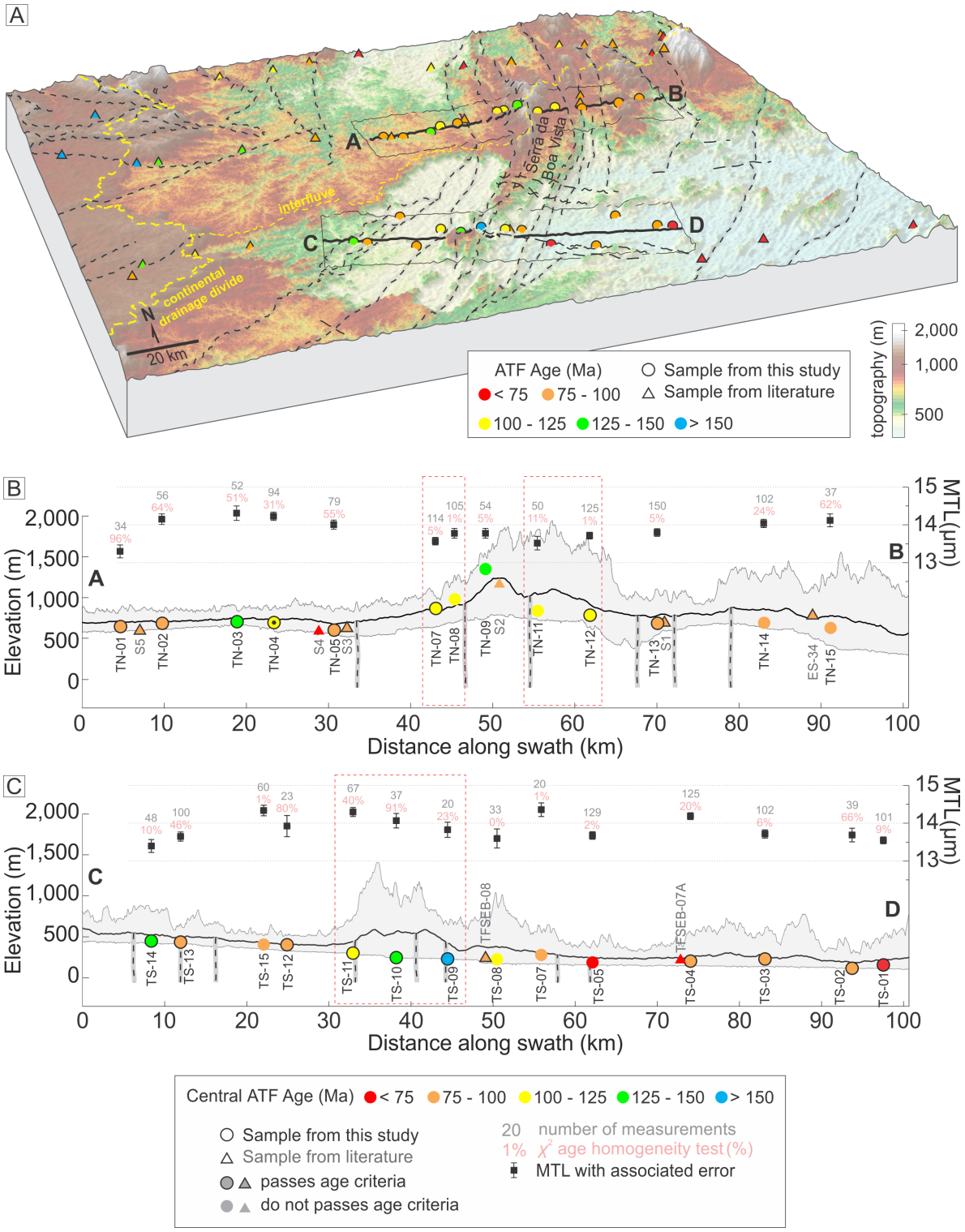

Figure 23 – A) 3D diagram of the digital elevation models of the Serra da Boa Vista region showing the main bedrock tectonic structures, regional and local AFT ages, and the position of the continental drainage divide and the coastal interfluve; B) Topographic Swath profile and the AFT data of the northern transect; C) Topographic Swath profile and the AFT data of the southern transect.

contrasting denudation rates rather than being associated with variations in the thermal reference frame (i.e. isothermal surface) such as the thermal influence of intrusive bodies or effect of the previous topography (cf. Malusà and Fitzgerald, 2019b). The age-elevation trends indicate that the study area's average denudation rates are highly variable. The strongly positive age-elevation correlation with a relatively small degree of dispersion showed by the samples from the northern transect may suggest an average denudation rate of 9.23 m/Ma. This value increases to 20.92 m/Ma if we only consider the samples at the Serra da Boa Vista (TN-07, TN-08, TN-09, TN-11), where the elevation range is maximum. In contrast, the relatively weak positive and highly-dispersed age-elevation trend showed by the samples from the southern transect suggests an average denudation rate of less than 1 m/Ma, and this value is negative if we consider only the samples associated with the Serra da Boa Vista morpho-structure (TS-07, TS-08, TS-09, TS-10).

The Serra da Boa Vista morpho-structure follows the main structural framework (i.e. the NNE-SSW shear zones)(Fig. 23A). The strong correlation between AFT ages and this spatial direction suggests that the bedrock inherited basement structures control the differential exhumation along the Serra da Boa Vista. This association is well illustrated by the samples from the southern transect where AFT ages vary considerably without significant variations in the elevation (Fig. 23C) indicating that the shear zones delimit portion of the crust that has experienced different amount of denudation. In this situation, the relative movement between blocks in response to the reactivation of basement inherited structures has induced differential denudation rates within the study area. Likewise, the differences between the southern and northern transects, mainly the variances regarding the age-elevation trend of different segments of the Serra da Boa Vista, suggest that, besides the influence of the NNE-SSW shear zones, the NW-SE structures (normal faults and other structural lineaments; Figs. 20) may also being reactivated and influenced the local exhumation pattern.

4.3.2 The regional context

Overall, our data agree with the regional thermochronology trends (Fig. 24). The study area is included in the segment of the Brazilian South Atlantic continental margin associated to the Espírito Santo offshore basin. The AFT data for this region characterizes the typical asymmetric denudation profile expected for a mature rifted setting (Fonte-Boa et al., 2022, Chapter 3). In this situation, a continental drainage divide delimits a coastal region, where AFT ages are generally younger or similar to the rifting event (ca. 138 Ma; Pérez-Díaz and Eagles, 2014), from a continental interior area, where AFT ages are older than continental breakup (Fig. 24A). Other important thermochronology pattern is that the post- to syn-rift AFT ages found at the coastal region tend to show a positive correlation with topography, whereas this correlation is not observed in the samples from the continental interior area (Fig. 24B). Great part of our new data, that include samples from both northern and southern transects, agrees with this tendency. This asymmetric denudation pattern is interpreted as the result of the asymmetric

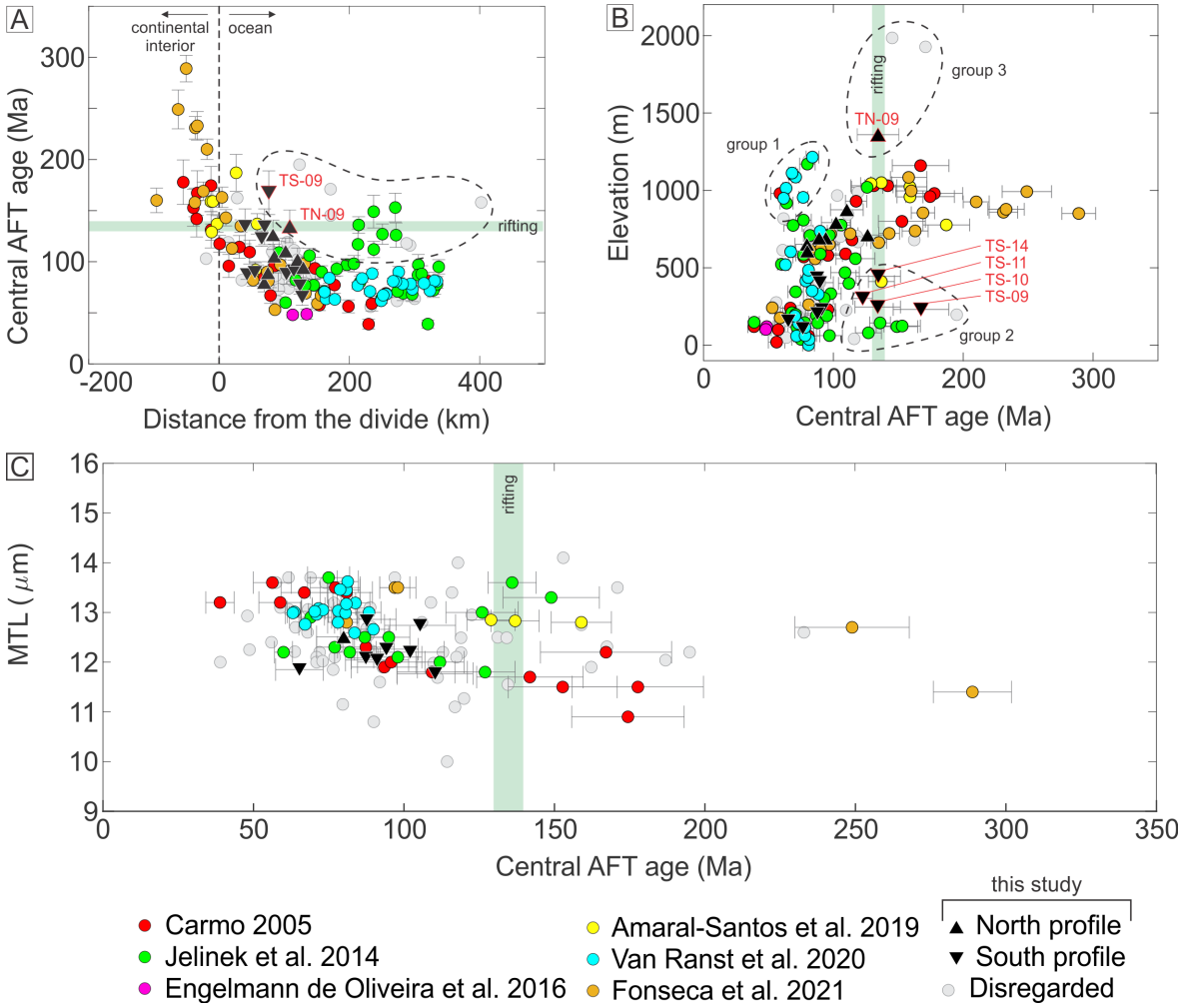

Figure 24 – **Regional apatite fission track plots**. A) Plot of AFT age against distance from divide; B) Plot of AFT age against elevation; C) Plot of AFT age against MTL (i.e., boomerang plot).

exhumation of the coastal region (i.e., area seaward from the continental divide) in comparison to the continental interior (i.e., area inland from the continental divide) in response to the operation of several process during the continental breakup, such as the differential exhumation due to the development of a new baselevel for continental erosion and the associated isostatic rebound.

The samples that stand apart from this general pattern are interpreted as the result of relative movement of blocks (i.e., uplift and subsidence) occurred during the post-rift evolution of the margin. The post-rift ages found at relatively high elevation (group 1 in Fig. 24B) represent areas of the coastal region that experienced uplift, while the low-elevation pre- to syn-rift ages include areas of subsidence (group 2 in Fig. 24B). Several samples from the southern transect agree with group 2 (TS-14, TS-11, TS-10, TS-09) indicating that the southern segment of the Serra da Boa Vista experienced relative subsidence. In the set of pre- to syn-rift ages found in the coast region, a minor number occur at high-elevation (group 3 in Fig. 24B). This specific set of samples generally occurs in high-elevation segments of the coastal interfluves interpreted as coastal less denudated portions that represent secondary water divides that delimits the coastal

drainage basins (i.e., coastal interfluves; Fonte-Boa et al., 2022, chapter 3 of this thesis). That is the case of the sample TS-09, a syn-rift samples located at a high-elevation segment of a costal interfluve (Fig. 24B).

This scenario is also observed in other segments of the Brazilian continental margin (e.g. Serra do Mar region that is adjacent to Santos and Campos offshore basins) and agrees with the local thermochronology pattern discussed before. Previous studies have suggested the importance of the basement inherited structures on the denudation pattern along other segments of the Brazilian South Atlantic continental margin (e.g., Gallagher et al., 1994; Hiruma et al., 2010; Cogné et al., 2011, 2012; Karl et al., 2013). Likewise, van Ranst et al. (2020) highlighted the importance of the inherited NNE-SSW trending structures on the thermochronologic pattern in the study area. However, this is the first time that the link between differential denudation pattern the reactivation of inherited structures is characterized in detail in the continental area related to Espírito Santo offshore basin.

5 General discussion and conclusions

The Brazilian continental margin evolved from the fragmentation of the Gondwana supercontinent after the development of a divergent plate boundary that led to continental rifting and subsequent opening of the South Atlantic Ocean in the Early Cretaceous. After a protracted period of seafloor spreading and continental drifting, this ancient active plate boundary is currently located in the South Atlantic plate interior comprising a segment of the Western South Atlantic passive margin.

The Brazilian thermochronology dataset shows that the southeast Brazilian coast region experienced a great cooling episode agreeing with the South Atlantic rifting phase (i.e., syn-rift phase). This syn-rift cooling event is broadly reported along the margin (Fig.25A) and is mainly associated with the generalized differential exhumation of coast region in response to the processes associated with the rupture of the continental lithosphere (cf. Peron-Pinvidic et al., 2019). This increased syn-rift exhumation resulted in an asymmetrical continental interior-coast denudation profile in which AFT ages tend to increase with elevation and toward the continental interior. The continental drainage divide roughly delimits the coast (i.e., region intensively exhumed after rifting) from the continental interior (i.e., relatively less denudated region). In the region of Serra do Caparaó the syn-rift denudation seems to have reached the east flanks of the Serra do Espinhaço and Quadrilátero Ferrífero region, while, in the region of Serra do Mar, it reached the borders of Poços de Caldas plateau (Fig. 25A).

In contrast to the proposed generic passive continental margins landscape models, the Brazilian coast shows AFT ages significantly younger than rifting event, suggesting that the Brazilian western South Atlantic passive margin segment experienced a surprising higher amount of denudation since continental breakup (e.g. more than 4 km; Gallagher et al., 1994). In addition, thermal models inferred from the thermochronology data frequently shows a pulse of denudation occurring long after rifting event, indicating that an additional transient factor than continued rifting-related denudation may have influenced the exhumation of the western South Atlantic passive margin. However, such empirical data indicate that the this post-rift denudation episode involves successive and spatial-heterogeneous events rather than a well-defined, single, and general event affecting the Brazilian margin as a whole (Figs. 25B and 25C).

A detailed analysis of the age-elevation thermochronology plots suggests that the denudation of the margin was not homogeneous. Some areas of the coastal region were prevented from syn- to post-rift denudation (i.e., relative old AFT ages from the coastal region), and some have experienced relative post-rift uplift/subsidence (i.e., age-elevation plot outliers). Parts of these relatively old coastal areas agree with the high elevation coastal interfluves segments (e.g., the Serra da Bocaina in the region of Serra do Mar; (Hiruma et al., 2010), and the norther segment

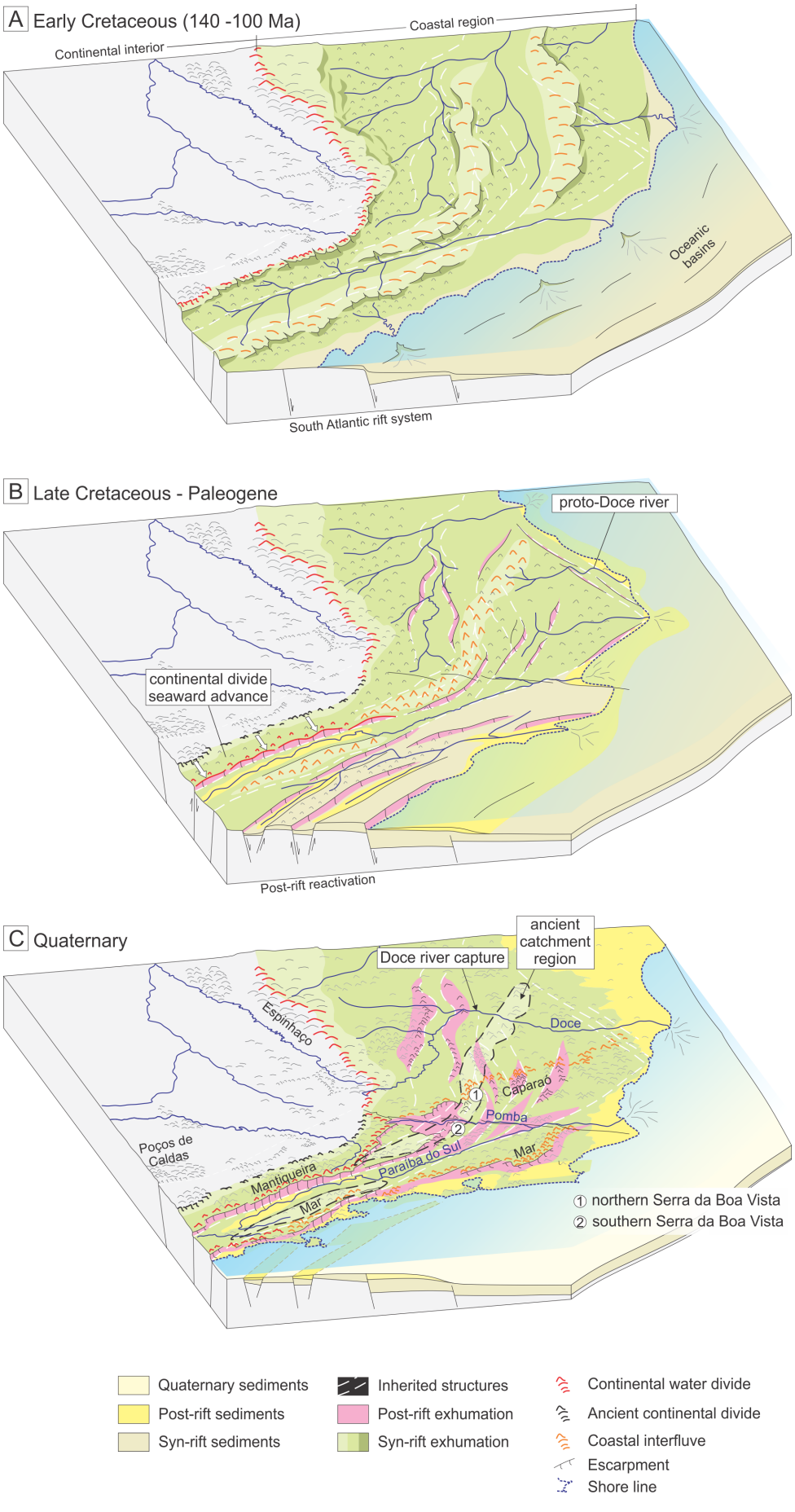
A Early Cretaceous (140 -100 Ma)
Continental interior
Coastal region
Oceanic basins
South Atlantic rift system
B Late Cretaceous - Paleogene
proto-Doce river
continental divide
seaward advance
Post-rift reactivation
C Quaternary
ancient
catchment
region
Doce river capture
Espinhaço
Doce
Caparaó
Pomba
Paraíba do Sul
Mar
Mantiqueira
Poços de
Caldas
① northern Serra da Boa Vista
② southern Serra da Boa Vista
Quaternary sediments
Post-rift sediments
Syn-rift sediments
Inherited structures
Post-rift exhumation
Syn-rift exhumation
Continental water divide
Ancient continental divide
Coastal interfluve
Escarpment
Shore line

Figure 25 – **Sechematic illustration of the evolution of the southeast Brazilian continental margin**. A)Syn-rift phase, highlighting the influence of the basement inherited structures in the rift geometry, and the position of the continental divide and coastal interfluves; B)The post-rift reactivation event(s), showing the relative uplift/subsidence of fault-bounded blocks, the seaward advance of the southern continental divisor segment due to the Serra da Mantiqueira uplift; C)Actual configuration of the coastal drainage system highlighting the position of the ancient interfluve region.

of Serra da Boa Vista in Serra do Capraó), suggesting that these elevated old coastal portions represent ling-lived long-lived catchments segments that, due to small upstream contribution area, have experienced reduced denudation since rifting (see the ancient catchment regions in Fig. 25C). On the other hand, some relative old coastal samples are found at low elevation areas. This old lowered areas include segments of river valleys (e.g., medium Doce river valley, the southern segment of the Serra da Boa Vista drained by Pomba river) and are interpreted as ancient coastal catchment segments that has experienced post-rift subsidence. This relative post-rift uplift/subsidence is associated to intense changes in the coastal drainage system that leads to the capture of Doce and Paraíba do Sul rivers (Cogné et al., 2011; Jelinek et al., 2014; Souza et al., 2019; van Ranst et al., 2020)(Fig. 25C). The contrasting AFT age pattern seems to be linked with the basement structural framework, suggesting that the main ancient lithospheric weaknesses have been reactivated and controlled the post-rift exhumation; that is, relative movement between fault-bounded blocks induced contrasting denudation patterns along the margin. Thus, in addition to the importance of the lithospheric structural framework on rift geometry (Mohriak et al., 2008)(Fig. 25A), inherited structures have accommodated post-rift deformation in response to tilting and relative movement between shear zone-bounded basement blocks (Fig. 25B) triggering drastic changes in the surface runoff and controlling the denudation pattern along the Brazilian South Atlantic continental margin (Fig. 25C).

Differences regarding the morphology and the denudation pattern along Serra do Mar and Serra do Caparaó region suggests that the tectonic evolution of the South Atlantic margin was not uniform. In the segment related to Santos and Campos offshore basins, the continental drainage divide has advanced seaward due to relative post-rift uplift (i.e., faulting). Faulting have also contributed to the maintenance of steep escarpment features along the Serra do Mar and the Serra da Mantiqueira. On the other hand, in the segment related to Espírito Santo offshore basin, the continental drainage divide has been anchored deeply in the continental interior (Serra do Espinhaço) resulting on an unusually wide coastal region with no escarpment morphology (Fig. 25C). Despite the numerous proposed mechanisms operating during the evolution of the margin (e.g., secondary convection cells in the mantle; (Sacek, 2017), underplating magma; (Hackspacher et al., 2004; Gallagher et al., 1994), mantle plume activity (Franco-Magalhaes et al., 2010), 2014, intraplate-wide compressive stress transmitted from the Andean orogeny and the Atlantic spreading axis (Cogné et al., 2011, 2012; Jelinek et al., 2014; Amaral-Santos

et al., 2019; van Ranst et al., 2020; Fonseca et al., 2021) that have contributed for the different geologic histories within different segments of the margin, the tectonic inheritance (i.e, structural framework, lithology, effective flexural strength of the lithosphere) performed a fundamental role in setting up geomorphic diversification along the Brazilian South Atlantic rifted margin.

In this situation, Serra do Caparaó region is interpreted as part of an ancient coastal catchment system developed during the rearrangement of the first order drainage system in response to Gondwana breakup and the opening of the South Atlantic Ocean in Early Cretaceous. By this time, this region may comprise a less denudated and relative elevated region evolved from the reactivation of the inherited N-S shear zones that have controlled the rift geometry (Fig. 25A). The post-rift reactivation of these inherited lithospheric structures during the post-rift evolution of the margin resulted in local uplift/subsidence and the intense reconfiguration of the drainage system geometry (Fig. 25B). Nowadays, Serra do Caparaó comprises a high elevation portion of the coastal interfluve that includes segments of long-lived syn-rift coastal catchment (e.g., northern segment of Serra da Boa Vista; (1) in Fig. 25C) and uplifted syn-rift costal valleys.

Bibliography

Ahnert, F. (1970). Functional relationships between denudation, relief, and uplift in large, mid-latitude drainage basins. *American Journal of Science*, 268(3):243–263.

Alkmim, F. F. & Marshak, S. (1998). Transamazonian orogeny in the Southern São Francisco craton region, Minas Gerais, Brazil: evidence for Paleoproterozoic collision and collapse in the Quadrilátero Ferrífero. *Precambrian Research*, 90(1-2):29–58.

Alkmim, F. F., Marshak, S., Pedrosa-Soares, A. C., Peres, G. G., Cruz, S. C. P., & Whittington, A. (2006). Kinematic evolution of the Araçuaí-West Congo orogen in Brazil and Africa: Nutcracker tectonics during the Neoproterozoic assembly of Gondwana. *Precambrian research*, 149(1-2):43–64.

Almeida, F., Hasui, Y., de Brito Neves, B., & Fuck, R. A. (1981). Brazilian structural provinces: an introduction. *Earth-Science Reviews*, 17:1–29.

Almeida, F. F. M. (1976). The system of continental rifts bordering the Santos basin, Brazil. *An. Acad. Bras. Cienc.*, 48:15–26.

Amaral, G., Born, H., Hadler, J., Iunes, P., Kawashita, K., Machado Jr, D., Oliveira, E., Paulo, S., & Tello, C. (1997). Fission track analysis of apatites from São Francisco craton and Mesozoic alcaline-carbonatite complexes from central and southeastern Brazil. *Journal of South American Earth Sciences*, 10(3-4):285–294.

Amaral-Santos, E., Jelinek, A., Almeida-Abreu, P., & Genezine, F. (2019). Phanerozoic cooling history of Archean/Paleoproterozoic basement in the southern Espinhaço range, southeastern Brazil, through apatite fission-track analysis. *Journal of South American Earth Sciences*, 96:102352.

Araujo, L. E. d. A. B., Heilbron, M., Teixeira, W., Dussin, I. A., de Morisson Valeriano, C., Bruno, H., Sato, K., Paravidini, G., & Castro, M. (2021). Siderian to Rhyacian evolution of the Juiz de Fora Complex: Arc fingerprints and correlations within the Minas-Bahia Orogen and the Western Central Africa Belt. *Precambrian Research*, 359:106118.

Armitage, J., Jaupart, C., Fourel, L., & Allen, P. (2013). The instability of continental passive margins and its effect on continental topography and heat flow. *Journal of Geophysical Research: Solid Earth*, 118(4):1817–1836.

Asmus, H. & Ponte, F. (1973). The brazilian marginal basins. In: *The ocean basins and margins - The South Atlantic*, volume 1, chapter 3, pages 87–133. Springer.

Asmus, H. & Porto, R. (1972). Classificação das bacias sedimentares brasileiras segundo a tectônica de placas. In: *Congresso Brasileiro de Geologia*, volume 26, pages 67–90.

Ávila, C. A., Teixeira, W., Cordani, U. G., Moura, C. A. V., & Pereira, R. M. (2010). Rhyacian (2.23–2.20 ga) juvenile accretion in the southern São Francisco craton, Brazil: Geochemical and isotopic evidence from the Serrinha magmatic suite, Mineiro belt. *Journal of South American Earth Sciences*, 29(2):464–482.

Bally, A., Roberts, D., Sawyer, D., & Sinkewich, A. (2012). Tectonic and basin maps of the world. In: *Regional Geology and Tectonics: Phanerozoic Passive Margins, Cratonic Basins and Global Tectonic Maps*, pages 970–1151. Elsevier.

Barbarand, J., Hurford, T., & Carter, A. (2003). Variation in apatite fission-track length measurement: implications for thermal history modelling. *Chemical Geology*, 198(1-2):77–106.

Barreto, H. N., Varajão, C. A., Braucher, R., Bourlès, D. L., Salgado, A. A., & Varajão, A. F. (2013). Denudation rates of the Southern Espinhaço range, Minas Gerais, Brazil, determined by in situ-produced cosmogenic beryllium-10. *Geomorphology*, 191:1–13.

Batezelli, A. & Ladeira, F. S. B. (2016). Stratigraphic framework and evolution of the Cretaceous continental sequences of the Bauru, Sanfranciscana, and Parecis basins, Brazil. *Journal of South American Earth Sciences*, 65:1–24.

Behling, H. (2002). South and southeast Brazilian grasslands during Late Quaternary times: a synthesis. *Palaeogeography, Palaeoclimatology, Palaeoecology*, 177(1-2):19–27.

Bezerra, F. H. & Vita-Finzi, C. (2000). How active is a passive margin? Paleoseismicity in northeastern Brazil. *Geology*, 28(7):591–594.

Bishop, P. (2007). Long-term landscape evolution: linking tectonics and surface processes. *Earth Surface Processes and Landforms: the Journal of the British Geomorphological Research Group*, 32(3):329–365.

Boone, S. C., Kohn, B. P., Gleadow, A. J., Morley, C. K., Seiler, C., & Foster, D. A. (2019). Birth of the East African Rift System: Nucleation of magmatism and strain in the Turkana Depression. *Geology*, 47(9):886–890.

Bradley, D. C. (2008). Passive margins through earth history. *Earth-Science Reviews*, 91(1-4):1–26.

Braun, J. (2018). A review of numerical modeling studies of passive margin escarpments leading to a new analytical expression for the rate of escarpment migration velocity. *Gondwana Research*, 53:209–224.

Braun, J. (2019). Response to comment by Japsen et al. on "A review of numerical modeling studies of passive margin escarpments leading to a new analytical expression for the rate of escarpment migration velocity". *Gondwana Research*, 65:174–176.

Braun, J. & Beaumont, C. (1989). A physical explanation of the relation between flank uplifts and the breakup unconformity at rifted continental margins. *Geology*, 17(8):760–764.

Braun, J., Simon-Labric, T., Murray, K. E., & Reiners, P. W. (2014). Topographic relief driven by variations in surface rock density. *Nature Geoscience*, 7(7):534–540.

Braun, J. & van der Beek, P. (2004). Evolution of passive margin escarpments: What can we learn from low-temperature thermochronology? *Journal of Geophysical Research: Earth Surface*, 109:F04009.

Brown, R. W., Summerfield, M. A., & Gleadow, A. J. (2002). Denudational history along a transect across the Drakensberg Escarpment of southern Africa derived from apatite fission track thermochronology. *Journal of Geophysical Research: Solid Earth*, 107(B12):2350.

Brune, S. (2016). Rifts and rifted margins: A review of geodynamic processes and natural hazards. *Plate Boundaries and Natural Hazards*, 219:13.

Bruno, H., Elizeu, V., Heilbron, M., de Morisson Valeriano, C., Strachan, R., Fowler, M., Bersan, S., Moreira, H., Dussin, I., do Eirado Silva, L. G., et al. (2020). Neoarchean and Rhyacian TTG-Sanukitoid suites in the southern São Francisco Paleocontinent, Brazil: evidence for diachronous change towards modern tectonics. *Geoscience Frontiers*, 11(5):1763–1787.

Calegari, S. S., Neves, M. A., Guadagnin, F., França, G. S., & Vincentelli, M. G. C. (2016). The Alegre Lineament and its role over the tectonic evolution of the Campos Basin and adjacent continental margin, Southeastern Brazil. *Journal of South American Earth Sciences*, 69:226–242.

Calegari, S. S., Peifer, D., Neves, M. A., & de Andrade Caxito, F. (2021). Post-Miocene topographic rejuvenation in an elevated passive continental margin not characterized by a sharp escarpment (northern end of the Mantiqueira Range, Brazil). *Geomorphology*, 393:107946.

Carlson, W. D., Donelick, R. A., & Ketcham, R. A. (1999). Variability of apatite fission-track annealing kinetics: I. experimental results. *American mineralogist*, 84(9):1213–1223.

Carmo, I. d. O. (2005). *Geocronologia do intemperismo Cenozóico no sudeste do Brasil*. PhD thesis, Universidade Federal do Rio de Janeiro.

Caxito, F., Heilbron, M., Valeriano, C., Bruno, H., Pedrosa-Soares, A., Alkmim, F., Chemale, F., Hartmann, L., Dantas, E., & Basei, M. (2021). Integration of elemental and isotope data supports a Neoproterozoic Adamastor Ocean realm. *Geochemical Perspectives Letters*, 17:6–10.

Chang, H. K., Kowsmann, R. O., Figueiredo, A. M. F., & Bender, A. (1992). Tectonics and stratigraphy of the East Brazil Rift system: an overview. *Tectonophysics*, 213(1-2):97–138.

Chemale Jr, F., Dussin, I. A., Alkmim, F. F., Martins, M. S., Queiroga, G., Armstrong, R., & Santos, M. N. (2012). Unravelling a Proterozoic basin history through detrital zircon geochronology: the case of the Espinhaço Supergroup, Minas Gerais, Brazil. *Gondwana Research*, 22(1):200–206.

Codilean, A. T., Fülöp, R.-H., Munack, H., Wilcken, K. M., Cohen, T. J., Rood, D. H., Fink, D., Bartley, R., Croke, J., & Fifield, L. (2021). Controls on denudation along the East Australian continental margin. *Earth-Science Reviews*, 214:103543.

Cogné, N., Chew, D. M., Donelick, R. A., & Ansberque, C. (2020). LA-ICP-MS apatite fission track dating: A practical zeta-based approach. *Chemical Geology*, 531:119302.

Cogné, N., Cobbold, P. R., Riccomini, C., & Gallagher, K. (2013). Tectonic setting of the Taubaté Basin (Southeastern Brazil): Insights from regional seismic profiles and outcrop data. *Journal of South American Earth Sciences*, 42:194–204.

Cogné, N., Gallagher, K., & Cobbold, P. R. (2011). Post-rift reactivation of the onshore margin of southeast Brazil: Evidence from apatite (U–Th)/He and fission-track data. *Earth and Planetary Science Letters*, 309(1-2):118–130.

Cogné, N., Gallagher, K., Cobbold, P. R., Riccomini, C., & Gautheron, C. (2012). Post-breakup tectonics in southeast Brazil from thermochronological data and combined inverse-forward thermal history modeling. *Journal of Geophysical Research: Solid Earth*, 117(B11).

Cordani, U. G., Brito-Neves, B. B., & D'Agrella-Filho, M. S. (2003). From Rodinia to Gondwana: a review of the available evidence from South America. *Gondwana Research*, 6(2):275–283.

Cox, R., Košler, J., Sylvester, P., & Hodych, J. (2000). Apatite fission-track (FT) dating by LA-ICP-MS analysis. In: *Goldschmidt Conference, Oxford, UK: Journal of Conference Abstracts*, volume 5, page 322.

Crowley, K., Cameron, M., & Schaefer, R. (1991). Experimental studies of annealing of etched fission tracks in fluorapatite. *Geochimica et Cosmochimica Acta*, 55(5):1449–1465.

Dias, A., Guadagnin, F., Rangel, C., Chemale, F., Oliveira, T., Moura, C., Pereira, V., & Alves, J. (2021). Provenance of Neogene deposits of Barreiras Formation in the southeastern Brazilian continental margin. *International Journal of Earth Sciences*, 110:233–249.

Divins, D. (2003). Total sediment thickness of the world's oceans & marginal seas. *NOAA National Geophysical Data Center, Boulder, CO*.

Dodson, M. H. (1973). Closure temperature in cooling geochronological and petrological systems. *Contributions to Mineralogy and Petrology*, 40(3):259–274.

Donelick, R. A. (1991). Crystallographic orientation dependence of mean etchable fission track length in apatite: An empirical model and experimental observations. *American Mineralogist*, 76(1-2):83–91.

Donelick, R. A., Ketcham, R. A., & Carlson, W. D. (1999). Variability of apatite fission-track annealing kinetics: II. crystallographic orientation effects. *American Mineralogist*, 84(9):1224–1234.

Donelick, R. A., O'Sullivan, P. B., & Ketcham, R. A. (2005). Apatite fission-track analysis. *Reviews in Mineralogy and Geochemistry*, 58(1):49–94.

Egydio-Silva, M., Vauchez, A., Fossen, H., Cavalcante, G. C. G., & Xavier, B. C. (2018). Connecting the Araçuaí and Ribeira belts (SE–Brazil): Progressive transition from contractional to transpressive strain regime during the Brasiliano orogeny. *Journal of South American Earth Sciences*, 86:127–139.

Engelmann de Oliveira, C. H., Jelinek, A. R., Chemale Jr, F., & Cupertino, J. A. (2016). Thermotectonic history of the southeastern Brazilian margin: Evidence from apatite fission track data of the offshore Santos basin and continental basement. *Tectonophysics*, 685:21–34.

Engelmann de Oliveira, C. H., Jelinek, A. R., Timoteo, D., & Bernet, M. (2018). Thermotectonic history of the Maastrichtian reservoir in Campos basin. *Marine and Petroleum Geology*, 93:331–343.

England, P. & Molnar, P. (1990). Surface uplift, uplift of rocks, and exhumation of rocks. *Geology*, 18(12):1173–1177.

Ernesto, M., Marques, L., Piccirillo, E., Molina, E., Ussami, N., Comin-Chiaramonti, P., & Bellieni, G. (2002). Paraná Magmatic Province–Tristan da Cunha plume system: fixed versus mobile plume, petrogenetic considerations and alternative heat sources. *Journal of Volcanology and Geothermal Research*, 118(1-2):15–36.

Fermi, E. (1934). *Possible production of elements of atomic number higher than 92*. Macmillan & Company.

Figueiredo, A. & Gabaglia, G. (1986). Sistema classificatorio applicado as bacias sedimentares brasileiras. *Revista Brasileira de Geociências*, 16:350–369.

Fleischer, R., Price, P., & Walker, R. (1965a). Effects of temperature, pressure, and ionization of the formation and stability of fission tracks in minerals and glasses. *Journal of Geophysical Research*, 70(6):1497–1502.

Fleischer, R. L., Price, P. B., & Walker, R. M. (1965b). Tracks of charged particles in solids. *Science*, 149(3682):383–393.

Fleischer, R. L., Price, P. B., Walker, R. M., & Walker, R. M. (1975). *Nuclear tracks in solids: principles and applications*. Univ of California Press.

Fonseca, A. C. L., Novo, T. A., Nachtergaele, S., Fonte-Boa, T. M. R., Van Ranst, G., & De Grave, J. (2021). Differential Phanerozoic evolution of cratonic and non-cratonic lithosphere from a thermochronological perspective: São Francisco Craton and marginal orogens (Brazil). *Gondwana Research*, 93:106–126.

Fontainha, M. V., Trouw, R. A., Dantas, E. L., Polo, H. J., Serafim, I. C., Furtado, P. C., & Negrão, A. P. (2021). Reactivated shear zones: A case study in a tectonic superposition zone between the Southern Brasília and Ribeira orogens, southeastern Brazil. *Journal of South American Earth Sciences*, 112:103537.

França, R., Del Rey, A., Tagliari, C., Brandão, J., & Fontanelli, P. (2007). Bacia do Espírito Santo. *B. Geoci. Petrobras*, 2(15):501–509.

Franco, A. O. B., Hackspacher, P. C., de Godoy, D. F., Ribeiro, L. F. B., & Guedes, S. (2005). História térmica do Maciço Alcalino de Poços de Caldas (SP/MG) e adjacências através da análise de datação por traços de fissão em apatitas. *Revista Brasileira de Geociências*, 35(3):351–358.

Franco-Magalhaes, A., Cuglieri, M., Hackspacher, P., & Saad, A. (2014). Long-term landscape evolution and post-rift reactivation in the southeastern Brazilian passive continental margin: Taubaté basin. *International Journal of Earth Sciences*, 103(2):441–453.

Franco-Magalhaes, A. O., Hackspacher, P. C., Glasmacher, U. A., & Saad, A. (2010). Rift to post-rift evolution of a "passive" continental margin: the Ponta Grossa arch, SE Brazil. *International Journal of Earth Sciences*, 99(7):1599–1613.

Frisch, W., Meschede, M., & Blakey, R. (2011). Passive continental margins and abyssal plains. In: *Plate Tectonics*, pages 43–57. Springer.

Galbraith, R. F. (2002). Some remarks on fission-track observational biases and crystallographic orientation effects. *American Mineralogist*, 87(7):991–995.

Galbraith, R. F. (2005). *Statistics for fission track analysis*. CRC Press.

Gallagher, K. (1995). Evolving temperature histories from apatite fission-track data. *Earth and Planetary Science Letters*, 136(3-4):421–435.

Gallagher, K. (2012). Transdimensional inverse thermal history modeling for quantitative thermochronology. *Journal of Geophysical Research: Solid Earth*, 117(B2).

Gallagher, K. & Brown, R. (1997). The onshore record of passive margin evolution. *Journal of the Geological Society*, 154(3):451–457.

Gallagher, K. & Brown, R. (1999). The Mesozoic denudation history of the Atlantic margins of southern Africa and southeast Brazil and the relationship to offshore sedimentation. *Geological Society, London, Special Publications*, 153(1):41–53.

Gallagher, K., Brown, R., & Johnson, C. (1998). Fission track analysis and its applications to geological problems. *Annual Review of Earth and Planetary Sciences*, 26(1):519–572.

Gallagher, K., Hawkesworth, C., & Mantovani, M. (1994). The denudation history of the onshore continental margin of SE Brazil inferred from apatite fission track data. *Journal of Geophysical Research: Solid Earth*, 99(B9):18117–18145.

Gallagher, K. & Sambridge, M. (1994). Genetic algorithms: a powerful tool for large-scale nonlinear optimization problems. *Computers & Geosciences*, 20(7-8):1229–1236.

Gallagher, K., Sambridge, M., & Drijkoningen, G. (1991). Genetic algorithms: An evolution from Monte Carlo Methods for strongly non-linear geophysical optimization problems. *Geophysical Research Letters*, 18(12):2177–2180.

Gezatt, J., Macdonald, D., Stephenson, R., Jelinek, A. R., & Carter, A. (2021). South Atlantic passive margin evolution: A thermochronology case study from the Rio de Janeiro-três Rios section, SE Brazil. *Journal of South American Earth Sciences*, 106:103051.

Gilchrist, A. & Summerfield, M. (1990). Differential denudation and flexural isostasy in formation of rifted-margin upwarps. *Nature*, 346(6286):739–742.

Gilchrist, A. R., Kooi, H., & Beaumont, C. (1994). Post-gondwana geomorphic evolution of southwestern Africa: Implications for the controls on landscape development from observations and numerical experiments. *Journal of Geophysical Research: Solid Earth*, 99(B6):12211–12228.

Gleadow, A. (1981). Fission-track dating methods: what are the real alternatives? *Nuclear Tracks*, 5(1-2):3–14.

Gleadow, A. & Duddy, I. (1981). A natural long-term track annealing experiment for apatite. *Nuclear tracks*, 5(1-2):169–174.

Gleadow, A., Duddy, I., & Lovering, J. (1983). Fission track analysis: a new tool for the evaluation of thermal histories and hydrocarbon potential. *The APPEA Journal*, 23(1):93–102.

Green, P. (1981). "Track-in-track" length measurements in annealed apatites. *Nuclear Tracks*, 5(1-2):121–128.

Green, P., Duddy, I., Gleadow, A., Tingate, P., & Laslett, G. (1985). Fission-track annealing in apatite: track length measurements and the form of the Arrhenius plot. *Nuclear Tracks and Radiation Measurements (1982)*, 10(3):323–328.

Green, P., Duddy, I., Gleadow, A., Tingate, P., & Laslett, G. (1986). Thermal annealing of fission tracks in apatite: 1. A qualitative description. *Chemical Geology: Isotope Geoscience Section*, 59:237–253.

Green, P. & Durrani, S. (1977). Annealing studies of tracks in crystals. *Nuclear Track Detection*, 1(1):33–39.

Green, P. F., Japsen, P., Chalmers, J. A., Bonow, J. M., & Duddy, I. R. (2018). Post-breakup burial and exhumation of passive continental margins: Seven propositions to inform geodynamic models. *Gondwana Research*, 53:58–81.

Green, P. F., Lidmar-Bergström, K., Japsen, P., Bonow, J. M., & Chalmers, J. A. (2013). Stratigraphic landscape analysis, thermochronology and the episodic development of elevated, passive continental margins. *Geological Survey of Denmark & Greenland Bulletin*, 30.

Gunnell, Y. & Harbor, D. (2010). Butte detachment: how pre-rift geological structure and drainage integration drive escarpment evolution at rifted continental margins. *Earth Surface Processes and Landforms*, 35(12):1373–1385.

Guth, P. L. & Geoffroy, T. M. (2021). LiDAR point cloud and ICESat-2 evaluation of 1 second global digital elevation models: Copernicus wins. *Transactions in GIS*, 25(5):2245–2261.

Hackspacher, P., Ribeiro, L., Ribeiro, M., Fetter, A., Neto, J. H., Tello, C., & Dantas, E. (2004). Consolidation and break-up of the South American platform in southeastern Brazil: tectonothermal and denudation histories. *Gondwana Research*, 7(1):91–101.

Hanna, G., Westcott, C., Lemmel, H., Leonard Jr, B., Story, J., & Attree, P. (1969). Revision of values for the 2200 m/s neutron constants for four fissile nuclides. Technical report, International Atomic Energy Agency.

Hasebe, N., Barbarand, J., Jarvis, K., Carter, A., & Hurford, A. J. (2004). Apatite fission-track chronometry using laser ablation ICP-MS. *Chemical Geology*, 207(3-4):135–145.

Heilbron, M., Cordani, U. G., & Alkmim, F. F. (2017). *The São Francisco craton and its margins*. Springer.

Heilbron, M., Duarte, B. P., de Morisson Valeriano, C., Simonetti, A., Machado, N., & Nogueira, J. R. (2010). Evolution of reworked Paleoproterozoic basement rocks within the Ribeira belt (Neoproterozoic), SE-Brazil, based on U –Pb geochronology: Implications for paleogeographic reconstructions of the são Francisco-Congo paleocontinent. *Precambrian Research*, 178(1-4):136–148.

Heilbron, M., Pedrosa-Soares, A. C., Campos Neto, M. d. C., Silva, L. d., Trouw, R. A. J., & Janasi, V. d. A. (2004). Província mantiqueira. In: *Geologia do continente sul-americano: evolução da obra de Fernando Flávio Marques de Almeida*, pages 203–235. Beca São Paulo.

Heilbron, M., Valeriano, C., Tassinari, C., Almeida, J., Tupinambá, M., Siga, O., & Trouw, R. (2008). Correlation of Neoproterozoic terranes between the Ribeira belt, SE Brazil and its African counterpart: comparative tectonic evolution and open questions. *Geological Society, London, Special Publications*, 294(1):211–237.

Hiruma, S. T., Riccomini, C., Modenesi-Gauttieri, M. C., Hackspacher, P. C., Neto, J. C. H., & Franco-Magalhães, A. O. (2010). Denudation history of the Bocaina Plateau, Serra do Mar, southeastern Brazil: Relationships to Gondwana breakup and passive margin development. *Gondwana Research*, 18(4):674–687.

Huismans, R. & Beaumont, C. (2011). Depth-dependent extension, two-stage breakup and cratonic underplating at rifted margins. *Nature*, 473(7345):74–78.

Hurford, A. J. (2019). An historical perspective on fission-track thermochronology. In: *Fission-Track Thermochronology and its application to geology*, pages 3–23. Springer.

Hurford, A. J. & Green, P. F. (1982). A users' guide to fission track dating calibration. *Earth and Planetary Science Letters*, 59(2):343–354.

Hurford, A. J. & Green, P. F. (1983). The zeta age calibration of fission-track dating. *Chemical Geology*, 41:285–317.

Janasi, V. A., de Freitas, V. A., & Heaman, L. H. (2011). The onset of flood basalt volcanism, Northern Paraná Basin, Brazil: a precise U–Pb baddeleyite/zircon age for a Chapecó-type dacite. *Earth and Planetary Science Letters*, 302(1-2):147–153.

Japsen, P., Bonow, J. M., Green, P. F., Chalmers, J. A., & Lidmar-Bergström, K. (2006). Elevated, passive continental margins: Long-term highs or Neogene uplifts? New evidence from West Greenland. *Earth and Planetary Science Letters*, 248(1-2):330–339.

Japsen, P. & Chalmers, J. A. (2000). Neogene uplift and tectonics around the north atlantic: overview. *Global and Planetary Change*, 24(3-4):165–173.

Japsen, P., Chalmers, J. A., Green, P. F., & Bonow, J. M. (2012). Elevated, passive continental margins: Not rift shoulders, but expressions of episodic, post-rift burial and exhumation. *Global and Planetary Change*, 90:73–86.

Japsen, P., Green, P. F., Chalmers, J. A., Duddy, I., & Bonow, J. M. (2019). Elevated passive continental margins: Numerical modeling vs observations. A comment on Braun (2018). *Gondwana Research*, 65:172–173.

Jelinek, A., Chemale Jr, F., van der Beek, P., Guadagnin, F., Cupertino, J., & Viana, A. (2014). Denudation history and landscape evolution of the northern east-Brazilian continental margin from apatite fission-track thermochronology. *Journal of South American Earth Sciences*, 54:158–181.

Jonckheere, R., Wauschkuhn, B., & Ratschbacher, L. (2019). On growth and form of etched fission tracks in apatite: A kinetic approach. *American Mineralogist: Journal of Earth and Planetary Materials*, 104(4):569–579.

Karl, M., Glasmacher, U. A., Kollenz, S., Franco-Magalhaes, A. O., Stockli, D. F., & Hackspacher, P. C. (2013). Evolution of the South Atlantic passive continental margin in southern Brazil derived from zircon and apatite (U–Th–Sm)/He and fission-track data. *Tectonophysics*, 604:224–244.

Ketcham, R. A. (2003). Observations on the relationship between crystallographic orientation and biasing in apatite fission-track measurements. *American Mineralogist*, 88(5-6):817–829.

Ketcham, R. A., Carter, A., Donelick, R. A., Barbarand, J., & Hurford, A. J. (2007). Improved modeling of fission-track annealing in apatite. *American Mineralogist*, 92(5-6):799–810.

Kooi, H. & Beaumont, C. (1994). Escarpment evolution on high-elevation rifted margins: Insights derived from a surface processes model that combines diffusion, advection, and reaction. *Journal of Geophysical Research: Solid Earth*, 99(B6):12191–12209.

Krob, F. C., Glasmacher, U. A., Karl, M., Perner, M., Hackspacher, P. C., & Stockli, D. F. (2019). Multi-chronometer thermochronological modelling of the Late Neoproterozoic to recent tT-evolution of the SE coastal region of Brazil. *Journal of South American Earth Sciences*, 92:77–94.

Kusznir, N. & Ziegler, P. (1992). The mechanics of continental extension and sedimentary basin formation: a simple-shear/pure-shear flexural cantilever model. *Tectonophysics*, 215(1-2):117–131.

Lal, D., Rajan, R., & Tamhane, A. (1969). Chemical composition of nuclei of Z> 22 in cosmic rays using meteoritic minerals as detectors. *Nature*, 221(5175):33–37.

Laslett, G., Gleadow, A., & Duddy, I. (1984). The relationship between fission track length and track density in apatite. *Nuclear Tracks and Radiation Measurements (1982)*, 9(1):29–38.

Laslett, G., Green, P. F., Duddy, I., & Gleadow, A. (1987). Thermal annealing of fission tracks in apatite 2. A quantitative analysis. *Chemical Geology: Isotope Geoscience Section*, 65(1):1–13.

Lister, G., Etheridge, M., & Symonds, P. (1991). Detachment models for the formation of passive continental margins. *Tectonics*, 10(5):1038–1064.

Lutz, T. M. & Omar, G. (1991). An inverse method of modeling thermal histories from apatite fission-track data. *Earth and Planetary Science Letters*, 104(2-4):181–195.

Malusà, M. G. & Fitzgerald, P. G. (2019a). *Fission-track thermochronology and its application to geology*. Springer.

Malusà, M. G. & Fitzgerald, P. G. (2019b). From cooling to exhumation: setting the reference frame for the interpretation of thermochronologic data. In: *Fission-track thermochronology and its application to geology*, pages 147–164. Springer.

Matmon, A., Bierman, P., & Enzel, Y. (2002). Pattern and tempo of great escarpment erosion. *Geology*, 30(12):1135–1138.

McKenzie, D. (1978). Some remarks on the development of sedimentary basins. *Earth and Planetary science letters*, 40(1):25–32.

McKenzie, D. (1984). A possible mechanism for epeirogenic uplift. *Nature*, 307(5952):616–618.

Meitner, L. & Frisch, O. R. (1939). Disintegration of uranium by neutrons: a new type of nuclear reaction. *Nature*, 143(3615):239–240.

Mello, C. L. (1997). *Sedimentação e tectônica cenozóicas no Médio Vale do Rio Doce (MG, Sudeste do Brasil) e suas implicações na evolução de um sistema de lagos*. PhD thesis, Universidade de São Paulo.

Mello, C. L., Metelo, C. M. S., Suguio, K., & KOHLER, H. C. (1999). Quaternary sedimentation, neotectonics and the evolution of the doce river middle valley lake system (southeastern Brazil). *Revista do Instituto Geológico*, 20(1-2):29–36.

Melo, M., Riccomini, C., Hasui, Y., Almeida, F., & Coimbra, A. (1985). Geologia e evolução do sistema de bacias tafrogênicas continentais do sudeste do Brasil. *Revista Brasileira de Geociências*, 15(3):193–201.

Menegazzo, M. C., Catuneanu, O., & Chang, H. K. (2016). The south american retroarc foreland system: the development of the Bauru Basin in the back-bulge province. *Marine and Petroleum Geology*, 73:131–156.

Milani, E. J. & Thomaz Filho, A. (2000). Sedimentary basins of South America. *Tectonic Evolution of South America*, 31:389–449.

Mohriak, W., Nemčok, M., & Enciso, G. (2008). South Atlantic divergent margin evolution: rift-border uplift and salt tectonics in the basins of SE Brazil. *Geological Society, London, Special Publications*, 294(1):365–398.

Montgomery, D. R. & Brandon, M. T. (2002). Topographic controls on erosion rates in tectonically active mountain ranges. *Earth and Planetary Science Letters*, 201(3-4):481–489.

Moreira, J., Madeira, C., Gil, J., & Machado, M. (2007). Bacia de Santos. *B. Geoci. Petrobras*, 2(15):531–549.

Moulin, M., Aslanian, D., & Unternehr, P. (2010). A new starting point for the South and Equatorial Atlantic Ocean. *Earth-Science Reviews*, 98(1-2):1–37.

Negrão, A. P., Mello, C. L., Ramos, R. R. C., Sanson, M. d. S. R., Louro, V. H. A., & Bauli, P. G. (2020). Tectonosedimentary evolution of the resende and Volta Redonda basins (Cenozoic, central segment of the Continental Rift of Southeastern Brazil). *Journal of South American Earth Sciences*, 104:102789.

Nóbrega, M., Sá, J., Bezerra, F., Neto, J. H., Iunes, P. J., Guedes, S., Saenz, C. T., Hackspacher, P., & Lima-Filho, F. (2005). The use of apatite fission track thermochronology to constrain fault movements and sedimentary basin evolution in northeastern Brazil. *Radiation Measurements*, 39(6):627–633.

Noce, C. M., Pedrosa-Soares, A. C., da Silva, L. C., Armstrong, R., & Piuzana, D. (2007). Evolution of polycyclic basement complexes in the Araçuaí Orogen, based on U–Pb SHRIMP data: Implications for Brazil–Africa links in Paleoproterozoic time. *Precambrian Research*, 159(1-2):60–78.

Noce, C. M., Romano, A., Pinheiro, C., Mol, V., & Pedrosa-Soares, A. (2003). Geologia das folhas Ubá e Muriaé. *Projeto Sul de Minas–Etapa I: Geologia e Recursos Minerais do Sudeste Mineiro, Belo Horizonte, COMIG/UFMG/UFRJ/UERJ, Cap.*, 12:623–659.

Novo, T., Fonte-Boa, T., Rolim, J., & Fonseca, A. C. (2021). The state of the art of Low-temperature Thermochronology in Brazil. *Journal of the Geological Survey of Brazil*, 4(3):239–256.

Ollier, C. (1982). The great escarpment of eastern australia: tectonic and geomorphic significance. *Journal of the Geological Society of Australia*, 29(1-2):13–23.

Ollier, C. & Pain, C. (1997). Equating the basal unconformity with the palaeoplain: a model for passive margins. *Geomorphology*, 19(1-2):1–15.

Paton, D. (2012). Post-rift deformation of the north east and south atlantic margins: Are "passive margins" really passive? *Tectonics of sedimentary basins: recent advances*, pages 249–269.

Pedrosa-Soares, A., De Campos, C. P., Noce, C., Silva, L. C., Novo, T., Roncato, J., Medeiros, S., Castañeda, C., Queiroga, G., Dantas, E., Dussin, I., & Alkmim, F. (2011). Late Neoproterozoic-Cambrian granitic magmatism in the Araçuaí orogen (Brazil), the Eastern Brazilian Pegmatite Province and related mineral resources. *Geological Society, London, Special Publications*, 350(1):25–51.

Pedrosa-Soares, A. C., Alkmim, F., Tack, L., Noce, C. M., Babinski, M., Silva, L. C. d., & Martins-Neto, M. (2008). Similarities and differences between the Brazilian and African counterparts of the Neoproterozoic Araçuaí-West Congo orogen. *Geological Society, London, Special Publications*, 294(1):153–172.

Pedrosa-Soares, A. C., Noce, C., Wiedemann, C., & Pinto, C. P. (2001). The Araçuaı-West-Congo Orogen in Brazil: an overview of a confined orogen formed during Gondwanaland assembly. *Precambrian research*, 110(1-4):307–323.

Peifer, D., Persano, C., Hurst, M. D., Bishop, P., & Fabel, D. (2021). Growing topography due to contrasting rock types in a tectonically dead landscape. *Earth Surface Dynamics*, 9(2):167–181.

Peifer Bezerra, D. (2018). *The pattern and style of landscape evolution in post-orogenic settings*. PhD thesis, University of Glasgow.

Pérez-Díaz, L. & Eagles, G. (2014). Constraining south atlantic growth with seafloor spreading data. *Tectonics*, 33(9):1848–1873.

Péron-Pinvidic, G. & Manatschal, G. (2009). The final rifting evolution at deep magma-poor passive margins from iberia-newfoundland: a new point of view. *International Journal of Earth Sciences*, 98(7):1581–1597.

Peron-Pinvidic, G., Manatschal, G., et al. (2019). Rifted margins: state of the art and future challenges. *Frontiers in Earth Science*, 7:218.

Peron-Pinvidic, G., Manatschal, G., & Osmundsen, P. T. (2013). Structural comparison of archetypal atlantic rifted margins: A review of observations and concepts. *Marine and petroleum geology*, 43:21–47.

Persano, C., Bishop, P., & Stuart, F. (2006). Apatite (U–Th)/He age constraints on the Mesozoic and Cenozoic evolution of the Bathurst region, New South Wales: evidence for antiquity of the continental drainage divide along a passive margin. *Australian Journal of Earth Sciences*, 53(6):1041–1050.

Persano, C., Stuart, F. M., Bishop, P., & Barfod, D. N. (2002). Apatite (U–Th)/He age constraints on the development of the great escarpment on the southeastern Australian passive margin. *Earth and Planetary Science Letters*, 200(1-2):79–90.

Price, P. & Walker, R. (1963). Fossil tracks of charged particles in mica and the age of minerals. *Journal of Geophysical Research*, 68(16):4847–4862.

Purinton, B. & Bookhagen, B. (2021). Beyond Vertical Point Accuracy: Assessing Inter-pixel Consistency in 30 m Global DEMs for the Arid Central Andes. *Frontiers in Earth Science*, 9:758606.

Ravenhurst, C. E., Roden-Tice, M. K., & Miller, D. S. (2003). Thermal annealing of fission tracks in fluorapatite, chlorapatite, manganoanapatite, and durango apatite: experimental results. *Canadian Journal of Earth Sciences*, 40(7):995–1007.

Redfield, T., Osmundsen, P., & Hendriks, B. (2005). The role of fault reactivation and growth in the uplift of western fennoscandia. *Journal of the Geological Society*, 162(6):1013–1030.

Reiners, P. W., Ehlers, T. A., & Zeitler, P. K. (2005). Past, present, and future of thermochronology. *Reviews in Mineralogy and Geochemistry*, 58(1):1–18.

Reno, B. L., Brown, M., Kobayashi, K., Nakamura, E., Piccoli, P. M., & Trouw, R. A. (2009). Eclogite–high-pressure granulite metamorphism records early collision in West Gondwana: new data from the Southern Brasília Belt, Brazil. *Journal of the Geological Society*, 166(6):1013–1032.

Ribeiro, L., Hackspacher, P., Ribeiro, M., Neto, J. H., Tello, S., Iunes, P., Franco, A., & Godoy, D. (2005a). Thermotectonic and fault dynamic analysis of Precambrian basement and tectonic constraints with the Paraná basin. *Radiation Measurements*, 39(6):669–673.

Ribeiro, L. F. B., Saenz, C. A. T., Iunes, P. J., Hackspacher, P. C., Neto, J. C. H., & Paulo, S. R. (2005b). Phanerozoic brittle tectonics in the South American continental platform, southeast Brazil: new insights from Fission Track studies on Apatite in reactivated fault zones. *Revista Brasileira de Geociências*, 35(2):151–164.

Riccomini, C. (1989). *O rift continental do sudeste do Brasil*. PhD thesis, Universidade de São Paulo.

Riccomini, C. & Assumpção, M. (1999). Quaternary tectonics in Brazil. *Episodes*, 22:221–225.

Riccomini, C., Sant'Anna, L. G., & Ferrari, A. L. (2004). Evolução geológica do rift continental do sudeste do Brasil. *Geologia do continente Sul-Americano: evolução da obra de Fernando Flávio Marques de Almeida*, pages 383–405.

Romano, A. W. & Castañeda, C. (2006). A tectônica distensiva pós-mesozóica na origem dos depósitos de bauxita da zona da mata mineira. *Geonomos*.

Royden, L. & Keen, C. (1980). Rifting process and thermal evolution of the continental margin of eastern Canada determined from subsidence curves. *Earth and Planetary Science Letters*, 51(2):343–361.

Ruetenik, G. A., Moucha, R., & Hoke, G. D. (2016). Landscape response to changes in dynamic topography. *Terra Nova*, 28(4):289–296.

Sacek, V. (2017). Post-rift influence of small-scale convection on the landscape evolution at divergent continental margins. *Earth and Planetary Science Letters*, 459:48–57.

Salgado, A. A. R., de Andrade Rezende, E., Bourles, D., Braucher, R., da Silva, J. R., & Garcia, R. A. (2016). Relief evolution of the continental rift of southeast brazil revealed by in situ-produced 10be concentrations in river-borne sediments. *Journal of South American Earth Sciences*, 67:89–99.

Salomon, E., Koehn, D., Passchier, C., Hackspacher, P. C., & Glasmacher, U. A. (2015). Contrasting stress fields on correlating margins of the South Atlantic. *Gondwana research*, 28(3):1152–1167.

Sambridge, M. & Mosegaard, K. (2002). Monte Carlo methods in geophysical inverse problems. *Reviews of Geophysics*, 40(3):3–1.

Sant'Anna, L. G., Schorscher, H. D., & Riccomini, C. (1997). Cenozoic tectonics of the Fonseca basin region, eastern Quadrilátero Ferrífero, MG, Brazil. *Journal of South American Earth Sciences*, 10(3-4):275–284.

Scherler, D. & Schwanghart, W. (2020a). Drainage divide networks–Part 1: Identification and ordering in digital elevation models. *Earth Surface Dynamics*, 8(2):245–259.

Scherler, D. & Schwanghart, W. (2020b). Drainage divide networks–Part 2: Response to perturbations. *Earth Surface Dynamics*, 8(2):261–274.

Schildgen, T. F. & Hoke, G. D. (2018). The topographic evolution of the central Andes. *Elements: An International Magazine of Mineralogy, Geochemistry, and Petrology*, 14(4):231–236.

Schmitt, R. d. S., de Araújo Fragoso, R., & Collins, A. S. (2018). Suturing Gondwana in the Cambrian: the orogenic events of the final amalgamation. In: *Geology of Southwest Gondwana*, pages 411–432. Springer.

Schneider, D. A. & Issler, D. R. (2019). Application of low-temperature thermochronology to hydrocarbon exploration. In: *Fission-Track Thermochronology and its Application to Geology*, pages 315–333. Springer.

Schwanghart, W. & Scherler, D. (2014). TopoToolbox 2–MATLAB-based software for topographic analysis and modeling in Earth surface sciences. *Earth Surface Dynamics*, 2(1):1–7.

Silk, E. & Barnes, R. (1959). Examination of fission fragment tracks with an electron microscope. *Philosophical Magazine*, 4(44):970–972.

Silva, C. M. T. d., Alkmim, F. F., & Pedrosa-Soares, A. C. (2009). Geometria e evolução do feixe de zonas de cisalhamento Manhuaçu–Santa Margarida, Orógeno Araçuaí, MG. *Rem: Revista Escola de Minas*, 62:23–34.

Smith, M. & Leigh-Jones, P. (1985). An automated microscope scanning stage for fission-track dating. *Nuclear Tracks and Radiation Measurements (1982)*, 10(3):395–400.

Soares, C., Guedes, S., Jonckheere, R., Hadler, J., Passarella, S., & Dias, A. (2016). Apatite fission-track analysis of Cretaceous alkaline rocks of Ponta Grossa and Alto Paranaíba arches, Brazil. *Geological Journal*, 51(5):805–810.

Souza, D. H., Hackspacher, P. C., Silva, B. V., Siqueira-Ribeiro, M. C., & Hiruma, S. T. (2021). Temporal and spatial denudation trends in the continental margin of southeastern Brazil. *Journal of South American Earth Sciences*, 105:102931.

Souza, D. H., Stuart, F. M., Ángel Rodés, Pupim, F. N., & Hackspacher, P. C. (2019). Controls on the erosion of the continental margin of southeast Brazil from cosmogenic 10Be in river sediments. *Geomorphology*, 330:163–176.

Spiegel, C., Kohn, B., Raza, A., Rainer, T., & Gleadow, A. (2007). The effect of long-term low-temperature exposure on apatite fission track stability: A natural annealing experiment in the deep ocean. *Geochimica et Cosmochimica Acta*, 71(18):4512–4537.

Stanton, N., Gordon, A., Cardozo, C., & Kusznir, N. (2021). Morphostructure, emplacement and duration of the Abrolhos Magmatic Province: A geophysical analysis of the largest post-breakup magmatism of the south-eastern Brazilian margin. *Marine and Petroleum Geology*, 133:105230.

Steiger, R. H. & Jäger, E. (1977). Subcommission on geochronology: convention on the use of decay constants in geo-and cosmochronology. *Earth and planetary science letters*, 36(3):359–362.

Stríkis, N. M., Cruz, F. W., Barreto, E. A., Naughton, F., Vuille, M., Cheng, H., Voelker, A. H., Zhang, H., Karmann, I., Edwards, R. L., et al. (2018). South American monsoon response to iceberg discharge in the North Atlantic. *Proceedings of the National Academy of Sciences*, 115(15):3788–3793.

Summerfield, M. A. (1991). *Global geomorphology*. Longman.

Tagami, T. & O'Sullivan, P. B. (2005). Fundamentals of fission-track thermochronology. *Reviews in Mineralogy and Geochemistry*, 58(1):19–47.

Tamer, M. & Ketcham, R. (2020). Is Low-Temperature Fission-Track Annealing in Apatite a Thermally Controlled Process? *Geochemistry, Geophysics, Geosystems*, 21(3):e2019GC008877.

Tamer, M. T., Chung, L., Ketcham, R. A., & Gleadow, A. J. (2019). Analyst and etching protocol effects on the reproducibility of apatite confined fission-track length measurement, and ambient-temperature annealing at decadal timescales. *American Mineralogist: Journal of Earth and Planetary Materials*, 104(10):1421–1435.

Tello Saenz, C., Hackspacher, P., Neto, J. H., Iunes, P., Guedes, S., Ribeiro, L., & Paulo, S. (2003). Recognition of Cretaceous, Paleocene, and Neogene tectonic reactivation through apatite fission-track analysis in Precambrian areas of southeast Brazil: association with the opening of the South Atlantic Ocean. *Journal of South American Earth Sciences*, 15(7):765–774.

Thiel, K. & Herr, W. (1976). The 238U spontaneous fission decay constant re-determined by fission tracks. *Earth and Planetary Science Letters*, 30(1):50–56.

Thompson, R., Gibson, S., Mitchell, J., Dickin, A., Leonardos, O., Brod, J., & Greenwood, J. (1998). Migrating Cretaceous–Eocene magmatismin the Serra do Mar alkaline province, SE Brazil: Melts from the deflected Trindade mantle plume? *Journal of Petrology*, 39(8):1493–1526.

Trouw, R. A., Peternel, R., Ribeiro, A., Heilbron, M., Vinagre, R., Duffles, P., Trouw, C. C., Fontainha, M., & Kussama, H. H. (2013). A new interpretation for the interference zone between the southern Brasília belt and the central Ribeira belt, SE Brazil. *Journal of South American Earth Sciences*, 48:43–57.

Trouw, R. A. J., Heilbron, M., Ribeiro, A., Paciullo, F., Valeriano, C., Almeida, J., Tupinambá, M., & Andreis, R. (2000). The central segment of the Ribeira belt. *Tectonic Evolution of South America*, 31:287–310.

Tucker, G. E. & Slingerland, R. L. (1994). Erosional dynamics, flexural isostasy, and long-lived escarpments: A numerical modeling study. *Journal of Geophysical Research: Solid Earth*, 99(B6):12229–12243.

van der Beek, P., Andriessen, P., & Cloetingh, S. (1995). Morphotectonic evolution of rifted continental margins: Inferences from a coupled tectonic-surface processes model and fission track thermochronology. *Tectonics*, 14(2):406–421.

van der Beek, P., Summerfield, M. A., Braun, J., Brown, R. W., & Fleming, A. (2002). Modeling postbreakup landscape development and denudational history across the southeast African (Drakensberg Escarpment) margin. *Journal of Geophysical Research: Solid Earth*, 107(B12):2351.

van Ranst, G., Pedrosa-Soares, A. C., Novo, T., Vermeesch, P., & De Grave, J. (2020). New insights from low-temperature thermochronology into the tectonic and geomorphologic evolution of the south-eastern Brazilian highlands and passive margin. *Geoscience Frontiers*, 11(1):303–324.

Wagner, G. & van der Haute, P. (1992). *Fission-track dating*. Kluwer Academic Publishers, Dordrecht.

Wang, Y. & Willett, S. D. (2021). Escarpment retreat rates derived from detrital cosmogenic nuclide concentrations. *Earth Surface Dynamics*, 9(5):1301–1322.

Wernicke, B. (1985). Uniform-sense normal simple shear of the continental lithosphere. *canadian Journal of earth sciences*, 22(1):108–125.

Wildman, M. (2015). *Reassessing the structural and geomorphic evolution of a'classic'Atlantic type passive margin: an integrated study of the Namaqualand sector of the South African continental margin*. PhD thesis, University of Glasgow.

Wildman, M., Brown, R., Beucher, R., Persano, C., Stuart, F., Gallagher, K., Schwanethal, J., & Carter, A. (2016). The chronology and tectonic style of landscape evolution along the elevated Atlantic continental margin of South Africa resolved by joint apatite fission track and (U-Th-Sm)/He thermochronology. *Tectonics*, 35(3):511–545.

Wildman, M., Brown, R., Persano, C., Beucher, R., Stuart, F. M., Mackintosh, V., Gallagher, K., Schwanethal, J., & Carter, A. (2017). Contrasting Mesozoic evolution across the boundary between on and off craton regions of the South African plateau inferred from apatite fission track and (U-Th-Sm)/He thermochronology. *Journal of Geophysical Research: Solid Earth*, 122(2):1517–1547.

Wildman, M., Brown, R., Watkins, R., Carter, A., Gleadow, A., & Summerfield, M. (2015). Post break-up tectonic inversion across the southwestern cape of South Africa: New insights from apatite and zircon fission track thermochronometry. *Tectonophysics*, 654:30–55.

Wildman, M., Cogné, N., & Beucher, R. (2019). Fission-track thermochronology applied to the evolution of passive continental margins. In: *Fission-track thermochronology and its application to geology*, pages 351–371. Springer.

Willett, S. D. (1997). Inverse modeling of annealing of fission tracks in apatite; 1, A controlled random search method. *American Journal of Science*, 297(10):939–969.

Winter, W., Jahnert, R., & França, A. (2007). Bacia de Campos. *B. Geoci. Petrobras*, 2(15):511–529.

Young, D. (1958). Etching of radiation damage in lithium fluoride. *Nature*, 182(4632):375–377.

Zachos, J., Pagani, M., Sloan, L., Thomas, E., & Billups, K. (2001). Trends, rhythms, and aberrations in global climate 65 Ma to present. *Science*, 292(5517):686–693.

Zalán, P. & Oliveira, J. (2005). Origin and structural evolution of the Cenozoic rift system of southeastern Brazil. *Bol Geoc Petrobras*, 13(2):269–300.

Ziegler, P. A. & Cloetingh, S. (2004). Dynamic processes controlling evolution of rifted basins. *Earth-Science Reviews*, 64(1-2):1–50.

Appendix

APPENDIX A – Supplementary material

A.1 Supplementary material of chapter 3

A.1.1 Apatite fission track thermochronology dataset of the continental margin of southeast Brazil

The apatite fission track thermochronology dataset of the continental margin of southeast Brazil approached in chapter 3 is presented in the file **'AppendixA_Brazilian_ rifted_continental_margin.xlsx'**.

A.1.2 Supporting images of the chapter 3

The supporting images for the chapter 3 is presented in the file **'AppendixB_ supporting images_Brazilian_rifted_continental_margin.pdf'**.

A.2 Supplementary material of the chapter 4

A.2.1 Apatite fission track thermochronology dataset of the Serra da Boa Vista

The apatite fission track thermochronology dataset (e.g., fission track age data, mean track length data, radial plots) of the Serra da Boa Vista region is presented in the folder **'Serra_da_Boa_Vista_AFT_data'**.

Annex

ANNEX A – Complete papers

A.1 Vista Alegre Meta-Ultramaphic body: A key towards tectonometamorphic evolution of the Araçuaí orogen high-grade core

In: Journal of South American Earth Sciences(2018), 87:42-52. (Link to access)

Journal of South American Earth Sciences 87 (2018) 42–52

Contents lists available at ScienceDirect

Journal of South American Earth Sciences

journal homepage: www.elsevier.com/locate/jsames

Vista Alegre Meta-Ultramaphic body: A key towards tectono-metamorphic evolution of the Araçuaí orogen high-grade core

Tobias Maia Rabelo Fonte-Boa [a, *], Marco Antônio Couto Jr. [b], Tiago Amâncio Novo [a], Antônio Carlos Pedrosa-Soares [a, 1]

[a] Universidade Federal de Minas Gerais, Programa de Pos-graduação em Geologia, CPMTC-IGC, Campus Pampulha, Av. Antônio Carlos 6627, Belo Horizonte, 31270-901 MG, Brazil
[b] Serviço Geologico do Brasil (CPRM), Av. Brasil 1731, 30140-002, Belo Horizonte, MG, Brazil

ARTICLE INFO

Article history:
Received 27 July 2017
Received in revised form
2 December 2017
Accepted 2 December 2017
Available online 6 December 2017

Keywords:
Meta-ultramafic body
High-grade metamorphic core
Araçuaí orogen

ABSTRACT

The Vista Alegre Meta-Ultramafic body is part of a cluster of meta-ultramafic occurrences located in the internal tectonic domain of the Araçuaí-West Congo orogen in southeast Brazil. They consist of several small northeast-trending bodies hosted by an orthogneiss basement and metasedimentary package tectonized and intruded by granites during the Brasiliano orogenic cycle. To improve the existent models of the tectono-metamorphic evolution of the Araçuaí orogen high-grade metamorphic core, we performed a geophysical and detailed mineralogical study of the meta-ultramafic body and its host rocks. The magnetic response indicates three relatively shallow portions instead of one deep continue meta-ultramafic body. These portions are interpreted as mega boudins aligned parallel to the regional foliation. The petrographic and mineral chemistry studies indicate a high-grade progressive metamorphic path followed by a retrograde process. The metamorphic peak must have reached granulite facies conditions related to the collisional stage of the Araçuaí-West Congo orogen. The posterior stabilization, in greenschist facies conditions, represents a metamorphic retrogression related to the thermal event during the post-collisional stage.

A.2 A-type Medina batholith and post-collisional anatexis in the Araçuaí orogen (SE Brazil)

In: Lithos(2018), 320-321:515-536. (Link to access)

Lithos 320–321 (2018) 515–536

Contents lists available at ScienceDirect

Lithos

journal homepage: www.elsevier.com/locate/lithos

A-type Medina batholith and post-collisional anatexis in the Araçuaí orogen (SE Brazil)

Paula Serrano [a,*], Antonio Pedrosa-Soares [a], Edgar Medeiros-Júnior [b], Tobias Fonte-Boa [a], Cristina Araujo [a], Ivo Dussin [c], Gláucia Queiroga [b], Cristiano Lana [b]

[a] Universidade Federal de Minas Gerais, Programa de Pós-Graduação em Geologia, CPMTC-IGC, Campus Pampulha, 31270-901 Belo Horizonte, Brazil
[b] Departamento de Geologia, Escola de Minas, Universidade Federal de Ouro Preto, Morro do Cruzeiro, R. Diogo de Vasconcelos, 122 Ouro Preto, Brazil
[c] Universidade do Estado do Rio de Janeiro, Faculdade de Geologia, R. São Francisco Xavier, 524 Rio de Janeiro, Brazil

ARTICLE INFO

Article history:
Received 21 February 2018
Accepted 9 September 2018
Available online 12 September 2018

Keywords:
Geochronology
Thermobarometry
A-type granites
Medina batholith
Araçuaí orogen

ABSTRACT

The Medina batholith and its host granitic migmatites record intriguing plutonic processes in the northern Araçuaí orogen (SE Brazil). This orogen shows a long lasting (630–480 Ma) succession of granite production events from the earliest pre-collisional plutons to the latest post-collisional intrusions. The Medina batholith includes granite intrusions ascribed to the post-collisional stage. They show high alkali and halogen contents, low CaO (at $SiO_2 = 71\%$: $Na_2O + K_2O = 7$ to 9%; $CaO = 1.6\%$), and high $FeO_t/(FeO_t + MgO)$ ratios (0.78 to 0.92). The Medina granites are metaluminous to weakly peraluminous, with ASI (molecular ratio Al/(Ca-1.67P + Na_K)) values of 1.76 to 2.07, and have high concentrations of high field strength elements (Zr + Nb + Ce + Y > 700 ppm), as well as high Ga/Al ratios. Accordingly, the Medina intrusions are typical ferroan A-type granites. U—Pb ages from zircon (501 ± 2 Ma) and monazite (497 ± 2 Ma) constrain the emplacement timing of the Medina batholith. Surprisingly, all monazite ages from host rocks also cluster around 500 Ma, despite their nature and distance from the batholith, suggesting that they would have shared a same thermal process. The studied host rocks are granitic migmatites varying from patch metatexite to nebulitic diatexite, comprising paleosome of foliated sillimanite-garnet-biotite metagranite to gneiss, and non-foliated garnet-cordierite neosome poor to free of biotite. A metatexite (R14) located relatively far from the Medina batholith, and a diatexite (M26) found at the batholith contact were sampled for detailed studies. The paleosome of foliated metagranite (R14A) only shows zircon grains with igneous features and Th/U ratio from 1.64 to 0.26. Although the spreading of zircon spots, the main cluster yields a Concordia age at 556 ± 6 Ma, constraining the protolith magmatic crystallization. A minor cluster furnishes a Concordia age at 499 ± 7 Ma, in agreement with the U—Pb monazite age at 501 ± 2 Ma. Extracted from the same metatexite sample, the non-foliated garnet-cordierite neosome (R14B) shows both igneous and metamorphic zircon domains with Th/U ratios ranging from 1.47 to 0.00. Again, the U—Pb spots cluster at two distinct Concordia ages (562 ± 3 Ma and 499 ± 3 Ma). The youngest of them, fitting with the monazite age (495 ± 3 Ma), constrains melt crystallization, while the oldest age suggests paleosome inheritance. The nebulitic diatexite (M26) shows monazite (497 ± 2 Ma) and zircon (Th/U = 1.7 to 0.0; Concordia ages at 564 ± 2 Ma and 507 ± 3 Ma) populations similar to the metatexite neosome, also with the youngest ages bracketing the melt crystallization process around 500 Ma. Accordingly, all those ages at around 500 Ma disclose a partial melting episode coeval with the Medina batholith emplacement. Phase equilibrium modeling on a garnet-cordierite neosome furnished P-T conditions of 750–840 °C at 2.4–3.5 kbar for that post-collisional anatexis. Evidence for such a late thermal event are common in the Araçuaí orogen, even far from the post-collisional batholiths. Thus, a possible major heat source can be envisaged, like a mantle plume triggering crustal anatexis and regional fluid circulation during the gravitational collapse of the Araçuaí orogen.

A.3 Interpolation artifacts as a result of spatial aliasing: a case study of the airborne magnetic dataset of south-eastern Minas Gerais - Brazil

In: GEOPHYSICS(2020),85(6):B173-B185. (Link to access).

GEOPHYSICS, VOL. 85, NO. 6 (NOVEMBER-DECEMBER 2020); P. B173–B185, 10 FIGS., 1 TABLE.
10.1190/GEO2019-0782.1

Case History

Interpolation artifacts as a result of spatial aliasing: A case study of the airborne magnetic data set of southeastern Minas Gerais, Brazil

Tobias Maia Rabelo Fonte-Boa[1], Aline Tavares Melo[1], and Tiago Amâncio Novo[1]

ABSTRACT

Linear features at an acute angle with the flight direction are imaged as a series of aligned circular anomalies in the images of Area 15 aeromagnetic survey, which covered part of the Brazilian southeastern region. These features are interpolation artifacts, a recurring problem found in airborne magnetic images that cause problems for qualitative and quantitative geophysical-geologic interpretation. This imaging problem is attributed to spatial aliasing. By running simulations of magnetic data on a synthetic model, we have physically demonstrated that the interpolation artifacts from Area 15 are due to inappropriate survey design. Besides the most common expression of artifacts, we described a geologically noncoherent linear pattern as a new type of artifact. Supported by spectral analyses, we found that the Area 15 aliased spectrum is similar to geologic high-frequency magnetic features, which constitutes a motive for unearthing the correct geophysical signal. Thus, we made use of four techniques for removing the artifacts. The trend enforcement method partially improved the images, whereas the inverse interpolation method was ineffective, apparently because Area 15 data are severely aliased. The constrained coherence diffusion and multitrend gridding methods were able to significantly reduce the presence of artifacts. Despite the high-frequency attenuation, these tools adequately enhanced the magnetic trends and minimized the artifacts. Therefore, the improved images are better suited for reliable geologic interpretation.

A.4 Differential Phanerozoic evolution of cratonic and non-cratonic lithosphere from a thermochronological perspective: São Francisco Craton and marginal orogens (Brazil)

In: Gondwana Research(2021), 92:106–126. (Link to access).

Gondwana Research 93 (2021) 106–126

Contents lists available at ScienceDirect

Gondwana Research

journal homepage: www.elsevier.com/locate/gr

Differential Phanerozoic evolution of cratonic and non-cratonic lithosphere from a thermochronological perspective: São Francisco Craton and marginal orogens (Brazil)

Ana Carolina Liberal Fonseca [a,*], Tiago Amâncio Novo [a], Simon Nachtergaele [b], Tobias M.R. Fonte-Boa [a], Gerben Van Ranst [b], Johan De Grave [b]

[a] Universidade Federal de Minas Gerais, Programa de Pós-Graduação em Geologia, CPMTC-IGC, Campus Pampulha, Belo Horizonte, MG, Brazil
[b] Department of Geology, Ghent University, Ghent, Belgium

ARTICLE INFO

Article history:
Received 10 March 2020
Received in revised form 20 December 2020
Accepted 19 January 2021
Available online 24 January 2021

Handling Editor: T. Gerya

Keywords:
Brasília Orogen
Araçuaí Orogen
Continental lithosphere rigidity
Lithospheric inheritance
Apatite fission track thermochronology

ABSTRACT

The São Francisco Craton (SFC) and its marginal Araçuaí and Brasília orogens exhibit a significant diversity in their lithospheric architecture. These orogens were shaped during the Neoproterozoic–Cambrian amalgamation of West Gondwana. The rigid cratonic lithosphere of the SFC and the relatively weak lithosphere of the Araçuaí Orogen were disrupted during the Cretaceous opening of the South Atlantic Ocean, whereas the Brasília Orogen remained in the continental hinterland. In earlier research, the thermal effects of the Phanerozoic reactivations in the shallow crust of the Araçuaí Orogen have been revealed by low-temperature thermochronology, mainly by apatite fission track (AFT) analysis. However, analyses from the continental interior are scarce. Here we present new AFT data from forty-three samples from the Brasília Orogen, the SFC and the Araçuaí Orogen, far from the passive margin of the Atlantic coast (~150 to 800 km). Three main periods of basement exhumation were identified: (i) Paleozoic, recorded both by samples from the SFC and Brasília Orogen; (ii) Early Cretaceous to Cenomanian, recorded by samples from the Araçuaí Orogen; and (iii) Late Cretaceous to Paleocene, inferred in samples from all domains. We compare the differential exhumation pattern of the different geotectonic provinces with their lithospheric strengths. We suggest that the SFC likely concentrated the Meso-Cenozoic reactivations in narrow weak zones while the Araçuaí Orogen displayed a far-reaching Meso-Cenozoic deformation. The Brasília Orogen seems to be an example of a stronger orogenic lithosphere, inhibiting reworking, confirmed by our new AFT data. Understanding the role of the lithosphere rigidity may be decisive to comprehend the processes of differential denudation and the tectonic–morphological evolution over Phanerozoic events.

A.5 The state of the art of low-temperature thermochronology in Brazil

In: Journal of the Geological Survey of Brazil (2021), 4(3):239-256. (Link to access).

Journal of the Geological Survey of Brazil vol 4, nº 3, 239 - 256, December 2021

Journal of the Geological Survey of Brazil

The state of the art of low-temperature thermochronometry in Brazil

Tiago Amâncio Novo[1*], Tobias Maia Rabelo Fonte-Boa[1], Júlia Mattioli Rolim[1], Ana Carolina Fonseca[2]

[1]UFMG - Universidade Federal de Minas Gerais, Programa de Pós-Graduação em Geologia, CPMTC-IGC, Campus Pampulha, Belo Horizonte, MG, Brazil. CEP: 31270-901
[2]Department of Geology, Ghent University, Ghent, Belgium

Abstract

Low-temperature thermochronology focuses on the comprehension of the upper crust's thermal history, where morphotectonic processes take place. We present a robust compilation (1120 data in almost 30 years of research) of fission-track and (U-Th)/He studies and their implications to the understanding of Brazilian geomorphology development. Brazil has a complex geological evolution, involving multiple orogenic and taphrogenic episodes that shaped cratons, orogens, and basins together through time. The thermochronology data set is inconsistently distributed, most of it is concentrated in coastal regions, mainly in the southeastern region; while the intracontinental portions lack studies. The available data set suggests a complex reactivation scenario near the coast to a more stable situation inland. The Mantiqueira and Borborema provinces show a great Early Cretaceous denudation event and a less important Permian to Jurassic, and Paleogene denudation events. The cratonic areas show different patterns, with denudation related to the Devonian to the Jurassic. The data suggest that elastic thickness, structural network, and drainage system play an important role in the morphotectonic control of Brazilian landscape evolution.

Article Information

Publication type: Review Articles
Received 9 June 2021
Accepted 30 November 2021
Online pub. 28 December 2021
Editor: J.M. Lafon

Keywords:
Thermochronology
Thermochronometry
Apatite
Fission-track
(U-Th)/He

**Corresponding author
Tiago Amâncio Novo
tiagoanovo@gmail.com

ANNEX B – Extended abstracts

B.1 Magnetic artifacts due to aliasing effect: a case from southeast Minas Gerais aeromagnetic dataset

In: 16º International Congress of the Brazilian Geophysical Society, 2019, Rio de Janeiro.

(Link to access)

Magnetic artifacts due to spatial aliasing effect: a case from southeast Minas Gerais aeromagnetic dataset

Tobias Maia Rabelo Fonte-Boa, Aline Tavares Melo e Tiago Amâncio Novo

Abstract

We present a preliminary effort to solve the aliasing effect faced by aeromagnetic data processing and interpretation. The aliasing problem is caused by the survey arrangement and results in expressive magnetic artifacts after data interpolation. The spectral characteristics of the artifacts are similar to geological high-frequency magnetic features. Thus, it is very important to remove these artifacts to access the correct geophysical information. As the first approach, we applied two automated methods, the Keating and the Naprstek and Smith methods. Both methods were able to remove the undesired artifacts. They eliminate most of all the aliasing effects and enhanced the geophysical features. However, the procedures do not effectively remove all the artifacts. Therefore, further investigation applying other techniques (e.g. inverse interpolation and constrained coherence-enhancing diffusion filtering) is required to remove this effect that masks the true geological signal.

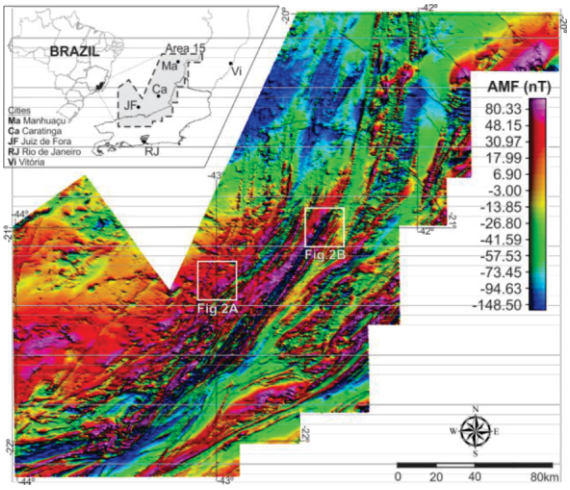

***Figure 1** – Anomalous Magnetic Field map of aerogeophysical data from Area 15 survey. The sensor height is 100 m, the line spacing is 500 m, and the grid-cell size is 100 m. Shading declination 45º.*

ANNEX C – Abstracts

C.1 Registros de Eventos Mesoproterozoicos no embasamento do Orógeno Araçuaí, sudeste do Brasil

In: 15º Simpósio de Geologia do Sudeste, 2017, Diamantina. (Link to access)

A história dos paleocontinentes se resume em longos períodos de fragmentação e pequenos intervalos de aglutinação. Um dos produtos de uma orogenia riaciana-orosiriana foi o paleocontinente São Francisco-Congo, representado nos crátons homônimos e no embasamento do Orógeno Araçuaí Congo Ocidental (AWCO). Durante o período de ca. 2 Ga até ca. 0,7 Ga aquela extensa região paleocontinental foi poupada de eventos orogênicos, mas por outro lado foi submetida a pelo menos cinco eventos tafrogênicos registrados por magmatismo anorogênico e sedimentação. Tais eventos tafrogênicos estão bem registrados nas zonas proximais do AWCO e regiões cratônicas adjacentes, mas suas evidências no núcleo de alto grau do AWCO são muito mais raras. Nossos estudos sobre lentes anfibolíticas intercaladas em ortognaisses do Complexo Pocrane, embasamento do Arco Magmático Rio Doce, permitiu reconhecer dois eventos tafrogênicos mesoproterozoicos distintos. O mais antigo deles, do Caliminiano, é caracterizado por anfibolitos com zircões cristalizados em 1529 ± 37 Ma (U-Pb SHRIMP). Outro conjunto de anfibolitos registra episódio tafrogênico mais jovem, do Esteniano, com zircões de idade magmática em 1096 ± 20 Ma (U-Pb SHRIMP). O episódio calimiano (ca. 1,5 Ga) é correlato com a bacia Espinhaço II e diques máficos dos domínios Espinhaço – Chapada Diamantina e Curaçá, enquanto que o episódio esteniano (ca. 1,1 Ga) correlaciona-se com a bacia Espinhaço III. Dados U-Pb de 87 grãos detríticos de zircão coletados em lentes do Quartzito Córrego Ubá, intercaladas no Complexo Pocrane, mostram um espectro de idades com picos em 1176 ± 21 Ma (35%), 1371 ± 30 Ma (18%), 1536 ± 22 Ma (19%), 1803 ± 36 Ma (17%) e 1977 ± 38 Ma (12%). Apesar de se ter encontrado um zircão com idade de 955 ± 66 Ma, o tratamento estatístico dos dados sugere uma idade máxima de deposição em ca. 1176 Ma. O espectro de idades mostra-se essencialmente limitado no intervalo 1-2 Ga; contrastando com os dados do setor oeste do AWCO e do Cráton São Francisco onde são comuns zircões do Toniano ou mais velhos que 2 Ga. Isso sugere uma bacia alimentada por fontes relativamente restritas. Os dois eventos tafrogênicos mesoproterozóicos aqui reportados evidenciam duas das tentativas de fragmentação mal sucedidas que incidiram sob o Paleocontinente São Francisco-Congo, o qual resistiu à completa fragmentação desde ca. 2 Ga até a abertura do Oceano Atlântico no Cretáceo.

C.2 Differential Phanerozoic denudation in the São Francisco craton and its surrounding mobile belts: insights from apatite fission track thermochronology

In: 4º SIMPÓSIO DO CRÁTON DO SÃO FRANCISCO, 2019, Aracajú. (Link to access)

DIFFERENTIAL PHANEROZOIC DENUDATION IN THE SÃO FRANCISCO CRATON AND ITS SURROUNDING MOBILE BELTS: INSIGHTS FROM APATITE FISSION TRACK THERMOCHRONOLOGY

Tiago Amâncio Novo[1], Ana Carolina Fonseca[1], Johan De Grave[2], Tobias Fonte Boa[1], Gabriella Piffer[1], Júlia Mattioli Rolim[1], Gerben Van Ranst[2], Simon Nachtergaele[2]

[1]UFMG-CPMTC (geoamancio@ufmg.br, analiberal7@gmail.com, tobiasfonteboa@gmail.com, gabriellavpiffer@gmail.com, julia.mattioli8@gmail.com); [2]Ghent University (Johan.DeGrave@ugent.be, gerben.vanranst@gmail.com, Simon.Nachtergaele@ugent.be)

This work brings new and compiled Apatite Fission Track (AFT) data from the São Francisco craton (SFC) and surrounding mobile belts (lithosphere weakness zones). The objective is to provide a regional view of the thermal behavior of the cratonic and orogenic belt lithospheres in front of the events that controlled their crustal denudation and geomorphological development. The SFC region has a complex, polycyclic history, involving multiple taphrogenic and orogenic events that result in a unique scenario. The São Francisco and Congo paleocontinental blocks were amalgamated during Rhyacian to Orosirian time constituting a cratonic area. After that, several extensional events have had given place from 1.75 Ga to 680 Ma. Two orogenic events occurred from the late Neoproterozoic to Permian (Brasiliano and Gondwanides, respectively). Afterwards the South American platform was stabilized. During the Mesozoic and Cenozoic taphrogenic processes took place; in the Early Cretaceous South America and Africa fall apart, resulting in the São Francisco-Congo craton disruption and the opening of the South Atlantic Ocean. The response to those taphrogenic and orogenic events was different in the cratonic and non-cratonic regions, resulting in differential denudation according to the terrain structure and rheology. To the east of the São Francisco craton, in the Araçuaí and Ribeira orogenic regions, the AFT central ages range from Jurassic to Neogene, showing different response to the late Mesozoic to Cenozoic extension efforts. This area registers mainly three thermal events: Early Cretaceous, Late Cretaceous and Paleogene-Neogene. On the one hand, the transect (from coast to hinterland) follows the expected model for passive margins in which there is an increase of ages from 30-90 Ma in the margin to 200 Ma in the continental hinterland. On the other hand, the range of younger AFT ages shows that the sensu strictu rifting process could not be the only responsible for the configuration of the relief on the coast. The discussion suggesting a post- breakup reactivation was already brought by other authors, involving the compressional event between the Andean subduction zone and the mid-Atlantic ridge; reburial and isostatic uplift events caused by the sedimentation of offshore basins. In the Bahia state coastal region, the cratonic lithosphere of the SFC registers older cooling ages, presenting a Permian-Early Jurasic thermal event. Countryside, in the Januária and Sete Lagoas highs (also cratonic lithosphere), the AFT ages range from Permian to Devonian, considerably older than the ages obtained in the Araçuaí-Ribeira orogenic region. The changes in the value of the AFT ages for the cratonic and orogenic lithosphere, suggest that the Mesozoic and Cenozoic extensive efforts did not act in a pervading way; implying that the higher mechanical resistance to deformation of the SFC constitute a long-lived, stable and almost deformational-free terrain. To the west of the SFC, the Brasilia Belt registers predominantly Carboniferous to Devonian AFT ages, with few younger ages; suggesting that the SFC acted as a physical barrier, sparing the Brasília belt from the Phanerozoic taphrogenic events.

KEYWORDS: THERMOCHRONOLOGY, DIFFERENTIAL DENUDATION

SUPPORT: CNPQ, CAPES, FAPEMIG

ANNEX D – Book chapters

D.1 Níquel e cobalto

In: Pedrosa-Soares, A.C; Voll, E; Cunha, E.C.. (Org.). Recursos Minerais de Minas Gerais Online. 1ed.Belo Horizonte: Companhia de Desenvolvimento de Minas Gerais (CODEMGE), 2018, v. , p. 1-24 (Link to access).

NÍQUEL E COBALTO

Tobias Maia Rabelo Fonte Boa
CPMTC – IGC/UFMG
tobiasfonteboa@gmail.com